UNCLASSIFIED

AD NUMBER

AD827108

NEW LIMITATION CHANGE

TO

Approved for public release, distribution unlimited

FROM

Distribution authorized to U.S. Gov't. agencies and their contractors; Administrative/Operational Use; FEB 1968. Other requests shall be referred to Air Force Rocket Propulsion Laboratory, Research and Technology Division, Edwards AFB, CA.

AUTHORITY

afrpl ltr, 27 oct 1971

THIS PAGE IS UNCLASSIFIED

AD827108

AFRPL-TR-67-320

STUDY AND DEMONSTRATION OF PAPER PHENOLIC COMPONENTS

FINAL REPORT

John W. Edwards, Principal Investigator
V. Singer, Structural Engineer
F. W. Mueller, Head, Applications Research and Development Group

DDC
RECEIVED
FEB 20 1968
B

THIOKOL CHEMICAL CORPORATION
ELKTON DIVISION
ELKTON, MARYLAND

TECHNICAL REPORT AFRPL-TR-67-320

FEBRUARY 1968

transmittal
made
RESEARCH AND TECHNOLOGY DIVISION

TELEPHONE
301-398-3000

Thiokol
CHEMICAL CORPORATION
ELKTON DIVISION
ELKTON, MARYLAND 21921

TWX
301-398-3914

In Reply Refer To:
E258-67

February 5, 1968

Air Force Rocket Propulsion Laboratory
Research and Technology Division
Edwards, California 93532

Attention: Mr. William F. Payne/RPMCH

Subject: Final Report - Study and Demonstration of Paper Phenolic Components

Reference: Contract AF04(611)-11621

Gentlemen:

Attached is Technical Report AFRPL-TR-67-320, the final report of a Study and Demonstration of Paper Phenolic Components. This document was prepared by the Elkton Division of Thiokol Chemical Corporation under Contract AF04(611)-11621, and covers work performed during the period of March 1966 to December 1967. Distribution has been made in accordance with the current CPIA mailing list.

We have appreciated the opportunity of working with you and look forward to future opportunities to serve you.

Very truly yours,

THIOKOL CHEMICAL CORPORATION
ELKTON DIVISION

H. G. Jones
General Manager

JJS/mp

When United States Government drawings, specifications, or other data are used for any purpose other than a definitely related government procurement operation, the Government thereby incurs no responsibility nor any obligation whatsoever, and the fact that the Government may have formulated, furnished, or in any way supplied the said drawings, specifications, or other data, is not to be regarded by implication or otherwise, or in any manner licensing the holder or any other person or corporation, or conveying any rights or permission to manufacture, use, or sell any patented invention that may in any way be related thereto.

AFRPL-TR-67-320

STUDY AND DEMONSTRATION OF PAPER PHENOLIC COMPONENTS

FINAL REPORT

John W. Edwards, Principal Investigator
V. Singer, Structural Engineer
F. W. Mueller, Head, Applications Research and Development Group

FOREWORD

This report was prepared by the Elkton Division of Thiokol Chemical Corporation, Elkton, Maryland under Contract AF04(611)-11621, Project 3059, Program Element No. 62405184. The report covers the period from May 2, 1966 through November 13, 1967. The Elkton Division report number is E258-67. The Air Force Project Officer is William F. Payne/RPMCH.

Acknowledgement is made of the assistance of Mr. E. G. Bittner and Mr. T. J. Crawford of the Micarta Division of Westinghouse Electric Corporation in the studies of manufacturing techniques and methods for improving the strength of paper phenolic materials.

This technical report has been reviewed and is approved.

ABSTRACT

The structural, thermal and mass properties of convolute-wrapped paper phenolic tubing were determined. This information was used to develop a satisfactory technique for performing a stress analysis for the preliminary design of several rocket devices, and for the detailed design and successful feasibility demonstration firing of a paper phenolic case, M58A2 rocket motor. The material is degraded by high temperature and humidity, although the effect is generally not permanent and the humidity problem can be overcome with a protective coating. The principal problem in the stress analysis technique was compensating for the non-linear anisotropic character of the material. The low strength-to-weight ratio and shear strength of the paper phenolic resulted in a decrease of seven percent in burnout velocity for the M58A2 and, consequently, a reduction of fifteen percent in cost effectiveness when compared to a metal case. In some applications, however, where the performance criterion is not sensitive to inert weight and where other properties of the paper phenolic offer overriding advantages (e.g., non-usability of debris) the material can be competitive.

TABLE OF CONTENTS

		PAGE
I.	Introduction	1
II.	Summary	3
III.	A Basis for Structural Analysis of Paper Phenolic Pressure Vessels	6
	1. Introduction	6
	2. General Description of the Nature of the Material in Tubular Form	7
	3. Mathematical Modeling of Pressurized Tube Elements	8
	4. Representations of Material Properties for Analysis	13
	5. Correlation of Analytical Strength Prediction with Experimental Results	15
IV.	Mechanical Properties of Paper Phenolic Laminates	20
	1. Uniaxial and Biaxial Tensile and Compressive Properties	20
	2. Effect of Environmental Conditioning on Tensile Properties	29
	3. Interlaminar Shear Strength	41
	4. Effect of Cyclic Loading on Tensile Properties	43
V.	Thermal and Mass Properties	46
VI.	Strength of Adhesive Bonds	47
VII.	Thermal Gradient Test of a Paper Phenolic M58A2 Analog	49
VIII.	Production Techniques for Paper Phenolic Components	53
	1. Introduction	53
	2. Production Techniques	54
	3. Dimensional Limitations	58
IX.	Generalized Design Studies and Comparisons of Paper Phenolic with Aluminum and Steel	63
	1. Wall Thickness and Mass Fraction	63
	2. Internal and External Insulation Requirements	66
	3. Propellant-Case Interactions	66
	4. Aeroelastic Bending	75
	5. Effects of Vehicle Interface Attachments on Case Structure	83
	6. Effect of Expected Handling and Storage Environments on Paper Phenolic Motor Structural Integrity and Performance	87

TABLE OF CONTENTS (Continued)

		PAGE
X.	Methods of Improving Physical Properties	89
	1. Increase Strength	89
	2. Anisotropy	89
	3. Composite Structures	90
	4. Composite Structures	90
	5. Tests	90
XI.	Preliminary Design Studies	91
	1. Introduction	91
	2. 2.75 Inch FFAR	91
	3. Tomahawk Igniter	94
	4. XM165 Parachute Flare	94
	5. 1.0-KS-25 Spin Motor	97
XII.	Design and Demonstration of a Prototype Paper Phenolic M58A2	100
	1. Introduction	100
	2. Design and Proof Tests	100
XIII.	Cost Effectiveness Studies	123
	1. Measures of Merit	123
	2. Actual Findings	124
XIV.	Conclusions and Recommendations	127
	APPENDIXES	
	I. Mechanical and Physical Properties Test Procedures	129
	II. Analytical Treatment of Flexural Effects	147
	III. Extensions of Hooke's Law	151
	IV. Strain Gauge Data for TE-M-49-1 Hydroburst	152
	V. Strain and Temperature Data for TE-M-49-1 Static Test	154
	REFERENCES	156

LIST OF ILLUSTRATIONS

		PAGE
1.	Typical Tensile Stress-Strain Relationship in Meridian Direction	10
2.	Representations of Stress-Strain Behavior	11
3.	Structural Model of Vessel	17
4.	Meridian Tensile Strength Versus Temperature	21
5.	Hoop Tensile Strength Versus Temperature	23
6.	Meridian Tensile Secant Modulus Versus Meridian Uniaxial Tensile Strain at 77°F	24
7.	Meridian Compressive Secant Modulus Versus Uniaxial Meridian Compressive Strain at 77°F (Five Specimens)	25
8.	Hoop Tensile Secant Modulus Versus Hoop Tensile Uniaxial Strain at 77°F	28
9.	Meridian Tensile Secant Modulus Versus Uniaxial Meridian Strain at -75°F	32
10.	Meridian Tensile Secant Modulus Versus Uniaxial Meridian Strain at 0°F	33
11.	Meridian Tensile Secant Modulus Versus Uniaxial Meridian Strain at 150°F	34
12.	Meridian Tensile Secant Modulus Versus Uniaxial Meridian Strain at 225°F	35
13.	Hoop Tensile Secant Modulus Versus Uniaxial Strain at -75°F	36
14.	Hoop Tensile Secant Modulus Versus Uniaxial Strain at 0°F	37
15.	Hoop Tensile Secant Modulus Versus Uniaxial Strain at 150°F	38
16.	Hoop Tensile Secant Modulus Versus Uniaxial Strain at 225°F	39
17.	Effect of Humidity, Salt Spray, Vacuum Storage and Thermal Cycling on Meridian Tensile Properties	40
18.	Effect of Humidity, Salt Spray, Vacuum Storage, and Thermal Cycling on Hoop Tensile Properties	41
19.	Interlaminar Shear Strength Versus Temperature for Tube Specimens of HY-488	43

LIST OF ILLUSTRATIONS (Continued)

		PAGE
20.	Effects of Cyclic Loading	45
21.	Gradient Study Motor	50
22.	Temperature Versus Time in Inert Paper Phenolic M58A2	51
23A.	Reduced Wall Thickness Versus Chamber Pressure for Paper Phenolic, Aluminum and Steel	64
23B.	Reduced Weight Versus Chamber Pressure for Paper Phenolic, Aluminum and Steel	65
24.	Temperature Gradient in Case Walls of Various Materials	67
25.	Model Geometry for Propellant-Grain Interaction Analysis	68
26.	Maximum Inner Bore Hoop Strain Versus Temperature	72
27.	Maximum Inner Bore Hoop Stress Versus Temperature	73
28.	Interface Radial Bond Stress Versus Temperature	74
29.	Aeroelastic Bending Analytical Model	76
30.	Structural Concepts for Fin and Closure Interfaces	85
31.	Paper Phenolic 2.75 inch FFAR	92
32.	Tomahawk Igniters. A. Steel Pyrogen Igniter B. Paper Phenolic Igniter	95
33.	XM165 Parachute Flare	96
34.	1.0-KS-25 Spin Motor Assembly A. Paper Phenolic Case B. Metal Case	98 99
35.	Concept I and Concept II Case Design	101
36.	Area of Failure, Concept II Hydrotest	104
37.	Adhesive Bond in Area of Failure, Concept II Hydrotest	105
38.	Adhesive Bond in Area of Failure, Concept II Hydrotest	106

LIST OF ILLUSTRATIONS (Continued)

		PAGE
39.	Burst Case, Concept I, Test I	107
40.	Adhesive Bond in Area of Failure, Concept I, Test I	108
41.	Burst Case, Concept I, Test II	109
42.	Burst Case, Concept I, Test III	110
43.	Concept III Loaded Case	112
44.	Burst Case, Concept III, Test I	113
45.	Burst Case, Concept III, Test II	114
46.	Motor Assembly, Concept III	117
47.	Static Test Arrangement, Concept III	118
48.	Post Static Test, Concept III	119
49.	Fired Components, Concept III	120
50.	Sectioned Case, Concept III	122
51.	NOL Ring Specimens	130
52.	Tube Tensile Specimen	131
53.	Hoop Tensile Test Apparatus	132
54.	Strain Measurement Locations for the NOL Ring Specimen	135
55.	Strain Measurement Locations for the Tube Specimen	136
56.	3.00-Inch I.D. Biaxial Test Vessel	138
57.	3.00-Inch I.D. Uniaxial Test Apparatus	139
58.	NOL Ring Interlaminar Shear Specimen	143
59.	Punch Interlaminar Shear Apparatus	145
60.	Strain Gauge Locations for Concept III Hydroburst	153
61.	Strain Gauge and Thermocouple Locations for Concept III Static Test	155

LIST OF TABLES

		PAGE
I.	Tensile Properties of Tube Specimens Versus Strain Rate	26
II.	Compressive Properties Versus Strain Rate	26
III.	Thermal and Mass Properties of Micarta HY-488	46
IV.	Tensile Shear Strength of Metal to Paper Phenolic Bonds	48
V.	Basic Cost Data for Paper Phenolic Tubing Produced to NEMA Standards	56
VI.	NEMA Standards for Dimensional Tolerances on Rolled Tubes	60
VII.	Thermal and Mechanical Properties for Propellant-Case Interaction Calculations	69
VIII.	Inner Band Hoop Strains Due to Internal Pressurization	71
IX.	Effect of Expected Handling and Storage Environments	87
X.	Weight Comparison of Metal and Paper Case 2.75 FFAR	93
XI.	Summary of Hydrotest Results	102
XII.	Hoop Tensile Results from Failed Cases	115
XIII.	Uniaxial Tensile Properties Test Program	134
XIV.	Thermal Cycling Program	141
XV.	Interlaminar Shear Strength Test Program	146
XVI.	Strain Data for TE-M-49-1, Concept III, Hydroburst I	152
XVII.	Strain and Temperature Data for TE-M-49-1 Static Test	154

LIST OF ABBREVIATIONS AND SYMBOLS

a	=	Acceleration (ft/sec)
A, B, C	=	Proportionality constants
D	=	Diameter (ft)
D_f	=	Flexural rigidity, defined in Eq. 2
$(C_{n\alpha}\ S)_N$	=	Lift coefficient slope of nose times reference area of the nose (ft^2/radians)
$(C_{n\alpha}\ S)_T$	=	Lift coefficient slope of tail times reference area of the tail (ft^2/radians)
E	=	Elastic modulus, $lb/in.^2$ or lb/ft^2
E_B	=	Propellant bulk modulus ($lb/in.^2/in.^3$)
E_e	=	Propellant equilibrium modulus (psi)
f_i	=	Inertial force distribution, defined in Eq. 14
F	=	Longitudinal force per circumferential inch (lbs/in.)
F_N	=	Force on nose, defined in Fig. 29 (lbf)
F_T	=	Force on tail, defined in Fig. 29 (lbf)
I	=	Moment of inertia (ft^4)
$\bar{k}$	=	Foundation modulus, defined in Eq. 3.
k	=	Defined by Eq. 26.
L	=	Length, ft.
m	=	Mass (slugs)
M	=	Longitudinal moment about mid-thickness, per circumferential inch or Longitudinal moment about center of gravity
P	=	Pressure, (psi)
q	=	Dynamic pressure = $\rho V^2/2$, (lb/ft^2)
R	=	Radius (inches)
r	=	Defined in Eq. 27.
t	=	Distance of a point from the surface of a cross section, illustrated in Appendix A (inches)
T	=	Thickness of cross-section or case (inches)
V	=	Velocity (ft/sec)
X	=	F/T
Y	=	M/T^2
α	=	Angle of attack, defined in Fig. 29, (radians)
δ	=	Misalignment angle, defined in Fig. 29, (radians)
ϵ	=	Strain (in./in.)
θ	=	Deflection angle, defined in Fig. 29 (radians)
ν	=	Poisson's Ratio
ξ	=	Length of moment arm (ft.)

ρ	=	Atmospheric density (slugs/ft^3)
λ	=	r_o/r_i
μ	=	Coefficient of thermal expansion
σ	=	Stress (psi)
T	=	Temperature (°F)
T_0	=	Grain zero strain temperature, °F
φ_p	=	Volumetric Cure Shrinkage
c	=	Case
f	=	Flexure
i	=	Inner
r	=	Radial Direction
o	=	Outer
n, p	=	Designate the extreme fibers on opposite sides of a cross section
p	=	Propellant
t	=	Through-thickness direction
φ	=	Meridian direction
θ	=	Hoop direction
sec	=	Secant
tan	=	Tangent

SUPERSCRIPTS

Over-bar (—) = Indicates through-thickness averaged value

NOTE: When more than one subscript is used (e.g., $\nu_{\varphi\theta}$) the first subscript refers to the stressed direction and the symbol represents the ratio of the strain in the direction of the second subscript to strain in the direction of the first subscript.

SECTION I

INTRODUCTION

SECTION I

INTRODUCTION

The objective of this program was to determine the potential of paper phenolic laminates as a structural material for solid propellant rocket motors. Both analytical and experimental studies were performed in a two-phase program to explore and assess the capabilities, limitations, and potential applications of the material. The first phase of the program consisted of laboratory tests to determine the structural and thermal properties of the material, a study of the production techniques for fabricating case components from paper phenolics, and parametric design and cost analysis of paper phenolic structural materials for various rocket motors and pyrotechnic devices. In the second phase we designed, fabricated, and successfully demonstrated in a static test a prototype M58A2 rocket motor with a paper phenolic case.

Based primarily on the results of a feasibility program conducted by the Huntsville Division of Thiokol Chemical Corporation, Micarta Grade HY-488 was selected as the material to be used for our investigations. The Huntsville Division had investigated several grades of material manufactured by the only two known producers of high strength paper phenolic laminates. These investigations had shown that the HY-488 was clearly stronger than the other materials investigated. HY-488 is a laminate of oriented fiber kraft paper and phenolic resin produced by the Micarta Division of Westinghouse Electric Company, Hampton, S. C. The material is normally available as convolute-wrapped tubing or as flat plate.

Since the material we are interested in for rocket motor case fabrication is tubing and since basic differences in the manufacturing processes for tubing and sheet result in differences in the material properties of the two forms, it was decided that all mechanical properties specimens and, insofar as possible, all mass and thermal properties specimens would be obtained from tubing. This necessitated the development of two different types of tensile specimens to take into account the configuration of the material and the anisotropy of the material.

We did not attempt to perform an all inclusive study of the physical properties nor did we attempt to perform sufficient tests of specific properties to provide an accurate statistical definition of their range. Instead, our objective was to obtain the minimum information about the material to provide a valid basis for an evaluation of its potential.

The environments and limits selected for evaluation were based on the common military operational requirements. The motors and devices selected for the preliminary design studies were selected as representative of specific classes of applications and as far as possible were items with which Thiokol had specific design and production experience.

SECTION II

SUMMARY

SECTION II

SUMMARY

During this program the mechanical, thermal and mass properties of Micarta HY-488 paper phenolic laminates were determined, and these data were used to develop structural analysis techniques; prepare preliminary designs of several rocket and pyrotechnic devices; design, build and fire a prototype M58A2; and prepare a cost effectiveness analysis of several of the preliminary designs. The demonstration firing was a success but the various studies showed that the material was cost effective only in limited applications.

An extensive laboratory test program was performed to determine the following properties of the paper phenolic tubing:

(1) uniaxial and biaxial tensile and compressive properties

(2) effect of cyclic loading and various military operational environments on the tensile properties

(3) density

(4) specific heat

(5) thermal conductivity

(6) linear coefficient of thermal expansion

In the course of these investigations several interesting characteristics were observed. First, the material is quite anisotropic, both with respect to mechanical properties and with respect to thermal conductivity; second, the stress-strain relationship is very nonlinear, without a yield point as is experienced with metals; third, both elevated temperature and humidity degrade the strength of the laminate. At 150°F the tensile strength is about 15 percent lower than at 70°F but the degradation is not permanent, except in the case of very thick walls. The humidity problem was overcome with a simple waterproof surface coating.

A nonlinear stress-strain relationship is not compatible with the ordinary means of performing stress analyses, particularly with respect to discontinuity analyses. Since the capability to perform an effective discontinuity analysis is essential to efficient design, considerable effort was expended in developing a satisfactory technique for treatment of the discontinuity problem. The technique developed is

based on the use of equivalent elastic properties and effective geometries and has been shown to produce analytical results in good agreement with experimental observations. It was also found that for the purposes of these analyses, it was convenient to express the stress-strain relationship in terms of the secant modulus, a linear parameter when expressed in terms of strain.

A number of generalized design and parametric studies were performed to assess the design problems, limitations and potential of the material. The strength to weight ratio is considerably lower than that of metals and this, combined with the low shear strength, leads to limitations in the design capabilities. An efficient design with this material must be optimized for paper phenolic from system conception. A structural design which is optimum for a metal is frequently not optimum for paper phenolic.

Preliminary designs were prepared of several contemporary motors and devices using paper phenolic as the primary structural materials. These designs were then compared to the existing metal case unit in terms of dimensional envelope, external and internal insulation requirements, center of gravity, vehicle performance and cost effectiveness. The units investigated were the 2.75 FFAR, Tomahawk Igniter, XM-165 parachute flare, 1.0-KS-25 Spin Motor, and the M58A2. It was found that such manufacturing cost savings as do exist are generally overcome by the low strength to weight ratio and, consequently, the lower performance of the system. This results in a decreased cost effectiveness if it is assumed that cost effectiveness is proportional to the square of the burnout velocity. However, in the case of systems with unique requirements which over-ride performance and capitalize on the special characteristics of the paper phenolics, the material does show promise.

In support of the cost effectiveness studies, a study was made of present and potential production techniques and of possible improvements in strength and cost. The results were not encouraging.

The preliminary design of the M58A2 was expanded into a detailed design for a feasibility demonstration test. Considerable difficulty was encountered in the design of an adequate joint and in finding a reliable adhesive bond. After a series of four failures with several bonding techniques and two joint designs, a successful joint design and bonding technique were developed. The first unit of the new design was successfully proof-tested and subsequently satisfactorily hydroburst. Unfortunately, the second unit of this design failed in hydrotest because of a material flaw. Appropriate adjustments were made and the third case was successfully proof-tested. This case was then loaded with propellant, assembled into a motor and static tested.

The static test was a successful demonstration of the feasibility of using paper phenolic as a structural material for rocket motors. A noncatastrophic gas leak and resultant burnthrough occurred at approximately 70% of web burn time, but the leak

was due to a poor gas seal around the metal nozzle threads and it was in no way associated with the use of the paper phenolic. All major test objectives were accomplished and the test was considered successful.

The conclusions of this study are that paper phenolic laminates offer potential as a competitive structural material in systems insensitive to strength to weight ratios, particularly where the other unique characteristics of the paper phenolic offer specific advantages. The paper phenolics are not suitable for systems which are sensitive to inert parts mass fraction and volume.

SECTION III

A BASIS FOR STRUCTURAL ANALYSIS OF PAPER PHENOLIC PRESSURE VESSELS

SECTION III

A BASIS FOR STRUCTURAL ANALYSIS OF PAPER PHENOLIC PRESSURE VESSELS

1. INTRODUCTION

This section serves as a demonstration that the structural behavior of critical regions of paper phenolic pressure vessels is predictable through the use of suitably modified ordinary analytical techniques. To this end, data obtained in routine mechanical tests are employed, but with extended data evaluation to develop a more complete description of the material's stress: strain behavior.

Critical regions of the vessel are approximated as problems in thin shell analysis, with test data developed in terms of average stress and average strain; test data is expressed for each principal direction as average modulus (as a function of average strain) and average Poisson ratio. Experimental verification is obtained that in a biaxial stress field, the strain dependence of modulus in either principal direction is referred to the value of strain that would occur at that stress level in a uniaxial field. Finally, uniaxial data is extended analytically to describe the behavior of an element experiencing combined pure bending with axial tension.

At this point, discontinuity analysis of a test vessel becomes possible. The non-linearly anisotropic material comprising various elements of the vessel is first represented as an equivalent linearly elastic anisotropic material using secant modulus values appropriate to the applied average stress levels at a particular pressure. Then, geometry and modulus parameters are manipulated for each element to develop a representation as an element of an analytically equivalent imaginary isotropic material. From this point, further treatment is routine.

For the test vessel first treated analytically at the actual failure pressure, the maximum meridional stress was analytically determined to be 14,000 psi, resulting from combined axial and flexural tension. In tests of specimens in pure tension, strengths of 12,000 psi were observed. Testing in flexure characteristically results in higher apparent strength levels because of the statistical significance of flaw populations; the incidence of the "weakest link" of the material in precisely that region of the flexural element which experiences the greatest tensile stress is not very likely, while in the pure tensile element, the "weakest link" cannot be avoided. On this basis, agreement between the analytical prediction of stress level at ultimate pressure and experimental pure tensile strength level is reasonable, and serves as verification of the analytical technique.

2. GENERAL DESCRIPTION OF THE NATURE OF THE MATERIAL IN TUBULAR FORM

Phenolic resin-impregnated paper laminate is a highly complex material; a complete analytical description would require eighteen mechanical property parameters, other than strength values, for normal stress considerations alone. Shearing stress considerations introduce still further complexity. When convolute wrapped, the material exhibits three mutually perpendicular principal directions: the hoop and longitudinal directions of the tube, and the through-thickness direction radial to the tube. These directions will henceforth be designated by the subcripts θ, φ, and t, respectively. Behavior under normal tensile stresses may be described by three uniaxial elastic modulus values, E_θ, E_φ, and E_t, and by six uniaxial Poisson ratio values, $V_{\theta\varphi}$, $V_{\theta t}$, $V_{\varphi\theta}$, $V_{\varphi t}$, V_{te} and $V_{t\varphi}$.

Description of compressive stress fields requires nine additional uniaxial values, similarly defined. Further, the θ and φ direction uniaxial modulus values which have been measured in this program, and presumably also the t direction modulus, are non-linear, their magnitudes being dependent upon strain. A further perturbation resulting from the non-linearity of modulus is the determination of the appropriate strain dependence for biaxial or triaxial stress fields, taking into consideration all the conceivable combinations of tensile, compressive and flexural forces. In addition, there is the question of what constitutes a failure condition — does failure occur upon development of some critical value of stress or upon some critical strain? If the latter, what is the effect of biaxiality or triaxiality?

As measured in this program, the value of hoop direction uniaxial tensile modulus is about three times the corresponding longitudinal value through a comparable strain range, and is approximately an order of magnitude higher than the longitudinal compressive modulus at low strain values. Hoop tensile strength is between two and three times the longitudinal tensile strength. The material appears to be capable of substantially higher longitudinal tensile strain and somewhat higher longitudinal tensile stress in flexure than in tension.

When a tube with closed ends, initially unstressed, is subjected to internal pressure, the state of stress in an element of material distant from discontinuity at the closures is as follows: the stress in the radial or through-thickness direction is compressive, varying from a value equal to the internal pressure at the inner surface to zero at the outer surface; the hoop stress averaged across the thickness is twice the longitudinal stress similarly averaged. For geometry appropriate to the purposes of this program, the hoop and longitudinal tensile stresses are at least an order of magnitude larger than the through-thickness compressive stress. Consideration of the nature of the fiber-resin composite suggests that the through-thickness compressive modulus should be no larger than the longitudinal direction compressure

modulus. Accordingly, for the internally pressurized tube and for modulus values as described in the previous paragraph, hoop stresses and strains on the inner face will be larger than on the outer face; this characteristic is analagous to the thick cylinder, or gun-barrel effect.

In regions close to the tube closures, where geometric and elastic discontinuity exists, the requirement of continuity of deflected position along the structure gives rise to radial shearing forces and longitudinal bending moments in the tube wall. Because of the low longitudinal tensile strength of the material, failure occurs as the result of the combination of longitudinal tensile and flexural stresses at the discontinuity, without evidence of significant interaction between longitudinal tensile stress and shearing stress.

3. MATHEMATICAL MODELING OF PRESSURIZED TUBE ELEMENTS

Where structural strength is the major factor, capability to design effectively in a material such as paper phenolic can be obtained only through development of sufficiently rigorous analytical techniques and appropriate material property parameters to permit prediction of the behavior of a candidate configuration. A technique is sufficiently rigorous when its application leads to close yet conservative predictions of strength; it is excessively rigorous when its complexity requires that the analyst and experimenter deal with aspects of behavior of only tangential importance to the problem in order to obtain any answer at all. With regard only to paper phenolic pressure vessels, rigorous treatment of the thick cylinder effect in regions remote from discontinuities is important, but rigorous treatment of the discontinuity condition is indispensable. The best possible mathematical model would allow treatment of both conditions simultaneously. For linearly elastic materials, finite element, three-dimensional solutions are available (e.g., propellant grain stress analyses) but are extremely tedious and not well adapted to the present problem; on the other hand, computerized, rigorous closed-form solutions for thin shell element discontinuity problems are readily available through Thiokol routine vessel analysis procedures. Adaptation of the thick cylinder methods for the nonlinear anisotropic material would require years of effort, plus evaluation of all the normal stress elastic property parameters above defined, as well as the corresponding shear stress parameters; most of these later ones would be of minor importance. The approach was adapted therefore, to employ the thin shell alternative with evaluations of gross material property parameters (elastic modulus and Poisson's ratio values based on stress and strain averaged across the thickness). The thick cylinder effect was considered only as a correction factor for results determined for the thin cylinder model, to be used or neglected, wherever appropriate. The only substantial constraint resulting from such a procedure is that the material property parameters cannot be considered appropriate for a very great range of thicknesses, because certain of the material properties must be determined using geometries similar to those of the intended application.

In conjunction with the consideration of modeling techniques, it is necessary to consider a means to represent analytically the various uniaxial stress-strain curves. All these determined in the program have been non-linear, with continuously decreasing tangent modulus, through the entire strain range (Figure 1). Because it simplified the handling of the data, the secant modulus was adapted as the key parameter, and was evaluated in polynominal form in terms of strain. This modulus is the slope of a straight line, secant to the stress-strain curve, intersecting at the origin where $\sigma = o$, and $\epsilon = o$ and at any other point σ and ϵ. For non-linearly elastic material, of course, the secant modulus is a variable; expressions may be developed for its value as a function either of stress or strain, the latter of which is used hereafter. Thus, in general terms, for any particular value of the abscissa, the following relations are obtained (Figures 1 and 2).

$$E_{sec} = A + B\epsilon + C\epsilon^2 \text{ etc} \qquad (1\text{-a})$$

$$\sigma = \epsilon E_{sec} = A\epsilon + B\epsilon^2 + C\epsilon^3 \text{ etc} \qquad (1\text{-b})$$

$$E_{tan} = d\sigma/d\epsilon = A + 2B\epsilon + 3C\epsilon^2 \text{ etc} \qquad (1\text{-c})$$

The character of the data obtained in this program is such that the secant modulus is linear with strain (Figure 2-b), so that the first two terms of the polynomial are sufficient with B negative for positive strain.

In effect, through the use of the secant modulus, an element of non-linear material experiencing some particular uniaxial normal stress and strain is represented by an equivalent linear material which would, at the same stress level, experience the same strain. However, as Figure 2-a shows, upon application of an increment of stress $d\sigma$, the increment of strain $d\epsilon$ would occur according to the appropriate tangent modulus value, or alternatively, according to the secant modulus value appropriate to the new strain value, $\epsilon + d\epsilon$. Using only the polynomial for secant modulus, and a known applied stress, appropriate values of strain and modulus may be easily determined by solution of equation 1-b for strain, and substitution into equation 1-a or 1-c.

Still another matter appropriate to discussion of modeling techniques is the manner of representation of flexural effects in the longitudinal direction of the tube. Early in the program it was decided that there was little to be gained from testing longitudinal flexural specimens since the non-linear behavior of the material obviates the classical method of reducing flexure test data according to assumptions of straight line stress distribution across the section, and equal tensile and compressive modulus. Also, except as an indication of maximum strain capability in flexure, any such test results would be of questionable usefulness because of complications due to substantial shearing stresses in the classical test, substantial longitudinal tensile stresses in the

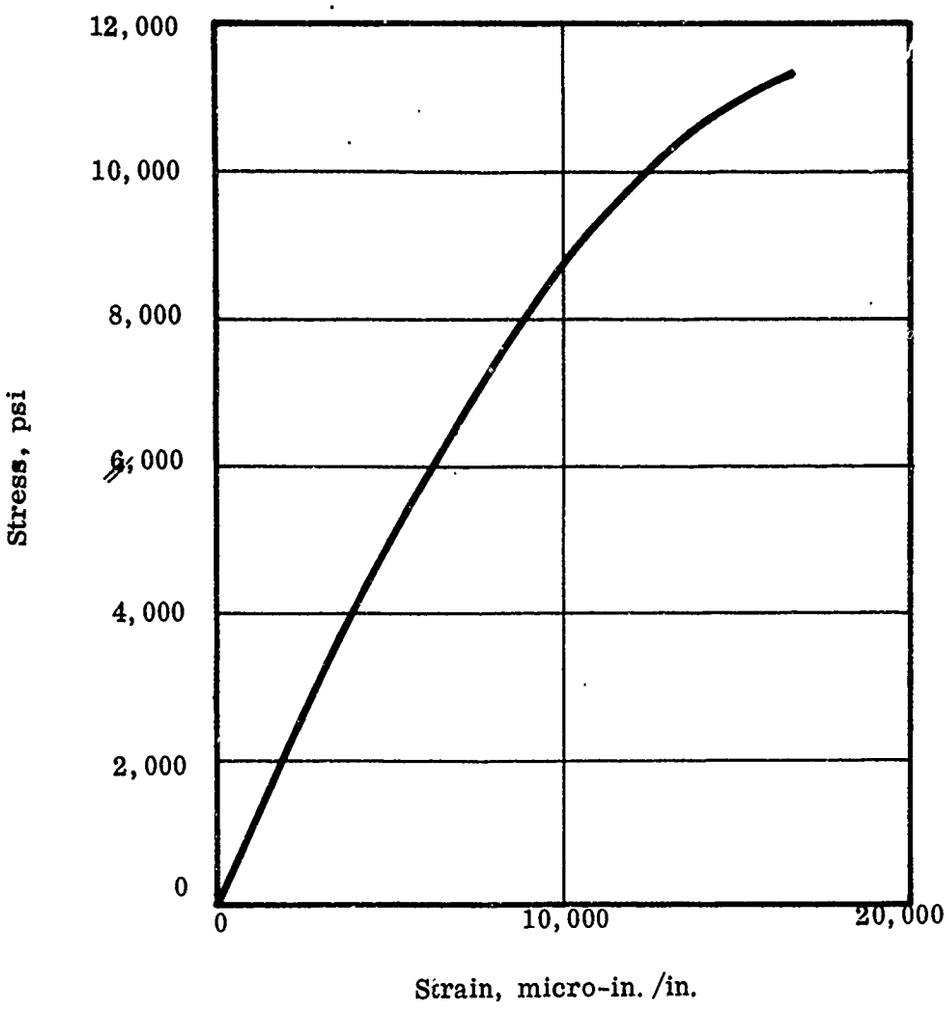


FIGURE 1. TYPICAL TENSILE STRESS-STRAIN RELATIONSHIP IN MERIDIAN DIRECTION

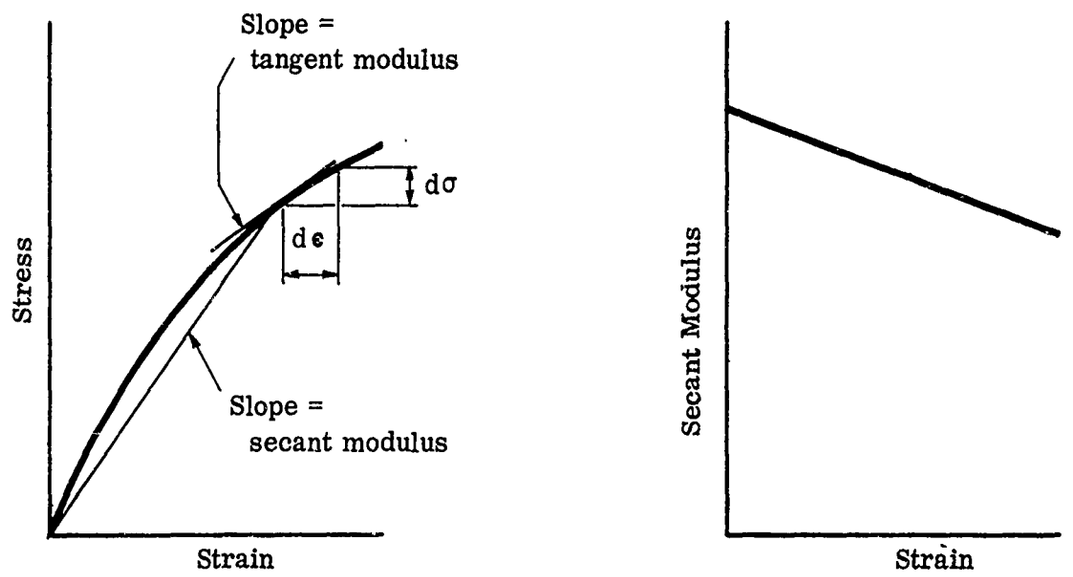


FIGURE 2. REPRESENTATIONS OF STRESS-STRAIN BEHAVIOR

intended pressure vessel application, and the problem of crosswise curvature in specimens cut longitudinally from tubes. Accordingly, analytical treatment based on tensile and compressive test data was adapted as the only real alternative, so long as verification of results could be obtained via later analysis of discontinuity effects in test vessels.

A beam analysis was established subject to the usual assumptions that only pure bending acts, and that the cross-section behaves as a bundle of fibers each independent of its neighbors except for continuity of elongations, for a cross-section experiencing an arbitrary strain at the extreme top and bottom fibers, and a linearly varying strain--not stress--in between. The stress for any fiber is given by the product of its strain and the appropriate value of secant modulus, tensile or compressive. Through integration across the section, expressions were obtained for the axial force and moment about the mid-thickness, in terms of the extreme fiber strains. Again making use of the figurative substitution of a linearly elastic material which would experience the same extreme fiber strains upon application of the same mid-thickness moment, an expression for flexural modulus was also obtained. The pertinent equations and their derivations are presented in Appendix II. Results of computer solution of the equations appear in later sections of this report as an expression of the analytical results of specific interest here.

It must be noted that since the effect of shearing stresses in the flexural element has been neglected, the flexural rigidity determined by this technique is greater than would occur in an actual element experiencing shearing stresses. If substantial overestimates of flexural rigidity were thus obtained, pressure vessel analyses using the high flexural rigidity would show higher than realistic values of flexural stresses. The assumption that shearing stresses in paper phenolic pressure vessels are not significant is reinforced by observation of the discontinuity failure mode in the test vessels. This, and the fact that the error is in the conservative direction, suggests that neglect of shear stresses at this stage is acceptable.

The final matter concerning modeling techniques is the manner of substituting a pressure vessel for the paper phenolic elements and comparable isotropic and linearly elastic elements so that available theoretical analyses and computer methods may be applied to the discontinuity problems. In previous paragraphs, use of secant modulus information has been interpreted as equivalent to substitution of an imaginary linearly elastic, anisotropic material for the actual material. The present technique is a further substitution of still another imaginary material. The key parameters which describe the behavior of isotropic, linearly elastic, cylindrical elements under axially symmetric loading, using the beam on elastic foundation method, are the longitudinal direction flexural rigidity, $\overline{D}$, and the foundation modulus, $\overline{k}$, descriptive of hoop stiffness:

$$\bar{D}_f = \frac{\bar{E}\,\bar{t}^3}{12\,(1-\nu^2)} = \frac{E_f\,t^3}{12\,(1-\nu^2)} \qquad (2)$$

$$\bar{k} = \frac{\bar{E}\quad\bar{t}}{R^2} = \frac{E_\theta\,t}{R^2} \qquad (3)$$

where the overbar indicates the equivalent isotropic linearly elastic material. Manipulation of these expressions yields values for the equivalent isotropic material as follows:

$$\bar{t} = t\,(E_f/E_\theta)^{1/2} \qquad (4)$$

$$\bar{E} = (E_\theta{}^3/E_f)^{1/2} \qquad (5)$$

Without further alternation, the above value of equivalent modulus is appropriate for E_f invariant with moment. The equivalent material represented as above will experience deformations corresponding to the secant modulus line in Figure 2-a. Further refinement may be obtained through use of the above representation for definition of the free radial deflection of a cylindrical element, together with another representation based on the tangent value of hoop modulus for definition of the smaller deflections caused by edge loads on a cylindrical element.

4. REPRESENTATIONS OF MATERIAL PROPERTIES FOR ANALYSIS

The various experimental techniques employed in the characterization of the material together with discussions of the basis for their use and limitations of the developed data are described in Appendix I. For the purpose of the pressure vessel discontinuity analyses conducted in this program at room temperature conditions, the material is described by the following parameters extracted from the data:

Longitudinal direction:

$$\begin{aligned} E_{\varphi\,\text{sec}}^{\text{tens}} &= 10^3 \times (1151. - \epsilon_\varphi \times 23875.)\ \text{psi} \\ \nu_{\varphi\theta} &= 0.178 \qquad (6) \\ E_{\varphi\,\text{sec}}^{\text{comp}} &= 10^3 \times (425. + \epsilon_\varphi \times 2689.)\ \text{psi} \end{aligned}$$

where ϵ_φ is positive when extensional.

Hoop direction:

$$E_{\theta_{sec}}^{tens} = 10^3 \times (3000. - \epsilon\theta \times 71667.) \text{ psi for } t = .070''$$

$$E_{\theta_{sec}}^{tens} = 10^3 \times (3430. - \epsilon\theta \times 92593.) \text{ psi for } t = .125'' \quad (7)$$

$$\nu_{\theta\varphi} = 0.367$$

Following the analytical procedure described above for flexural effects (see also Appendix II), and using the polynomial for longitudinal secant modulus, a large volume of data describing flexural effects has been developed through a special-purpose computer program. In the range of present interest, with combined axial tension and flexure such that uniaxial strains are extensional throughout the cross-section, this data is represented by the following expression:

Longitudinal direction flexural modulus·

$$E_f = 1192.65144 \times 10^3 = \frac{F}{T} \times 54.29694$$

$$-\frac{M}{T^2}\left(\frac{F}{T} \times 0.00801572 - 25.30865\right) \text{ psi} \quad (8)$$

The flexural modulus as analytically determined varies very little with moment so long as the axial force remains constant. This suggests that even though the material is quite non-linear in tension, it is, curiously, possible for a flexurally loaded section with constant axial tension to behave with a linear moment-deflection curve. (A similar effect for zero axial force would explain potentially deceptive behavior of flexural specimens).

5. CORRELATION OF ANALYTICAL STRENGTH PREDICTION WITH EXPERIMENTAL RESULTS

From the outset, an important program objective was to manufacture a vessel with burst strength close to, but in excess of, some analytically predicted value. As a basis for forming judgments in the prediction, a trial discontinuity analysis was conducted for one of the biaxial test vessels which had failed at a pressure of 916.6 psi with origin at the case-closure interface. The intent was to compare the analytically determined stress levels at the interface with uniaxial test data to

determine if they appeared reasonably related. The biaxial test vessel was a paper phenolic tube of 3.000-inch inside diameter and 0.070-inch wall thickness, fitted with aluminum closures in the form of a plate with an 0.161-inch thick skirt bonded to the outside face of the tube. (Figure 56). Strains at burst recorded at mid-length of the cylinder at orientations 180 degrees apart were:

	Point A	Point B
ϵ_θ inside	7992 "/" x 10^{-6}	7540 "/" x 10^{-6}
ϵ_θ outside	6385	6959
ϵ_φ inside	8572	9128
ϵ_φ outside	8497	8968
ϵ_θ mean	7188	7249
$\epsilon\varphi$ mean	8534.5	9048

Average hoop and longitudinal stresses σ_θ and σ_φ were 20,100 psi and 10,050 psi, respectively, as determined from statics.

Imposing the above value of hoop stress, as in equation (1-b), upon the expression for hoop secant modulus, equation (7), the uniaxial hoop strain, hoop secant modulus, and from equation (1-c), hoop tangent modulus are obtained. A similar operation produces the uniaxial longitudinal strain. Also, remembering that $F/T = \sigma_\varphi$, we obtain from equation (8) for trial values of M/T^2 of zero and 1,000, values for flexural modulus E_f. Thus,

$\epsilon_{\theta uniaxial} = 8375.8$ "/" x 10^{-6} $\quad \epsilon_{\theta uniaxial} = 11452$ "/" x 10^{-6}

$\epsilon_{\theta sec} = 2399.7 \times 10^3$ psi $\quad \epsilon_{\theta tan} = 1799.5 \times 10^3$ psi

$E_f = 647 \times 10^3$ psi for zero moment

$E_f = 591.7 \times 10^3$ psi for $M/T^2 = 1,000$

(The above strain values are consistent with the observed strains using values of Poisson's ratios $\nu_{\theta\varphi} = .35$ and $\nu_{\varphi\theta} = .10$, which are appropriate.)

Because the greater the longitudinal flexural rigidity, the greater will be the longitudinal bending moment at the discontinuity, we assume a high first value, $E_f = 635 \times 10^3$ psi, and determine, using equations (4) and (5) and the hoop secant modulus, that:

$$\bar{t} = 0.036008'' \quad \text{and} \quad \bar{E} = 4665.1 \times 10^3 \text{ psi}$$

These values are applicable for a first estimate of the free deflection of the cylindrical element and will result in over-estimates of edge load influence coefficients. Similarly, from the hoop tangent modulus, we obtain additional values of

$$\bar{t} = 0.041583'' \quad \text{and} \quad \bar{E} = 3029.2 \times 10^3 \text{ psi},$$

which are applicable to estimating the influence coefficients at the end of the cylindrical element. The final parameter for the equivalent material, Poisson's ratio, was taken as the square root of the product of the Poisson's ratios for the two directions.

Since the thickness of the closure skirt is so great in comparison with the portion of the paper tube bonded within it, and since the skirt modulus is also so much higher, the stiffness characteristics of the composite element -- skirt with internally-bonded paper tube -- was taken to be essentially the same as that of the aluminum tube alone. Accordingly, it is appropriate to arrange our structural model as in Figure 3 with the paper cylinder truncated at the beginning of the skirt, applying the moment due to eccentricity of longitudinal force at this point.

From here on, the thin shell analysis is quite routine up to the point of further modification of material property parameters for the equivalent material. Maximum bending moment in the paper phenolic is determined to be 6.6298 inch-lbs per circumferential inch, tension inside face, based on the first set of equivalent properties, or 5.8229 inch-lbs per circumferential inch, tension inside face, based on appropriate use of the two sets of equivalent properties. Radial deflection at the cylinder-skirt interface is 3.717×10^{-3} inches or 3.574×10^{-3} inches for the same two solutions, compared to a free deflection of the cylinder of 11.237×10^{-3} inches, showing that the actual hoop stress in the paper element near the interface is much lower than the PR/t value used in the initial determination of hoop modulus.

At this stage, it is possible to further subdivide the paper cylinder into short elements so that the properties may be varied according to the hoop stress and bending moment at any station as predicted in the first trial, thus by iteration developing the analysis to the point where the material property parameters, deflections, and bending moments are mutually consistent. A sufficient number of cycles were performed in the present instance to suggest that the above maximum moment values are not

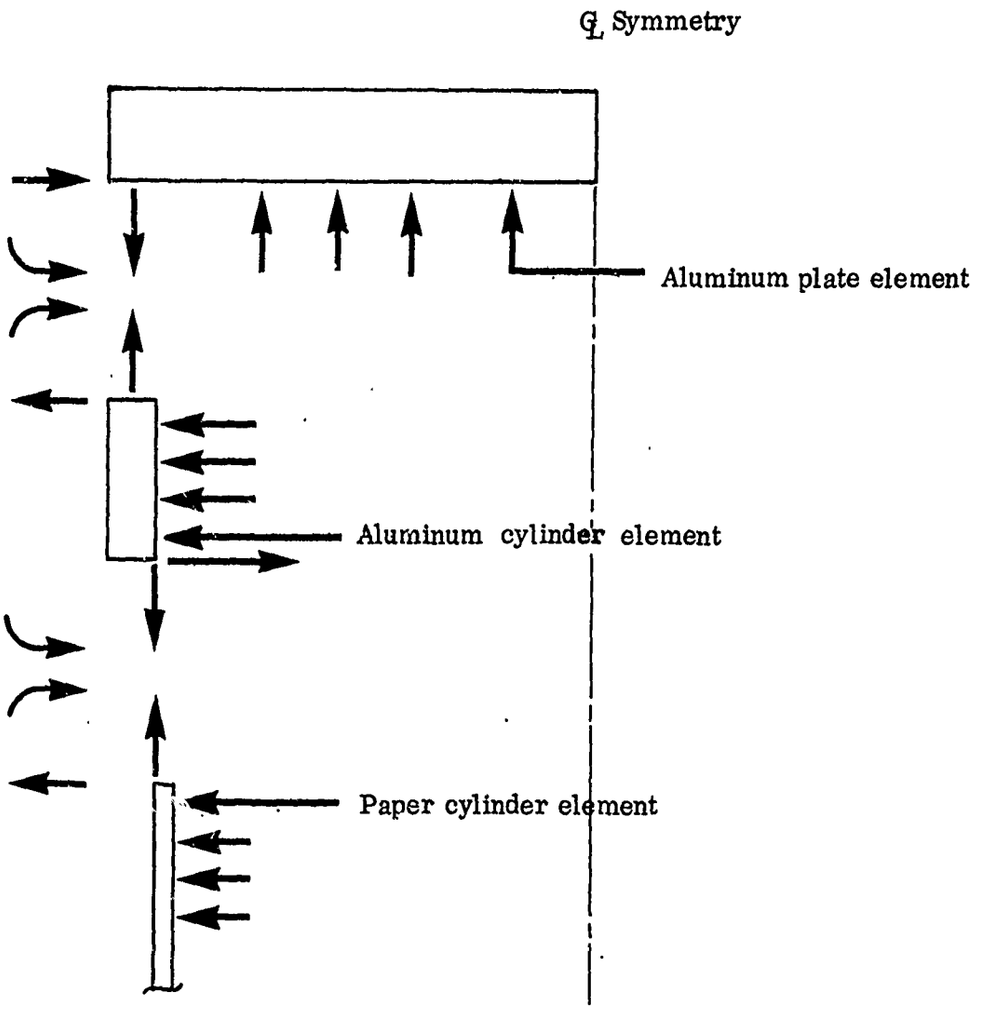


FIGURE 3. STRUCTURAL MODEL OF VESSEL

drastically affected by this iteration. Several trials using different values of Poisson's ratio were also conducted for the present vessel, without greatly changing the bending moment values.

The analytically determined moment corresponds to M/T^2 of 1188 inch-lbs/inch^2/ circumferential inch; F/T is 10,050 lbs/inch/circumferential inch. From the computer runs for flexural modulus, we may estimate final longitudinal tensile strains of about 25,000 μ"/" on the inside face and about 1000 μ"/" on the outside face at the discontinuity, corresponding to an extreme fiber tensile stress of about 14,000 psi on the inside face, assuming the longitudinal modulus polynomial to be valid for this high a strain. These values compare to average strains of about 15,000 μ"/" and average strengths of about 12,000 psi measured in longitudinal uniaxial tension. Though no simple flexure tests have been conducted in this program, manufacturer's data typically show apparent flexural tensile strengths greater than axial strengths by 50% or more. This data derives from the classical methods of treatment of flexure test results. More realistic treatment of flexural behavior as discussed in a previous section would show this to be actually a substantial increase in extreme fiber strain capability together with a moderate increase in extreme fiber stress capability over the values recorded in pure tension. Subject to this discussion, then, the predictions of the discontinuity analysis appear to be quite consistent with our understanding of the material strength parameters, and the failure condition appears to be stress-dependent rather than strain-dependent.

At this stage a design effort was undertaken with optimistic expectations of success, for two candidate vessel designs with 5.713-inch inside diameter, and wall thickness of approximately one-half inch. Analysis was pursued in a manner corresponding to the treatment of the 3.000-inch test vessel, but with greater complexity in the transition region due to more gradual transitions, which necessitated composite element treatment. The outcome of the effort was a pair of designs with cylinder thickness of 0.49 inch, which were expected to attain a burst pressure in excess of 3100 psi.

An unanticipated problem with the integrity of the adhesive bonds made it impossible to evaluate the behavior of the phenolic bond since bond failure occurred prematurely in every instance. This problem made it necessary to abandon the two candidate designs and a third interface configuration was established which offered the potential of eliminating the manufacturing difficulty. One such vessel attained a burst pressure of 3,200 psi, corresponding closely to the design objective.

In the final vessel configuration, discontinuity regions were of quite different character than in the two designs for which detailed discontinuity analyses were performed. Nevertheless, internal and external strains were recorded at the mid-length and adjacent to the closure. The internal strain readings at the closure however,

were of such character as to indicate apparent failure of the waterproofing. The record of mid-length gauges (Table XVI) indicates, as anticipated, that the thick-cylinder or gunbarrel effect was of greater significance in this vessel than in the thinner vessels previously tested. The average strains at this point are consistent with uniaxial values as predicted by the modulii of equations (4) and (5) using Poisson ratios $\nu_{\theta\varphi} = 0.399$ and $\nu_{\varphi\theta} = 0.066$, not far different from anticipated values. With these Poisson ratio values and the recorded total outer surface strains adjacent to the discontinuity, we can separate the portion due to Poisson effect from the portion due to stress in the same direction. The uniaxial longitudinal strain component is about 10,500 in./in., leading to a stress of about 9,900 psi. Since the total longitudinal force corresponds to only 8,000 psi average longitudinal stress, it is apparent that discontinuity bending moment at this point produced tension on the outer fiber. The location is sufficiently close to the failure origin to suggest that failure resulted from a condition not vastly different. Yet this longitudinal stress is lower than previously recorded strengths of the material.

A potential explanation develops from examination of some associated data from NOL rings cut from the same tube. Their average hoop strength, by hydrotest, seems to have been higher by about 10%, or 3,000 psi, than that of the bulk of previously tested material (Table XII). With fiber properties and resin properties unchanged, the only possible difference would be in fiber orientation. If we presume that enough more fibers were oriented in the hoop direction to increase the hoop strength by 3,000 psi, it would be reasonably consistent to expect a corresponding drop in the longitudinal strength. This is quite close to what has been observed.

These difficulties notwithstanding, verification of the analytical procedures described above is amply provided by first, a reasonable correlation between the analytical description and actual strength of the 3.000-inch biaxial test vessel, and second, by the vessel with 0.49-inch wall thickness which attained a burst pressure of 3,200 psi.

SECTION IV

MECHANICAL PROPERTIES OF PAPER PHENOLIC LAMINATES

SECTION IV

MECHANICAL PROPERTIES OF PAPER PHENOLIC LAMINATES

1. UNIAXIAL AND BIAXIAL TENSILE AND COMPRESSIVE PROPERTIES

Tensile and compressive data were determined in accordance with the procedures described in Appendix I and the results are presented in Figures 4-8 and Tables I and II.

a. Uniaxial Tensile Strength

The results of these tests are presented in Figures 4 and 5. Both figures are self-explanatory. The most interesting result is that the ultimate strength is only slightly affected by changes in temperature between -75° F and 77° F. At high temperatures the effect is very pronounced and the ultimate strength drops quite rapidly with any increase in temperature above 77° F.

No notable problems were encountered with the meridian tensile tests. This was not so with the hoop properties test method and specimen. It was our original intent to use the NOL Split Disc Method to evaluate hoop properties but early in the program it was discovered that an inherent deficiency of the Disc Method masks the actual behavior of this material and hoop tensile properties that are obtained with this test. The separation of the jaws of the split disc during the test introduced severe bending stresses in the ring of undetc.minable and erratic character, and resulted in premature flexural failure of the specimen rather than tensile failure. This failure mechanism was evide' ced by the form of the fracture in the specimens and by the output of strain gauges in the vicinity of the failure. The strain gauges indicated that the outer surface of the rings was compressed during the early stages of the tests and the fractures were at an acute angle to the extreme fibers of the ring. A true tensile failure, as was later demonstrated, will result in a fracture whose mean path is normal to the extreme fibers of the ring. This deficiency caused the rings to fail a! apparent hoop stresses about 20% below the actual hoop strength of the material.

It was apparent that a new technique had to be developed if we were to determine the hoop tensile properties of this material. There was one practical constraint on the design of this technique. Since all the specimens had been fabricated and a large number of them had been subjected to a rather expensive environmental conditioning program, the new technique would have to use the NOL ring. This requirement led to the development of the apparatus depicted in Figure 53 and described in Appendix I.

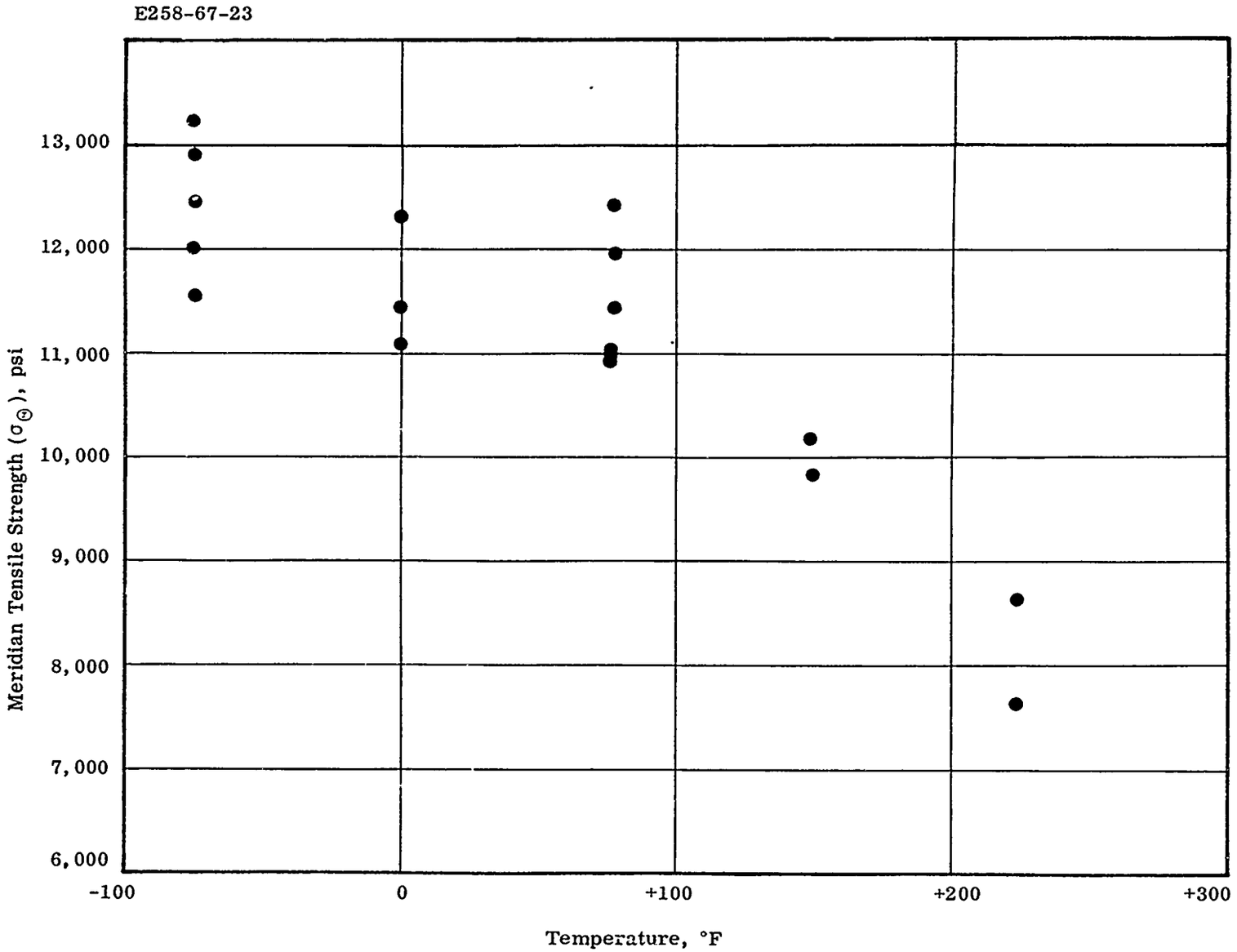


FIGURE 4. MERIDIAN TENSILE STRENGTH VERSUS TEMPERATURE

Results with the new apparatus have been quite successful but unfortunately the test is several times more expensive than the split-disc procedure. An occasional specimen has failed because of what appeared to be discontinuity stresses; it appeared that these resulted from localized radial restriction of the ring caused by a poor fit of the ring in the groove, various foreign particles lodged in the gap between the ring and groove walls, improper installation of the ring, or an abundance of the epoxy resin used to cover the strain gauges. All these can be attributed to operator error rather than a deficiency of the technique. At very low temperatures all these effects are exaggerated because of the increased modulus of the paper phenolic and, hence, experimental error increases with decreasing temperature. Even further accentuation of this effect can be attributed to the increased modulus of the O-ring. In fact, the O-ring became so stiff at -50° and lower that it is questionable whether it was transferring the load to the NOL ring in a uniform manner. Specimens which definitely appeared to have failed because of a discontinuity effect rather than simple hoop tension have been omitted from the data in this report. The mode of failure was verified by both visual inspection of the fracture and analysis of the strain data.

Figure 5 presents the hoop tensile strength of HY-488 versus temperature. The relationship is somewhat similar to that observed for the meridian tensile strength. Although the scatter is exceedingly large at -75° F, there was no justification for discarding either point. A third point, which failed at a far lower stress than either of these, was discarded because of the characteristics of the fracture.

Additional tests were performed to determine the effect of strain rate on the meridian tensile properties but no detectable effect could be determined, as shown in Table I.

b. Compressive Strength

The compression tests were quite straightforward with no noteworthy problems. Again, it appears that the elastic properties are not strain rate dependent, at least in the range investigated.

c. Analysis of the Results of Uniaxial and Biaxial Tensile and Compression Data

Figures 6 and 7 present plots of measured values of secant modulus in longitudinal uniaxial tensile and compression, respectively. These values were obtained from tube tensile specimens, from uniaxial compression tests reported last quarter, and from hydrotests of cylinders. Also shown in the figures are visual, linear approximations of the mean value through the entire strain range for tension and through the region of interest for compression.

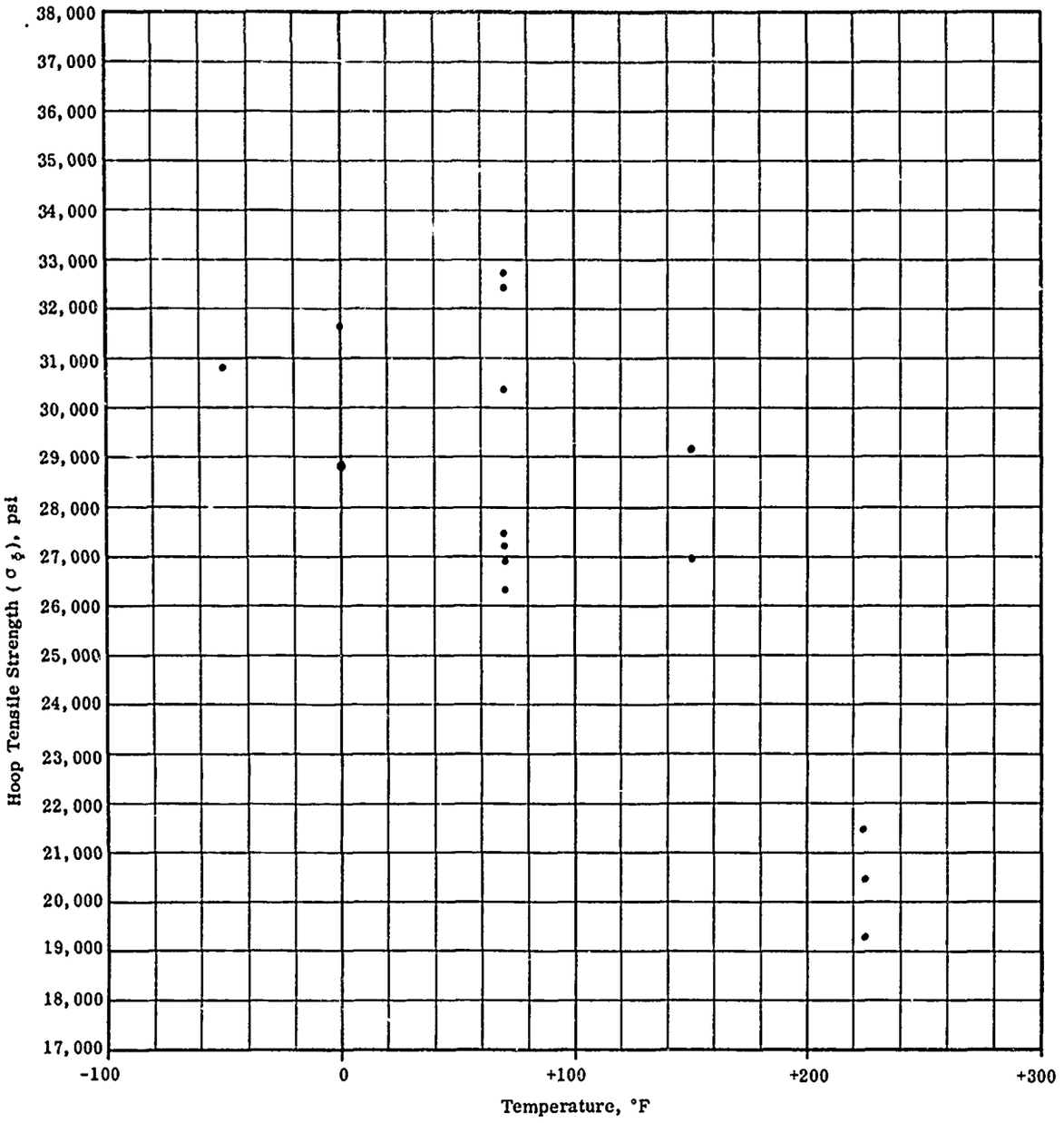


FIGURE 5. HOOP TENSILE STRENGTH VERSUS TEMPERATURE

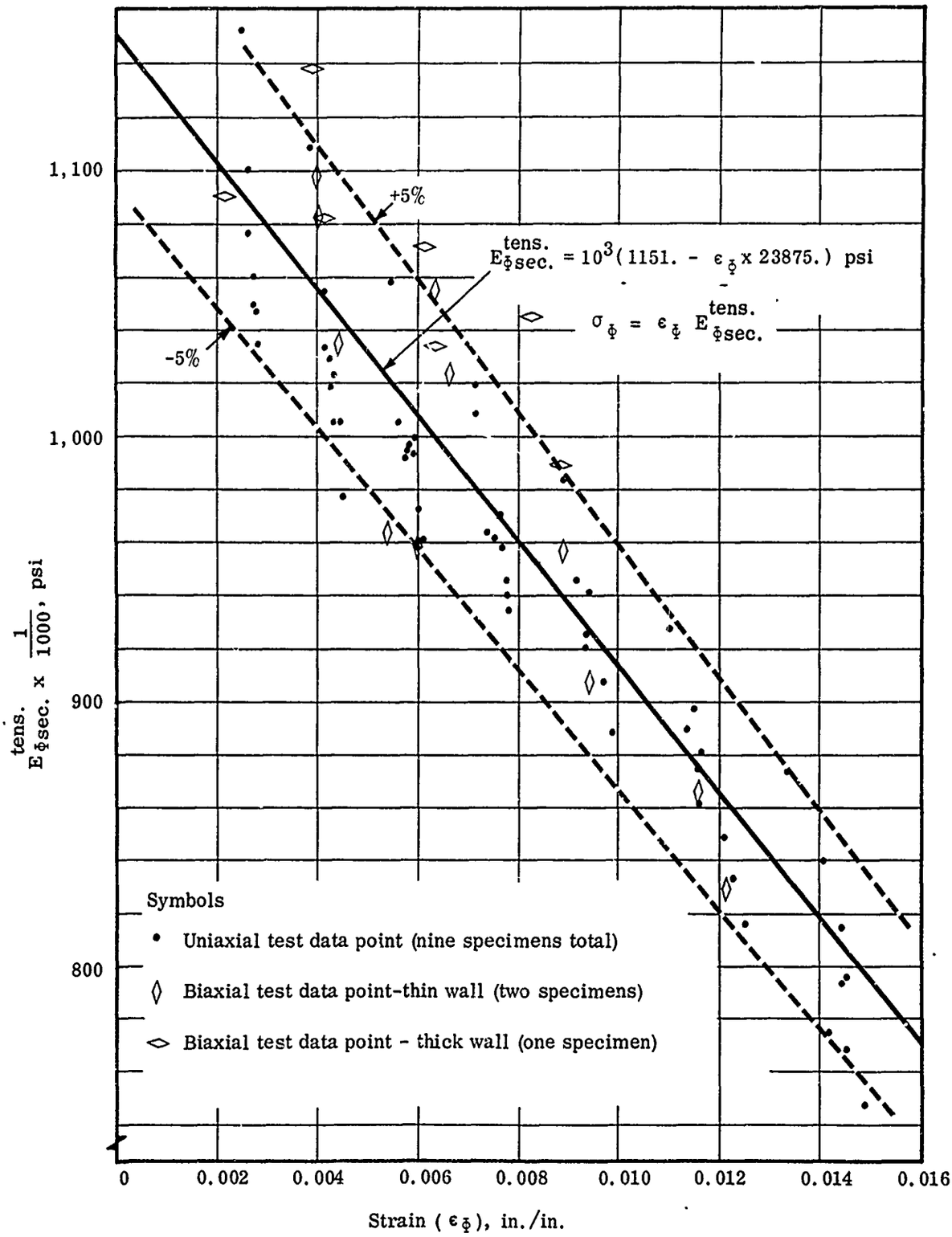


FIGURE 6. MERIDIAN TENSILE SECANT MODULUS VERSUS MERIDIAN UNIAXIAL TENSILE STRAIN AT 77°F

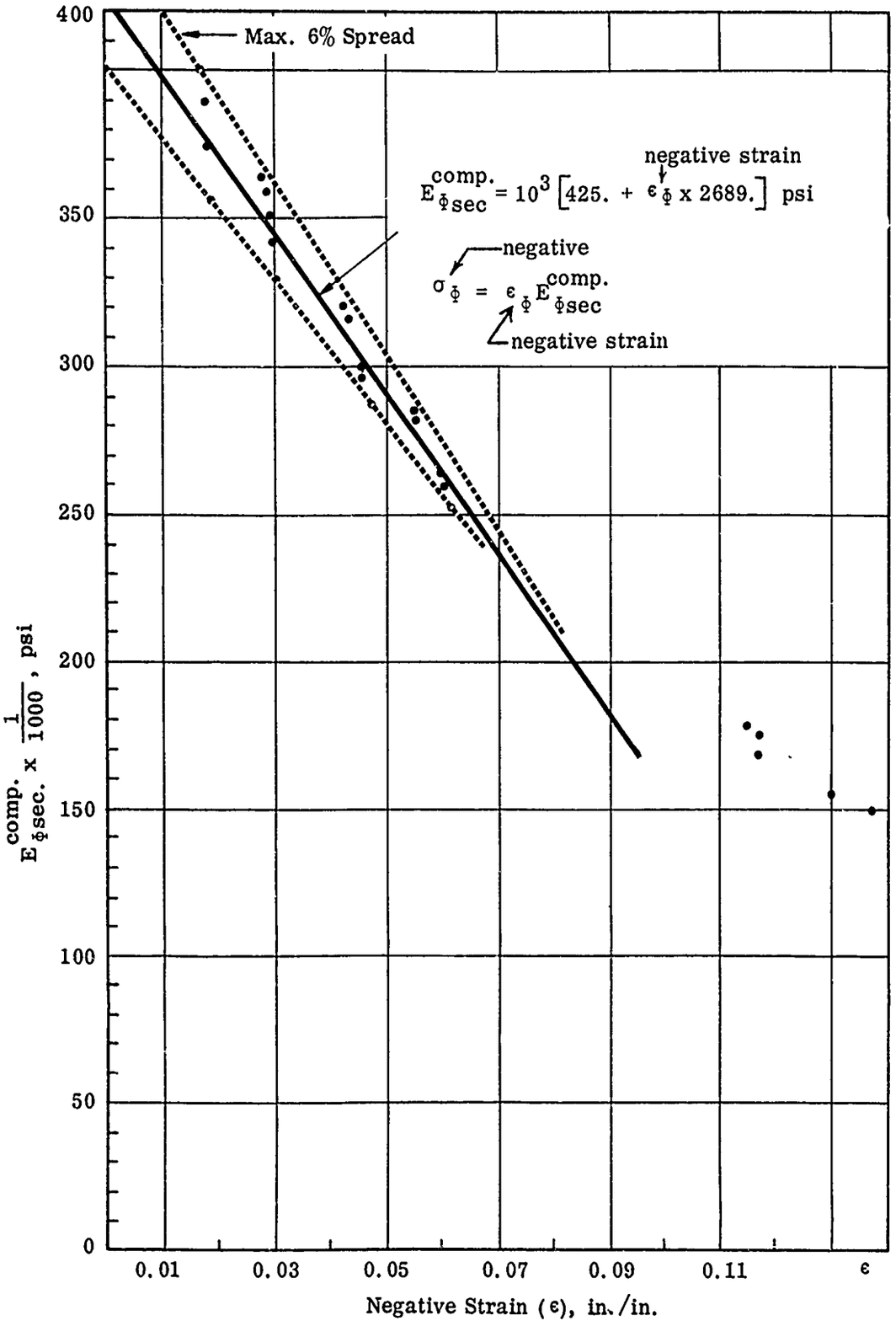


FIGURE 7. MERIDIAN COMPRESSIVE SECANT MODULUS VERSUS UNIAXIAL MERIDIAN COMPRESSIVE STRAIN AT 77°F (FIVE SPECIMENS)

TABLE I

TENSILE PROPERTIES OF TUBE SPECIMENS VERSUS STRAIN RATE

Strain Rate, in./Min	Ultimate Tensile Strength, psi
0.05	12,456
	10,930
	11,483
0.20	12,426
	12,442
	11,358
0.50	11,550
	11,850
	12,286

TABLE II

COMPRESSIVE PROPERTIES VERSUS STRAIN RATE

Strain Rate, in./min	Compressive Strength, psi	Failure Strain, %
0.02	23,347	16.50
	21,081	
	20,203	
	23,136	
	21,240	
0.05	20,000	17.02
	20,680	
	19,728	
	19,728	
	20,199	
0.10	20,270	17.84
	19,646	
	21,088	
	19,730	

Poisson's Ratio, $\nu_{\varphi\theta}$, was determined at several strain levels on each of five tube tensile specimens. The procedure followed is described in Appendix I. The average value obtained was 0.208; the maximum, 0.225, and the minimum, 0.167. We observed a decrease in Poisson's Ratio of from 2% to 15% with increasing stress. Since all our strain measurements were made on the outer fiber, this was possibly due to a combination of thick cylinder effects and a true variation of Poisson's Ratio with strain.

Figure 8 presents plots of secant modulus in hoop direction uniaxial tension, based on uniaxial hydrotests of cylinders and tests of NOL rings The values were computed by averaging the inside face and outside face hoop strains at each of two points for each cylinder and were determined for tests using two wall thicknesses. Note that for the thick cylinder, modulus values for very low strains appear too high. This evaluation results from a great disparity at low pressures between the actual thick cylinder behavior, as discussed under modeling techniques, and the thin cylinder treatment used in reduction of the data. It is of no great importance to strength predictions as long as it has disappeared at strains high enough to correspond to a failure condition. Our aim, after all, is to describe the situation at the failure pressure; we are not overly concerned with accurate stress-strain predictions at much lower pressures, as long as we can be assured that the failure condition corresponds to some sufficiently high pressure level. As with the longitudinal secant modulus, the data is quite well represented by straight lines. These cylinders also provided an evaluation of a Poisson's ratio, $\nu_{\varphi\theta}$, for longitudinal strains due to hoop stresses, since the cylinders experienced no normal force in the longitudinal direction. The determined value of $\nu_{\varphi\theta}$ was remarkably consistent beyond the point where the thick cylinder behavior washed out, even through the thick cylinder effect was persistent to higher pressures here than for the modulus determination. The test results are:

$$E^{\text{tens}}_{\theta\,\text{sec}} = (3.00 - 71.67\varepsilon_\theta)\ (10^6) \text{ for } T = 0.070 \text{ in.}$$

$$E^{\text{tens}}_{\theta\,\text{sec}} = (3.43 - 92.593\ \theta)\ (10^6) \text{ for } T = 1.26 \text{ in}$$

$$\nu_{\theta\varphi} = 0.367 \text{ average}$$

NOL rings were also used for obtaining the modulus. The data thus obtained appear to be slightly lower than tube data for the same thickness, even though the ring values are based only on outside face hoop strain values. Since inside face hoop strains must have been higher than the outside face values, the modulus values

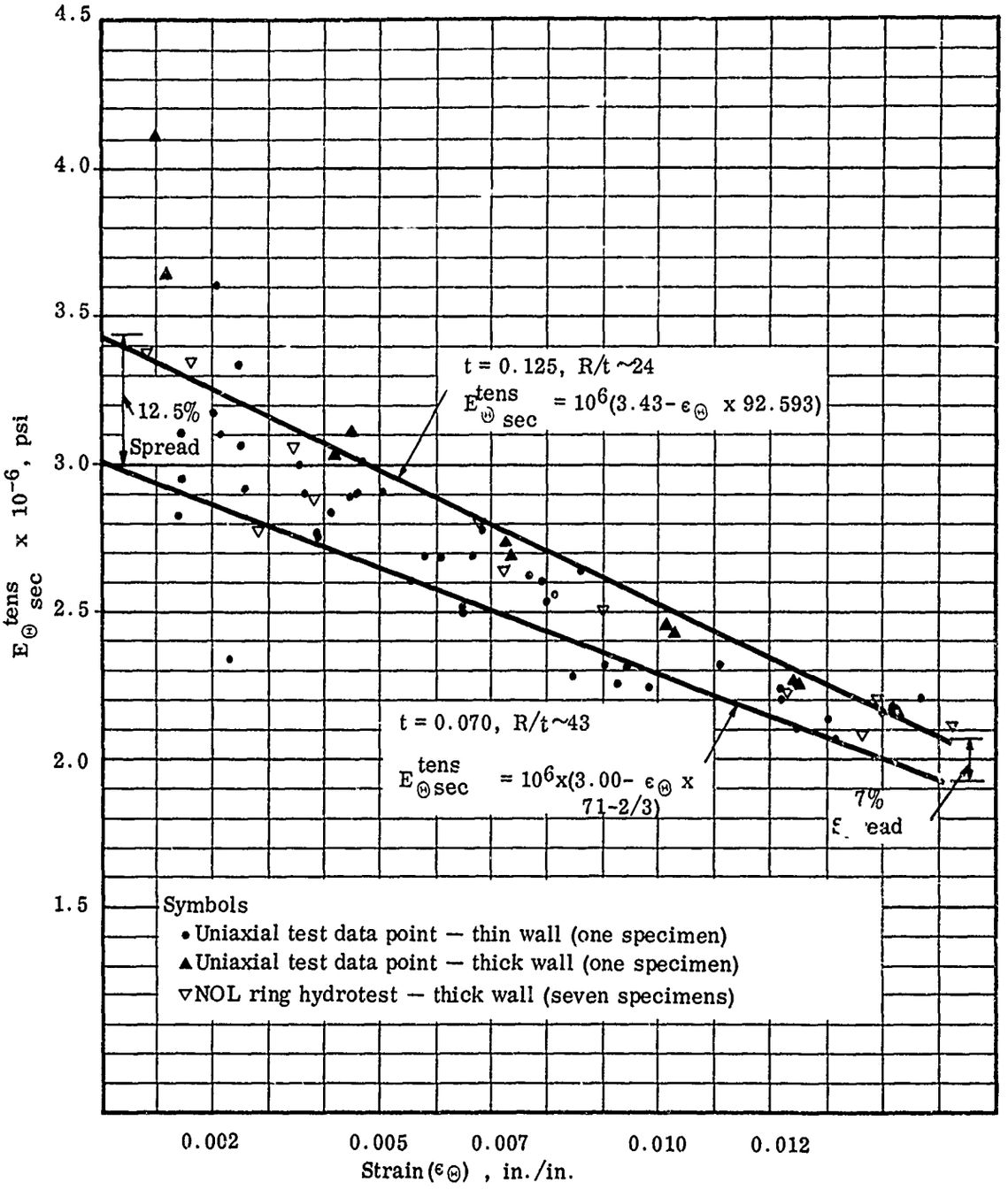


FIGURE 8. HOOP TENSILE SECANT MODULUS (ϵ_Θ sec) VERSUS HOOP TENSILE UNIAXIAL STRAIN AT 77° F

obtained for these rings should be slightly higher, i.e., the average strain should have been higher than the outside face strain. This is not borne out by the data. The difference must therefore be due either to variability in the material, or, as is more likely, to the distinction between the nearly plane stress condition in the ring and the plane strain condition in the tube. Under conditions of plane stress, longitudinal strain is not constant across the thickness and it follows that the thick cylinder effect would be less pronounced in the ring than in the tube, a point borne out qualitatively by the modulus values in Figure 6 at low values of strain. The extent of the thick cylinder effect is apparently dependent to comparable degree upon the low through-thickness modulus and the restraint offered by the plane strain condition It would be interesting to make comparisons with data which could be obtained through the use of a putty-like pressurizing medium in lieu of the fluid and O-ring combination used in this experiment. Such an extension would serve as the basis for definition of the character of the restraint which causes the plane strain condition.

Attempts were also made to measure the Poisson effect with the NOL ring. These efforts were uniformly unsuccessful in obtaining any rational results. A plane stress condition would explain the peculiar values obtained in these experiments.

The next series of tests consisted of pressurization of cylinders with full diameter bonded closures, so that known non-zero forces were applied in both the hoop and longitudinal directions. Based on the assumptions that the uniaxial hoop modulus, $E_{\theta sec}$, and Poisson's ratio $\nu_{\theta\phi}$, determined for cylinders without meridian loads would adequately describe the behavior in the biaxial field, independent determinations of the longitudinal modulus, $E_{\phi sec}$, and the Poisson effect, $\nu_{\phi\theta}$, for the biaxial field were obtained with the following equations (see Appendix II).

$$E_{\phi sec} = \frac{E_\theta \sigma_\phi}{E_\theta \epsilon_\phi + \nu_{\theta\phi} \sigma_\theta} \qquad (9)$$

$$\nu_{\phi\theta} = \frac{\sigma_\theta - E_\theta \epsilon_\theta}{E_\theta \epsilon_\phi + \nu_{\theta\phi} \sigma_\theta} \qquad (10)$$

The two stress components in the equations are actual mean normal stresses at pressure, as determined by geomerty and statics, and the two strain components are the means of measuring inside and outside face biaxial strains at the same pressure. The hoop modulus, however, is the secant value that would occur under uniaxial application of the same hoop stress, determined by solution of the appropriate polynominal of the form of Equation 1a. For the thin cylinders, a value of Poisson's ratio, $\nu_{\theta\phi}$, of 0.367 was used throughout, a value measured experimentally in the 1/16-inch wall cylinder. For the thick cylinder, however, higher values were used, comparable to the measured values at similar hoop stress levels in the uniaxial test.

A comparison was then made with the longitudinal modulus, $E_{\Phi sec}$ determined by uniaxial test, as follows. since the measured longitudinal strain in the biaxial field includes the effect of hoop stress. the measured longitudinal strain was increased by the product, $\nu_{\Theta\Phi} \times E_{\Theta}$ where E_{Θ} is the uniaxial hoop strain from the $E_{\Theta sec}$ polynominal solution. The resulting value of strain, when substituted into the polynominal for longitudinal modulus. $E_{\Phi sec}$ should give essentially the same modulus as was obtained in the previous paragraphs if all assumptions so far have been correct. Values thus obtained are plotted with the uniaxial values in Figure 7 and agreement is surprisingly close.

Not quite as good a comparison was obtained for the Poisson's ratio, $\nu_{\varphi\theta}$, value. This parameter seems to be quite an erratic one with measured values somewhere between zero and about 0.2 for pressure levels well beyond the point where the thick cylinder effect complicates the problem. The value of 0.208 obtained in the uniaxial test is at least in the range. Since the parameter can be shown to have only a minor effect on the most critical results of the discontinuity analysis, this kind of a comparison is probably sufficient.

It may thus be verified that the strain dependence of secant modulus for both hoop and longitudinal directions in a biaxial field is related to the particular value of strain that would occur in a uniaxial field with the same magnitude of stress. If may further be concluded that the value of 0.367 for $\nu_{\theta\varphi}$ is good after washout of thick cylinder behavior, that higher values are appropriate for the lower hoop stress range, and that $\nu_{\varphi\theta}$ has values between zero and 0.21, with evidence pointing to a valid value of 0.208.

2. EFFECT OF ENVIRONMENTAL CONDITIONING ON TENSILE PROPERTIES

Tests were performed on both Tube Tensile and NOL Ring specimens to determine the effects of temperature, humidity vacuum storage, thermal cycling, and salt spray on the mechanical properties of paper phenolic tubing. All investigations of the effect on meridian properties were performed with the Type A or Type B tensile specimens and using the standard test procedure Investigations of the effects of environment on hoop properties were performed by one of two techniques using the standard Type A and Type B, NOL ring specimens. All investigations of the effects of temperature on hoop properties were performed on the hydrostatic pressure apparatus described in Appendix I while the investigations of humidity, vacuum storage, thermal cycling, and salt spray on hoop properties were performed with the NOL Split Disc Apparatus. This diversity of procedures was an attempt to limit the cost of the tests as the hydrotest procedure is considerably more costly than the Split Disc procedure.

a. Effect of Temperature

The effect of temperature on the meridian tensile strength was discussed in Section IV-1 of this report. The effect on meridian tensile secant modulus is shown in Figure 9 to 12. As was the case with meridian tensile strength, the secant modulus does not appear to vary by any appreciable amount over the range of -75 to 77° F, but there is a marked decrease in modulus as the temperature rises above 77° F. No attempt has been made to fit a polynominal to the data at any of the temperature except 77° F. Both the paucity of data and the degree of scatter at the other temperatures would seem to make such an evaluation of questionable value.

Section IV-1 includes an analysis of the effect of temperature on hoop tensile strength and the results are shown in Figure 5. The data for hoop tensile secant modulus are presented in Figure 8, and 13 to 16. An almost unique dependence on temperature is noted here. In this case there was a distinct decrease in modulus with each increase in temperature, a result which does not seem to correlate with tensile strength tests, where no noticeable increase in strength was noted in going from 77 to 0° F. A possible explanation is a large normal spread of the measured parameter at a given temperature combined with a limited number of samples. As in the case of the meridian properties, no attempt was made to fit an equation to any of the data other than that at room temperature.

b. Effect of Humidity, Salt Spray, Vacuum Storage and Thermal Cycling

None of these environments had any effect on the meridian specimens that were coated with TA-D-311, and the uncoated specimens were affected by only the humidity and salt spray environments (Figure 17). This latter effect was serious enough to preclude consideration of uncoated material for any critical use in an operational environment.

As was noted earlier, the evaluation of the NOL Ring specimens was performed with the NOL Split Disc Apparatus. Although this apparatus was discredited as a means for determining tensile properties, it was hoped it would still be valid as a means of performing relative comparisons of environmental effect. This does not appear to be so, as evidenced by Figure 18. There is no apparent effect on the hoop properties as a result of the environments, a direct contradiction of the humidity and salt spray results with the meridian samples. We believe that this apparent lack of effect is again due to the flexural stresses induced by the NOL Split Disc. It is quite probable that the decrease in tensile strength to be expected in an uncoated specimen exposed to high humidity or salt spray would be accompanied by a compensating decrease in modulus; thus, flexural strength and apparent tensile strength would not change. Because of the complexity of the mode of failure, the NOL Split Disc Apparatus cannot be relied upon to provide even qualitative comparisons of the effect of

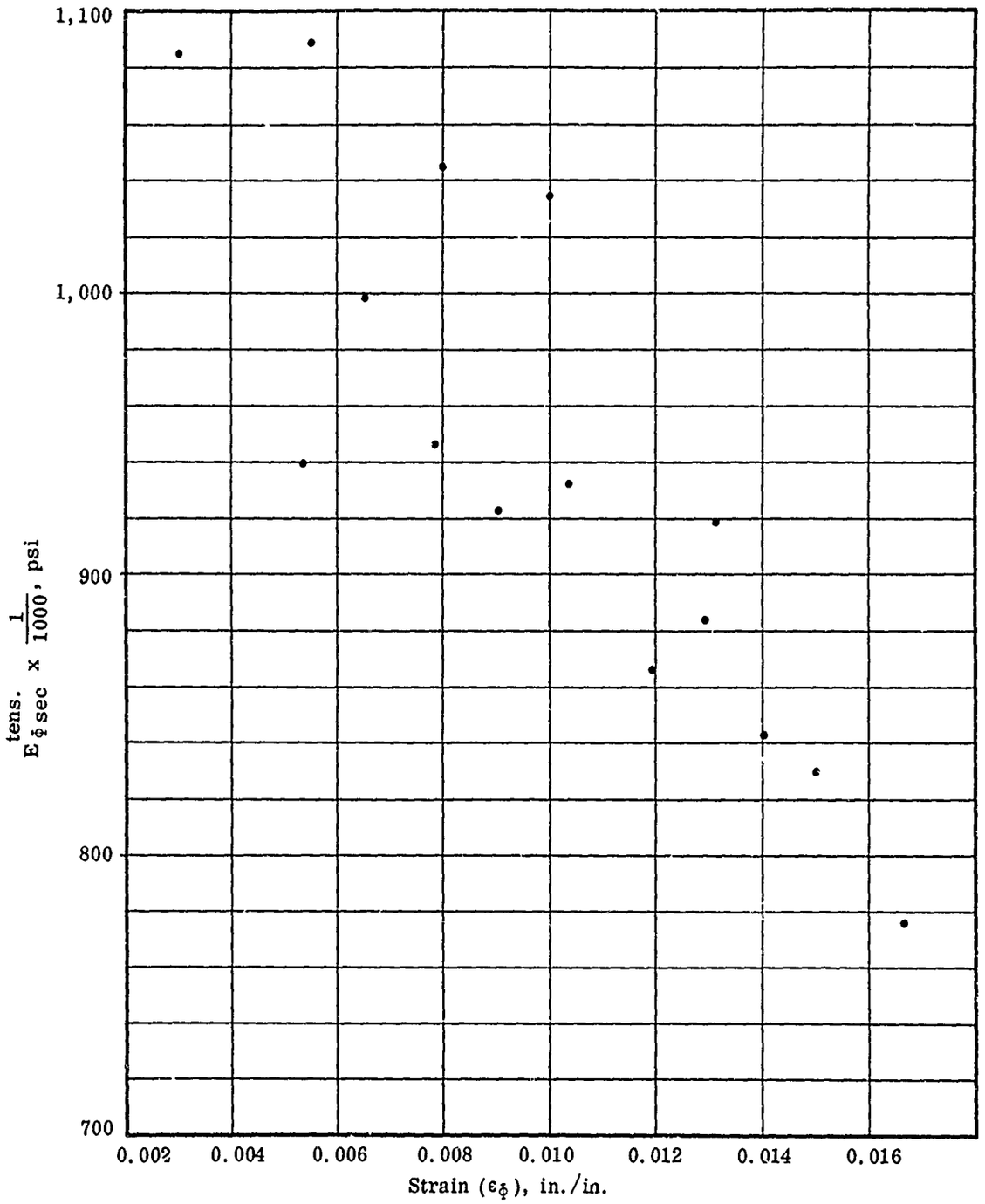


FIGURE 9. MERIDIAN TENSILE SECANT MODULUS ($E_{\phi sec}$) VERSUS UNIAXIAL MERIDIAN STRAIN AT -75°F

E258-67-13

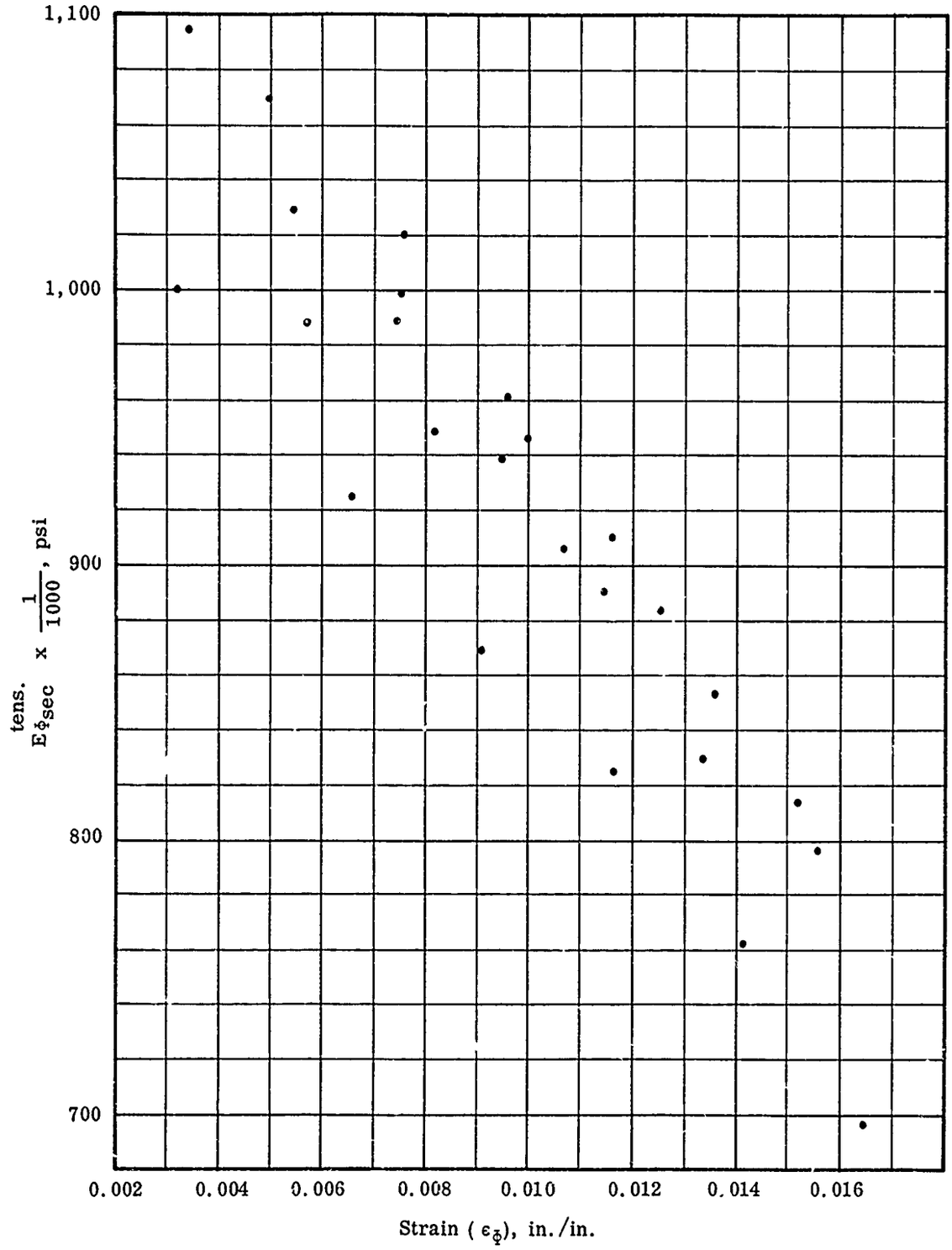


FIGURE 10. MERIDIAN TENSILE SECANT MODULUS ($E_{\phi\ sec}$) VERSUS UNIAXIAL MERIDIAN STRAIN AT 0°F

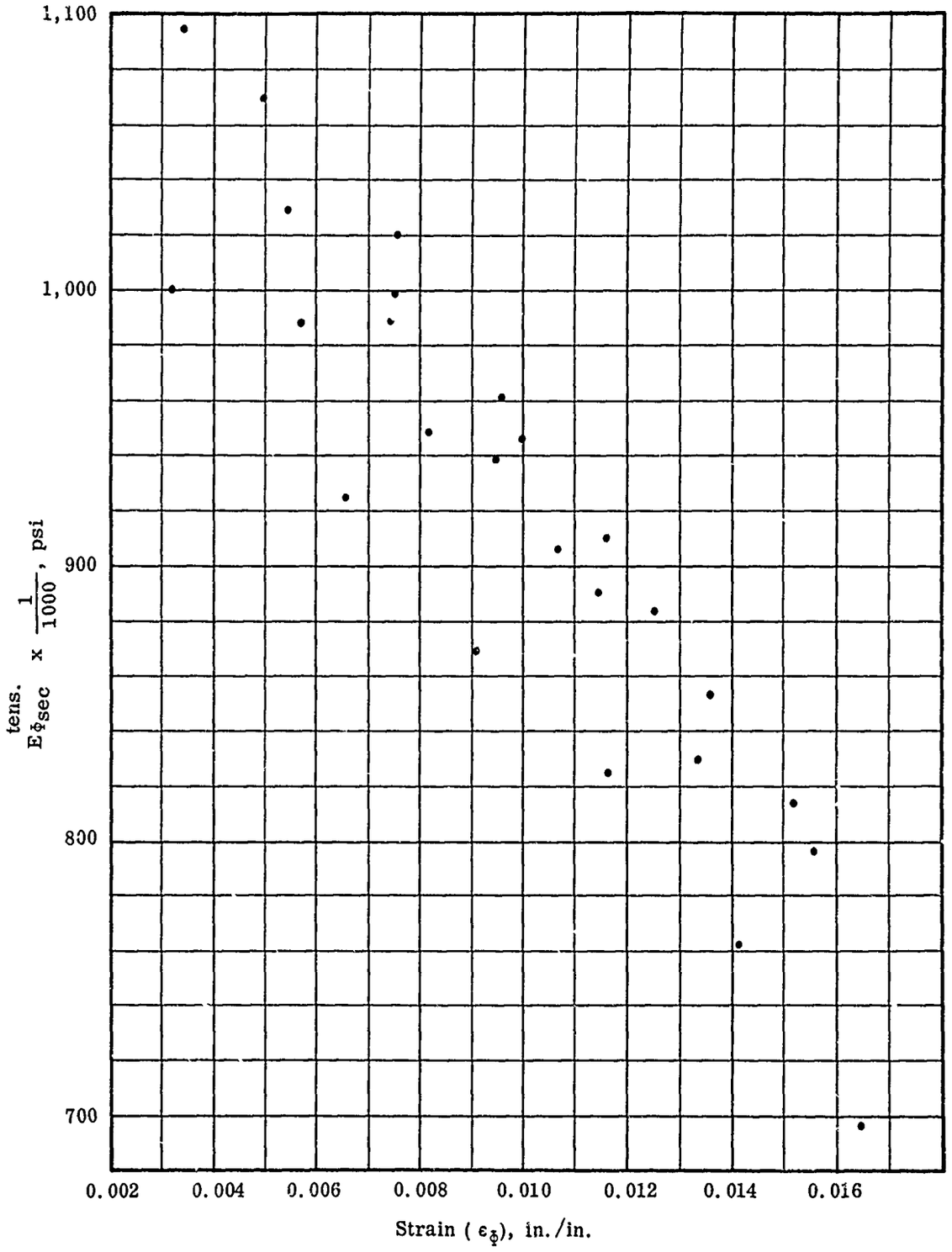


FIGURE 10. MERIDIAN TENSILE SECANT MODULUS ($E_{\Phi\ sec}$) VERSUS UNIAXIAL MERIDIAN STRAIN AT 0°F

E258-67-12

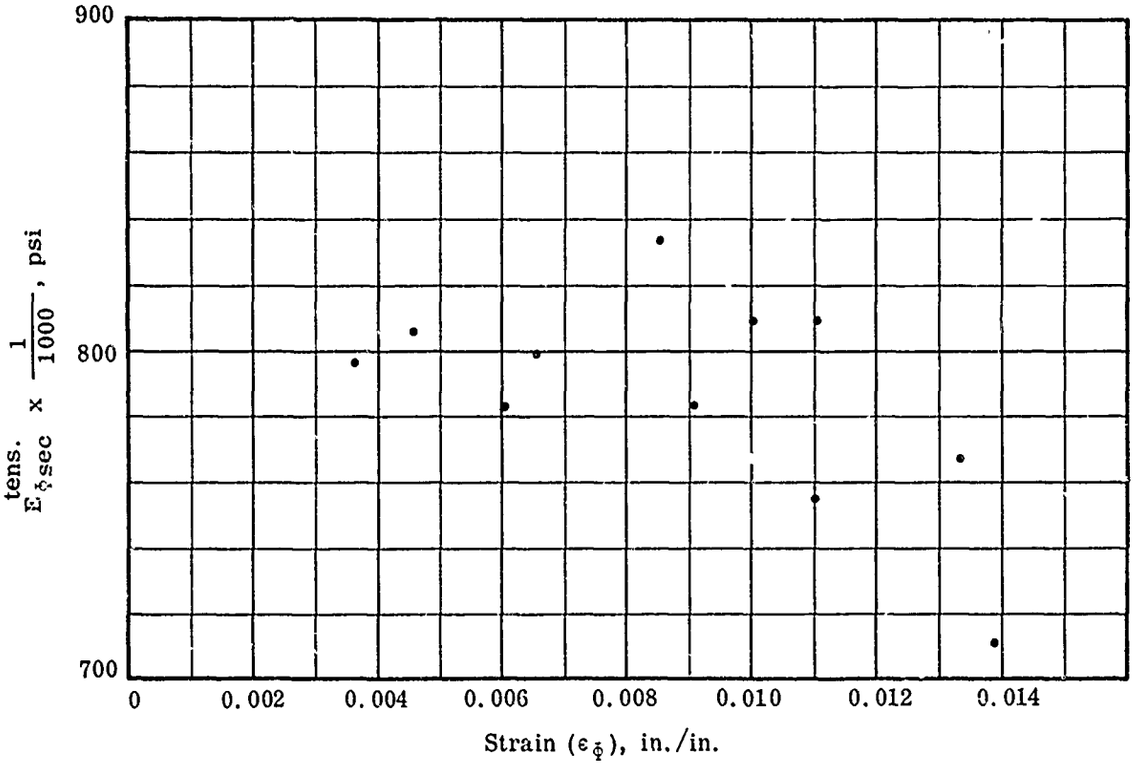


FIGURE 11. MERIDIAN TENSILE SECANT MODULUS ($E_{\phi sec}$) VERSUS UNIAXIAL MERIDIAN STRAIN AT 150° F

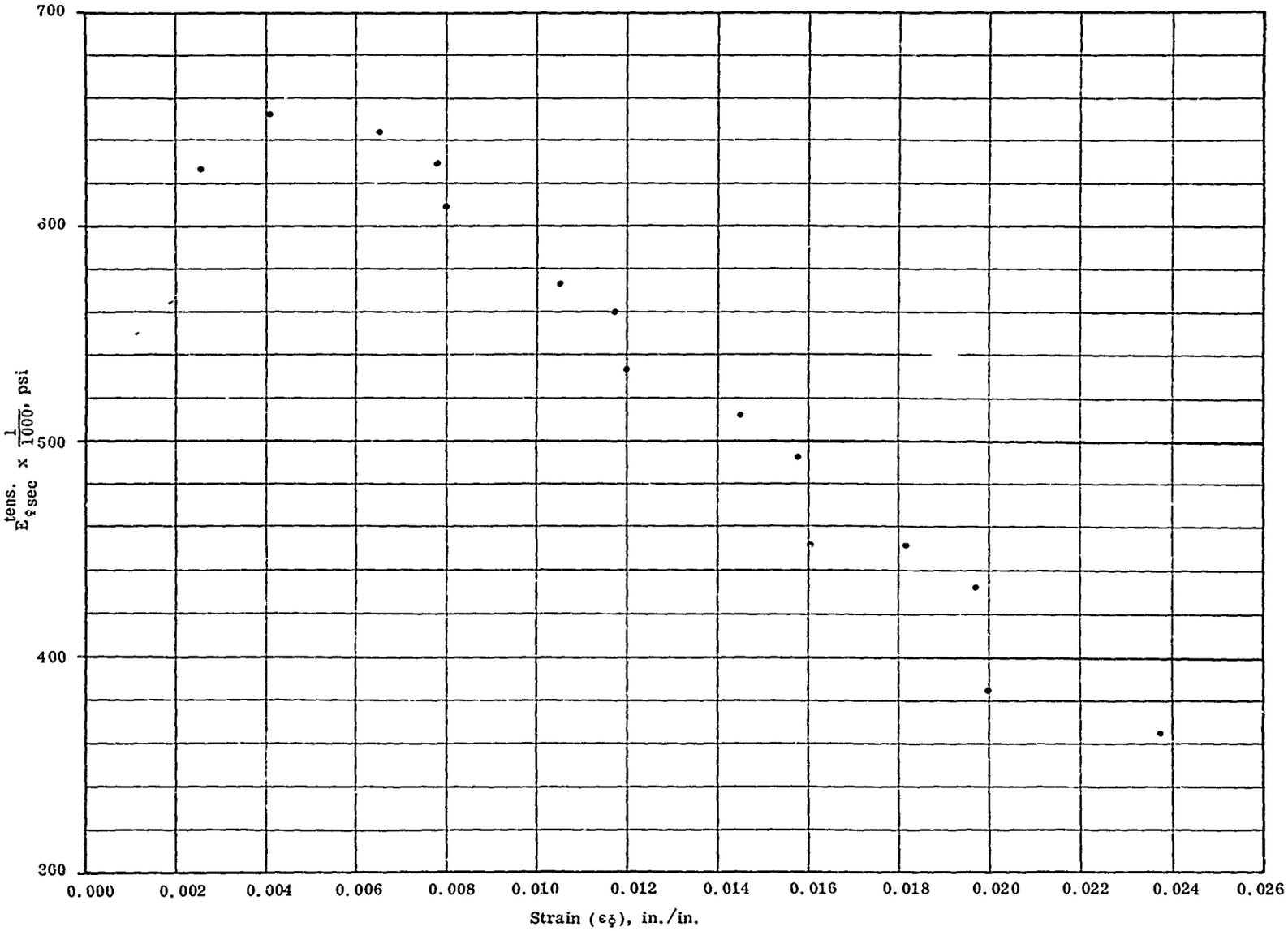


FIGURE 12. MERIDIAN TENSILE SECANT MODULUS ($E_{\xi sec}$) VERSUS UNIAXIAL MERIDIAN STRAIN AT 225°F

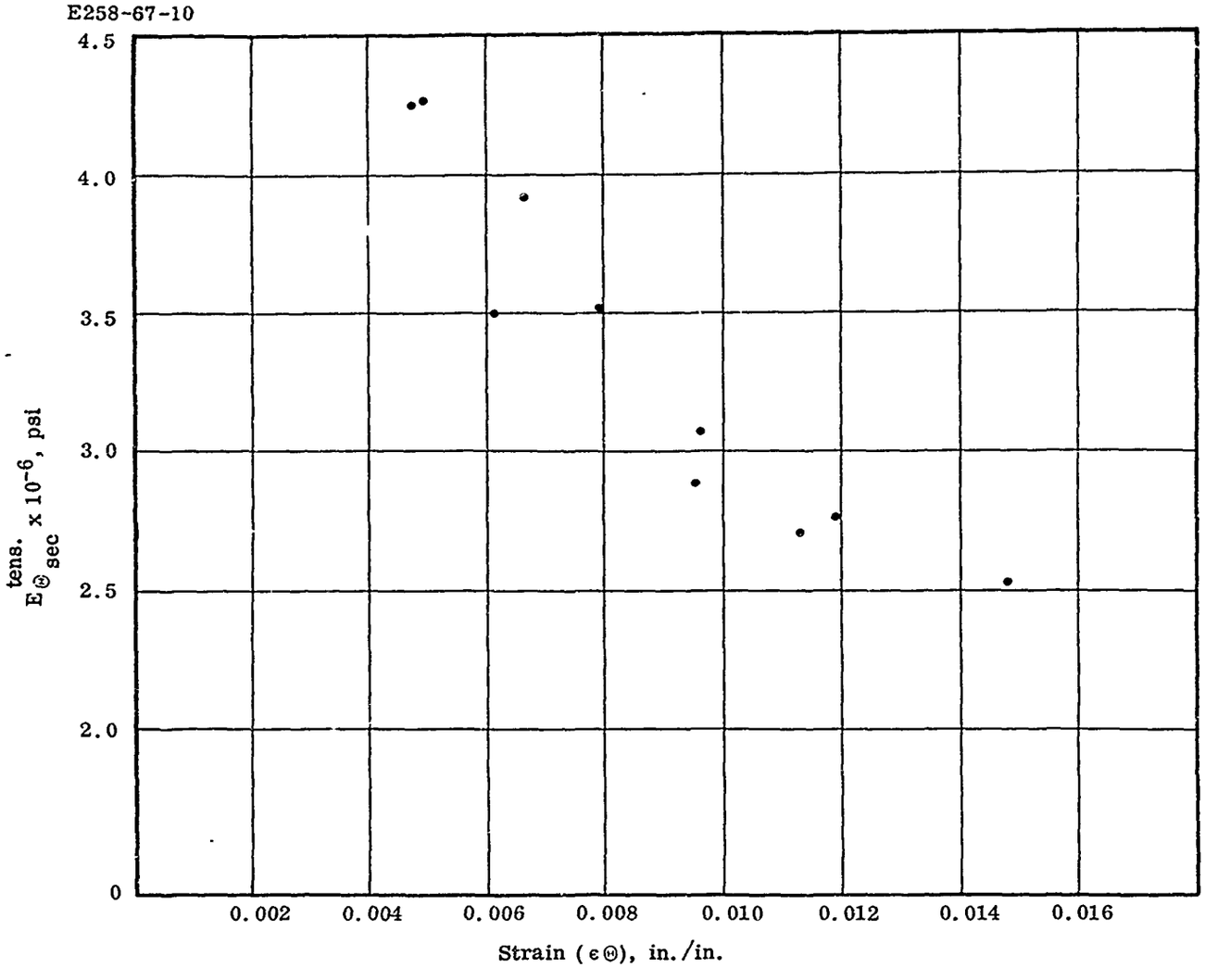


FIGURE 13. HOOP TENSILE SECANT MODULUS ($E_{\theta\,sec}$) VERSUS UNIAXIAL STRAIN AT -75°F

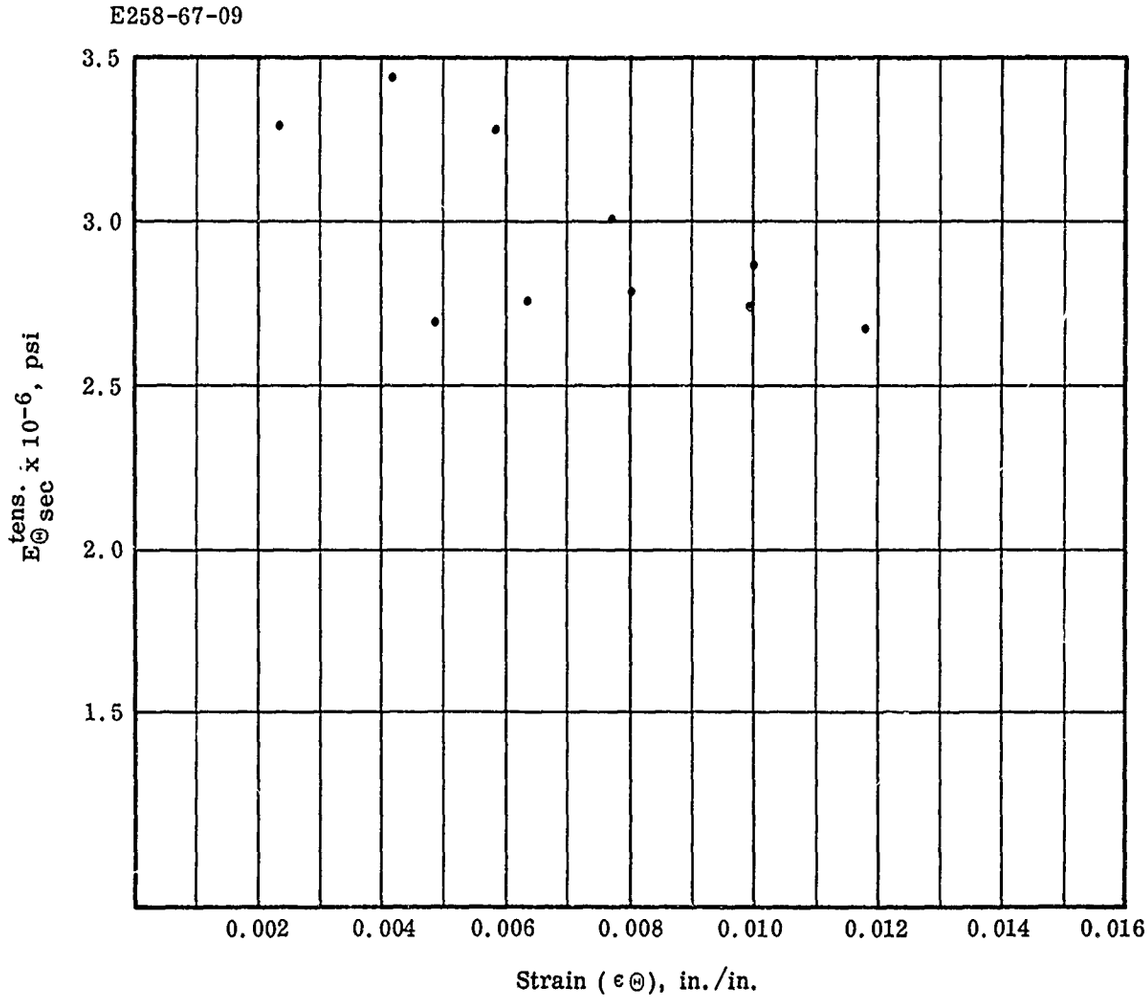


FIGURE 14. HOOP TENSILE SECANT MODULUS ($E_{\Theta\,sec}$) VERSUS UNIAXIAL STRAIN AT 0°F

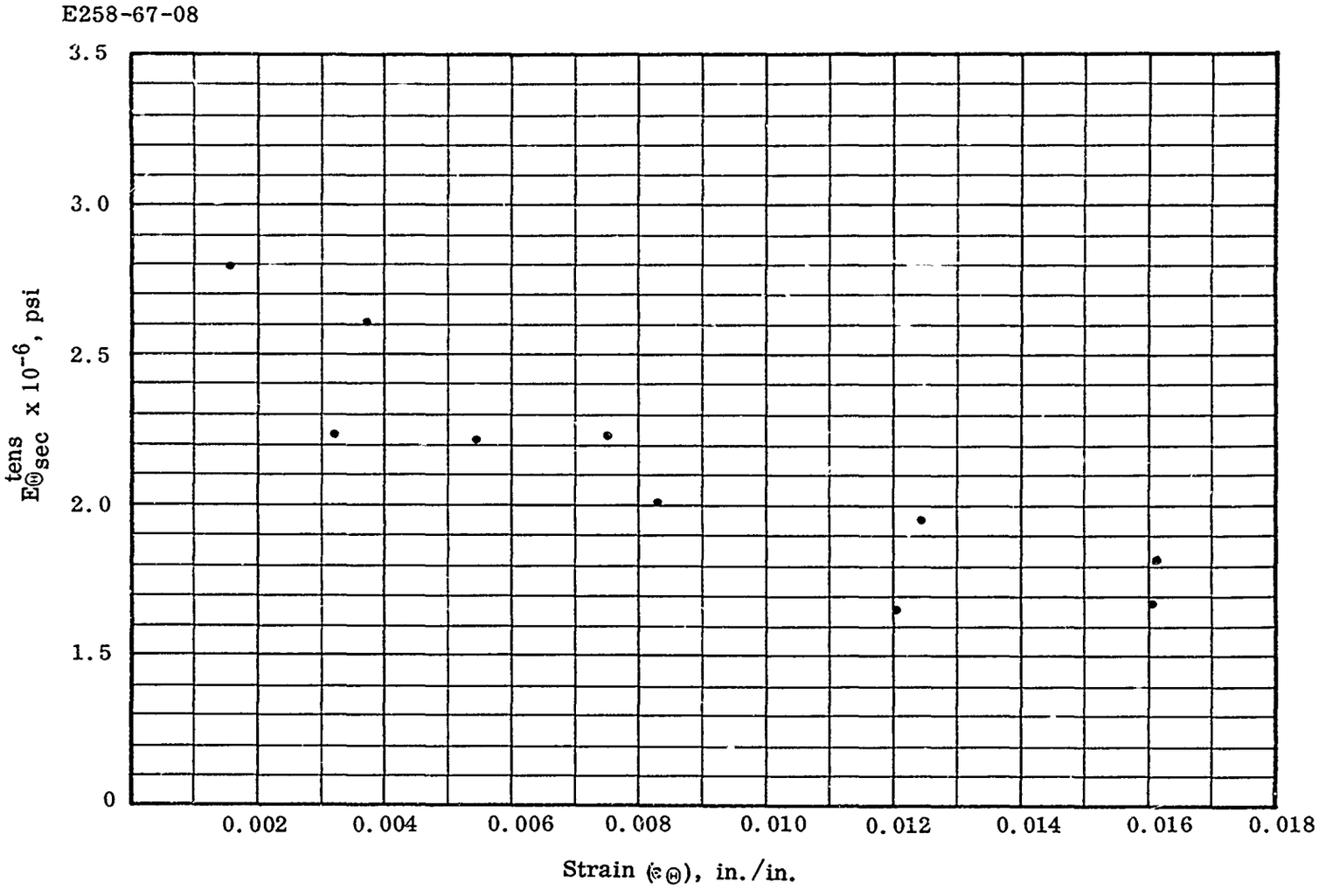


FIGURE 15. HOOP TENSILE SECANT MODULUS ($E_{\Theta sec}$) VERSUS UNIAXIAL STRAIN AT 150°F

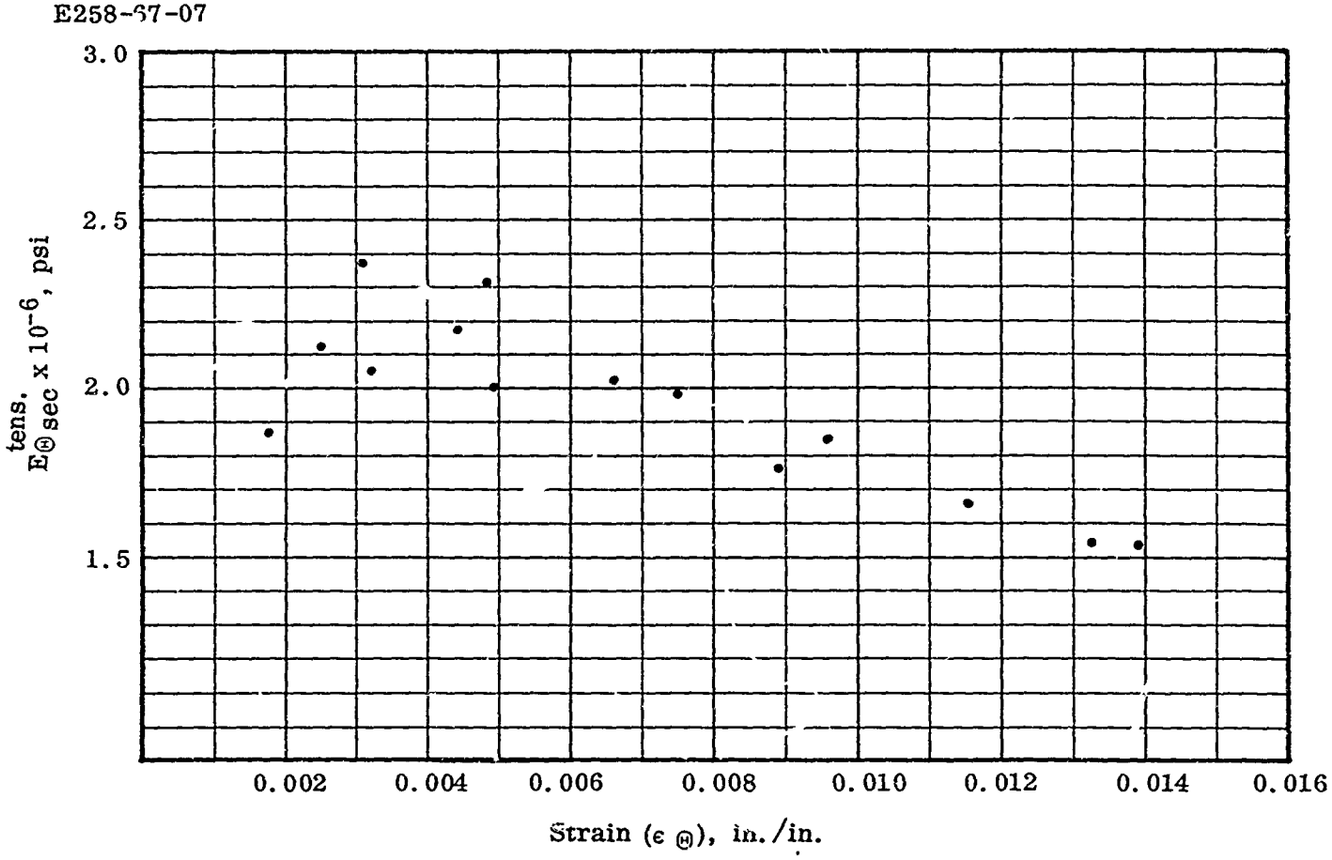


FIGURE 16. HOOP TENSILE SECANT MODULUS ($E_{@\,sec}$) VERSUS UNIAXIAL STRAIN AT 225°F

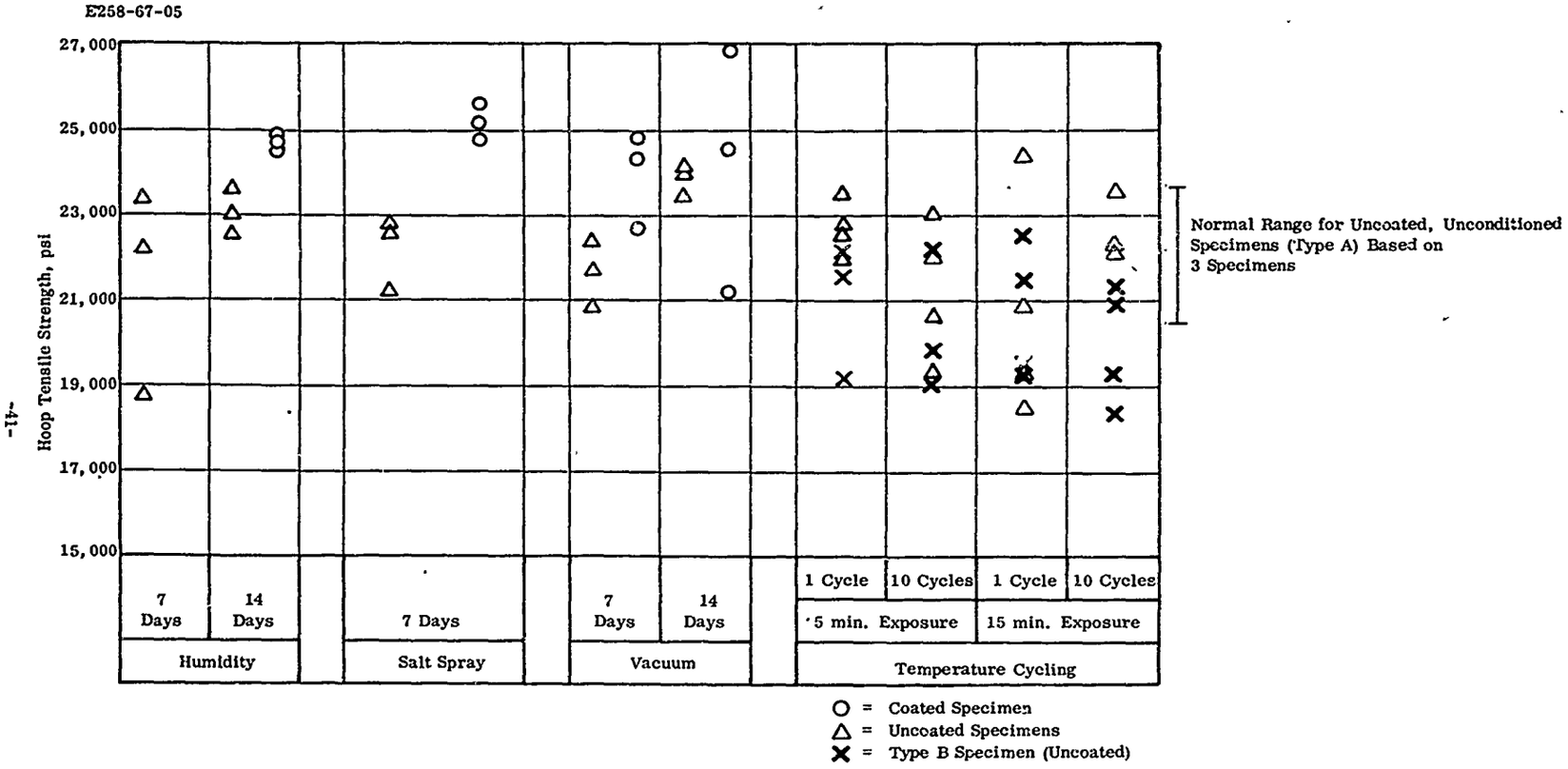


FIGURE 18. EFFECT OF HUMIDITY, SALT SPRAY, VACUUM STORAGE, AND THERMAL CYCLING ON HOOP TENSILE PROPERTIES

environment. All judgments on the effect of environment are therefore based on the tube tensile tests.

Meridian tensile strength was definitely degraded by both humidity and salt spray. The degree of degradation, however, is not as severe as would be assumed by a direct comparison of coated and uncoated specimens. A comparison of the range of strengths measured for unconditioned coated and uncoated tubes indicates that coated tubes are apparently 5 to 10 percent stronger. Since the stresses in both types of specimens were based on the uncoated dimensions, a simple analysis shows that this apparent increase in strength can be accounted for by considering the reinforcement due to the 0.005-inch coating of TA-D-311. When this is considered, the decrease in strength due to salt spray and humidity is still significant but the other environments are seen to have no effect on the meridian tensile properties of the Type A specimen.

The Type B specimen appears to be quite definitely degraded by thermal cycling. This specimen has the same outer diameter as the Type A specimen, but about twice the wall thickness. The cylinder has a very thick wall. In such a vessel thermal strains would be severe due to the low ratio of surface area to volume. In fact, producers of the tubing will not manufacture tubes of greater wall thickness than this in this diameter because of thermal stress problems during the cure cycle. During cycle, circumferential cracks are produced in the walls as a result of the severe thermal gradient across the wall. It is apparent that we have selected a specimen geometry that exaggerates the effects of thermal cycling. The results of the tests are in no sense derogatory, a rocket motor case would never approach the ratio of wall to diameter that we have in either the Type A or Type B specimen. Since the Type A specimen was not affected by temperature cycling, we would not expect any problems in a motor case. An interesting facet of the data was that the degradation seemed to be independent of the number of cycles.

3. INTERLAMINAR SHEAR STRENGTH

Two techniques were used for determining the interlaminar shear strength as described in Appendix A. In one technique a concentric tube was punched from a tube specimen and in the second a scored NOL ring was sheared in the hoop direction. As would be expected, the NOL Ring Shear Specimen had the same defects as the NOL Ring Tensile Specimen and the results obtained with this specimen were discarded.

The results obtained with the tube specimen are shown in Figure 19 and are most notable for the pronounced scatter at each temperature. The probable explanation for this is concerned with the nature of the material. Any tube of paper phenolic will undoubtedly have many small delaminations. Since the dimensions of the area in shear are small in our test specimens, the presence of one or more of these delaminations

E258-67-03

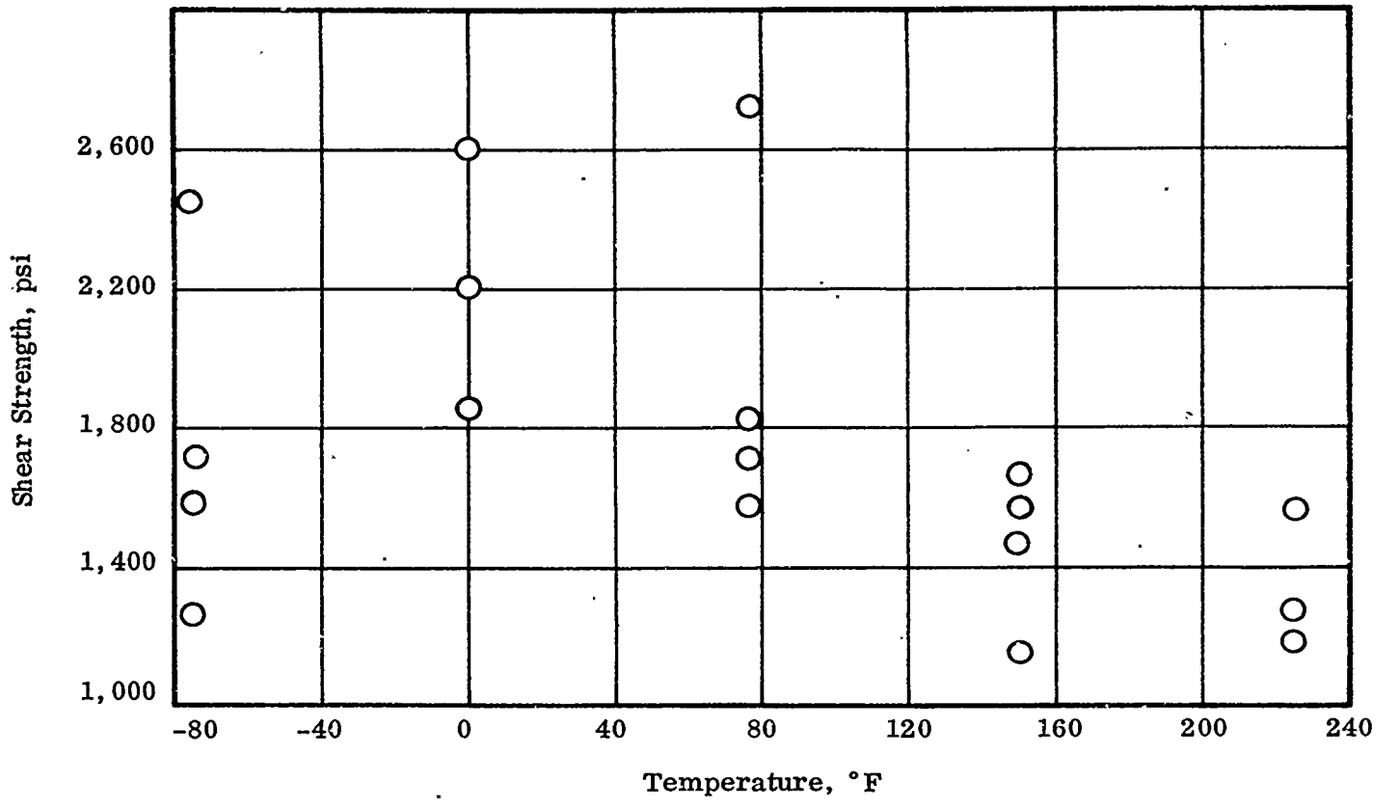


FIGURE 19. INTERLAMINAR SHEAR STRENGTH VERSUS TEMPERATURE FOR TUBE SPECIMENS OF HY-488

could have a major effect on the apparent shear strength of the material. The temperature dependence is probably overshadowed by this scatter.

It would probably be possible to achieve higher, more consistent values of the interlaminar shear strength if we used specimens with a much larger shear area and thus minimized the effect of delamination and other imperfections in the interlaminar bond. However, we feel that the values obtained by our specimens are realistic for use as conservative design strengths.

4. EFFECT OF CYCLIC LOADING ON TENSILE PROPERTIES

A total of five longitudinal pure tensile tests with zero to full load to zero cyclic loading were undertaken to establish a suitable maximum stress level for proof testing. In this sequence, the objective was to determine a level of stress or strain which would not significantly interfere with the material's strength or stiffness in further cycles of loading. In the tests for uniaxial longitudinal pure tensile strength, failures occurred characteristically at strains between 1.4% and 1.5%. The first cyclic test was accordingly pulled to a strain of 1.4%. Failure occurred in the fourth cycle (Figure 20). The remaining four samples were pulled to a strain of 1.2%. One of these failed at the peak of the seventh cycle, and three endured ten cycles each without failure. One of these three was then pulled to failure at 12, 000 psi, a value characteristic of the virgin samples. For both strain levels, load-deflection curves in the various cycles are not significantly different. Each curve is characteristically non-linear on the rising-load side, and nearly linear on the unloading side, with very small residual strain upon unloading.

The data supports the conclusion that for a longitudinal element to be designed for two or three cycles of pure tensile loading at or below some datum load level, a reasonable basis would employ a maximum strain of 1.2% corresponding to 10, 440 psi stress in comparison to a one-cycle failure strain of 1.5% approximately, corresponding to a one-cycle failure stress of 12, 000 psi. Assuming that a similar condition would obtain for flexural tension in a biaxial field, a reasonable design for a pressure vessel would employ a design safety factor not less than 1.15 on extreme fiber stress at proof pressure.

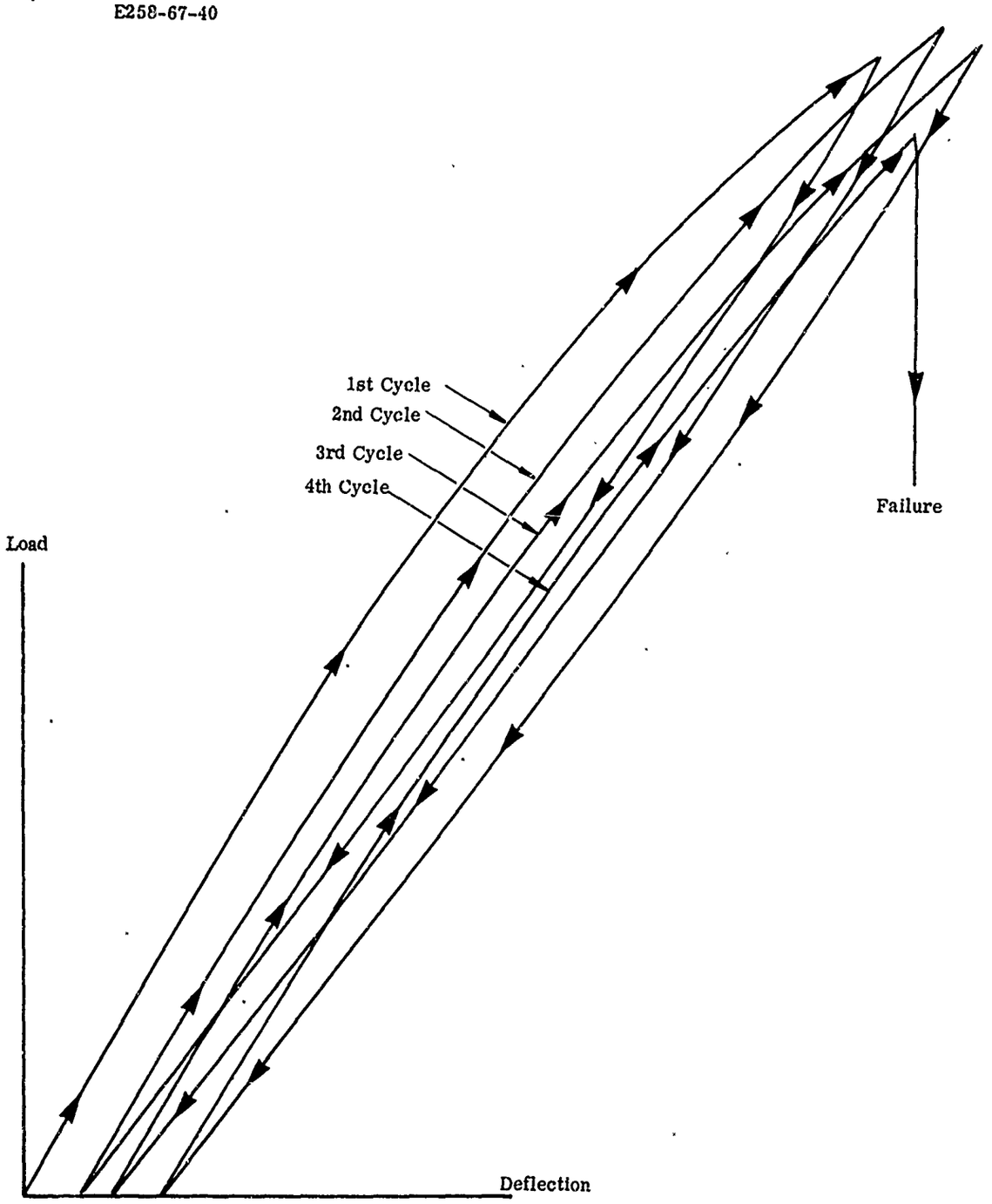


FIGURE 20. LOAD-DEFLECTION CURVE FOR
LONGITUDINAL SPECIMEN CYCLED TO 1.4% PURE TENSILE STRAIN.
FAILURE OCCURRED NEAR END OF 4TH CYCLE

SECTION V

THERMAL AND MASS PROPERTIES

SECTION V

THERMAL AND MASS PROPERTIES

The thermal and mass properties are given below. All determinations were made in accordance with the procedures described in Appendix I.

TABLE III

THERMAL & MASS PROPERTIES OF MICARTA HY-488

Property		Number of Specimens Tested	Value
Density at 23°F		3	1.316 gms/cc. 1.316 gms/cc. 1.315 gms/cc.
Specific Heat (-75°F to 200°F)		3	0.311 cal/gm/°c 0.335 cal/gm/°c 0.371 cal/gm/°c
Thermal Expansion*			
With Grain		2	1.55×10^{-5} in/in/°F
Across Grain		2	6.24×10^{-6} in/in/°F
Across Plies		2	7.59×10^{-6} in/in/°F
Thermal Conductivity			
Cold Side Temp.	Hot Side Temp.		
80°F	100°F	1	1.735 Btu/(hr-Ft^2-°F/in)
140°F	160°F	1	2.091 Btu/(hr-Ft^2-°F/in)
180°F	220°F	1	1.633 Btu/(hr-Ft^2-°F/in)
80°F	100°F	1	1.139 Btu/(hr-Ft^2-°F/in)
80°F	160°F	1	1.654 Btu/(hr-Ft^2-°F/in)
80°F	220°F	1	1.452 Btu/(hr-Ft^2-°F/in)

*Individual values not available. Values reported are averages.

SECTION VI

STRENGTH OF ADHESIVE BONDS

SECTION VI

STRENGTH OF ADHESIVE BONDS

In these tests our objective was to determine the strength of adhesive bonds between paper phenolic and 4130 steel and aluminum with each of several candidate epoxy adhesives in order to select an adhesive for use in the demonstration motor. The adhesives selected for evaluation were EPON 907, EPON 913, and EPON 929.

None of the test techniques we attempted were satisfactory and only general guidelines could be obtained from the results. The first series of tests was conducted in accordance with ASTM Method D816, Method B, using the Type 2, or single lap specimen. These samples were made up with one phenolic plate and one metal plate. In later tests we used double lap specimens in accordance with the Type 2 specimen of ASTM D816, Method B. Two versions of this specimen were used; one with plates of paper phenolic on the outside and a metal plate on the inside and the second with metal plates on the outside and a paper phenolic plate in the center. The results of these tests are compared in Table IV.

In the vast majority of the tests, with all types of specimens, the failure occurred in the paper phenolic rather than the adhesive and was generally due to flexure or shear in the phenolic laminate. In those few cases where adhesive failures occurred, poor sample preparation techniques were suspect. The single lap was by far the worst test because the highly unsymmetrical loading condition imposed severe flexural stresses on the phenolic plate, which has low flexural resistance, relative to the metal plate. The double lap specimen with two metal plates was apparently the best in this respect.

It is evident that adhesive tensile shear strength is not the limiting factor for phenolic-to-metal bonds using these adhesives. This was confirmed in several hydrotests of prototype motor cases. All but one of the failures originated in the paper phenolic; the only adhesion failure occurred when we used a primer whose shear strength was evidently quite low. Proper design of adhesive joints with paper phenolic must be based on the available strength of the paper phenolic and the effect of environment on this available length.

TABLE IV

TENSILE SHEAR STRENGTH OF METAL TO PAPER PHENOLIC BONDS*

		Tensile Shear Strength, psi		
Adhesive	Metal	Single Lap 1 Metal, 1 Phenolic	Double Lap 1 Metal, 2 Phenolic	Double Lap 2 Metal, 1 Phenolic
EPON 907	4130 Steel	>1100	> 980	>1350
EPON 913	4130 Steel	> 900	-	>1000
EPON 907	Aluminum	> 700	> 800	>1350
EPON 913	Aluminum	> 800	-	> 850
EPON 929	4130 Steel	> 400	-	-
EPON 929	Aluminum	> 650	-	-

*Six specimens of each type were tested

SECTION VII

THERMAL GRADIENT TEST OF A PAPER PHENOLIC M58A2 ANALOG

SECTION VII

THERMAL GRADIENT TEST OF A PAPER PHENOLIC M58A2 ANALOG

A thermal analog of a paper phenolic M58A2 was fabricated as shown in Figure 21. TN-L-3013 was selected as the inert propellant to be used in this study since its thermal properties are close to those of the live propellant used in the M58A2. The propellant was cast into an HY-488 tube 6 inches in diameter and 24 inches long with a wall thickness of 0.25 inch. This geometry approximated the expected geometry of the paper-phenolic M58A2 prototype. The tube was cast full of propellant using an M58A2 core, and the ends were sealed with 1-inch-thick discs of cork to minimize the heat transfer through the ends of the case.

Six thermocouples were imbedded in the propellant grain at points midway between the ends of the case. The thermocouples were grouped in two sets of three; one set at a star point and one at a star valley. In each set, one thermocouple was between the inner case wall and the case liner, one in the propellant immediately adjacent to the liner, and the third in the propellant and 1/2 inch from the case wall.

The inert motor was placed in an oven, preheated to 350° F, and kept there until the temperature of one of the thermocouples reached 240° F. This limitation was placed on the temperature so that the grain would not slump. The results of the test are shown in Figure 22 and appear quite normal with two exceptions. Both Thermocouple 3 and Thermocouple 6 give readings that appear to be inconsistent with their location.

Thermocouple 3 would be expected to see a temperature distinctly lower than either Thermocouple 1 or 2. As far as can be determined, it was in the proper location so no explanation can be given for its reading generally falling between those of 1 and 2. It is possible that Thermocouple 3 saw a temperature relatively lower than 1 or 2, but the differential was small enough to be concealed by the extremes of the respective error bands. However, it would be expected that the thermal gradient would be severe enough to produce distinct differences in temperature in a half inch of web.

Thermocouple 6 presents the opposite result. Its temperature is much below that of Thermocouples 4 and 5 and near Thermocouple 7. Peculiarly enough, when we X-rayed the motor to confirm the locations of the thermocouples we found that Thermocouple 6 was only 0.10 inch from the case wall instead of the intended 0.50 inch. The gradient is apparently quite severe under the star point.

E258-67-04

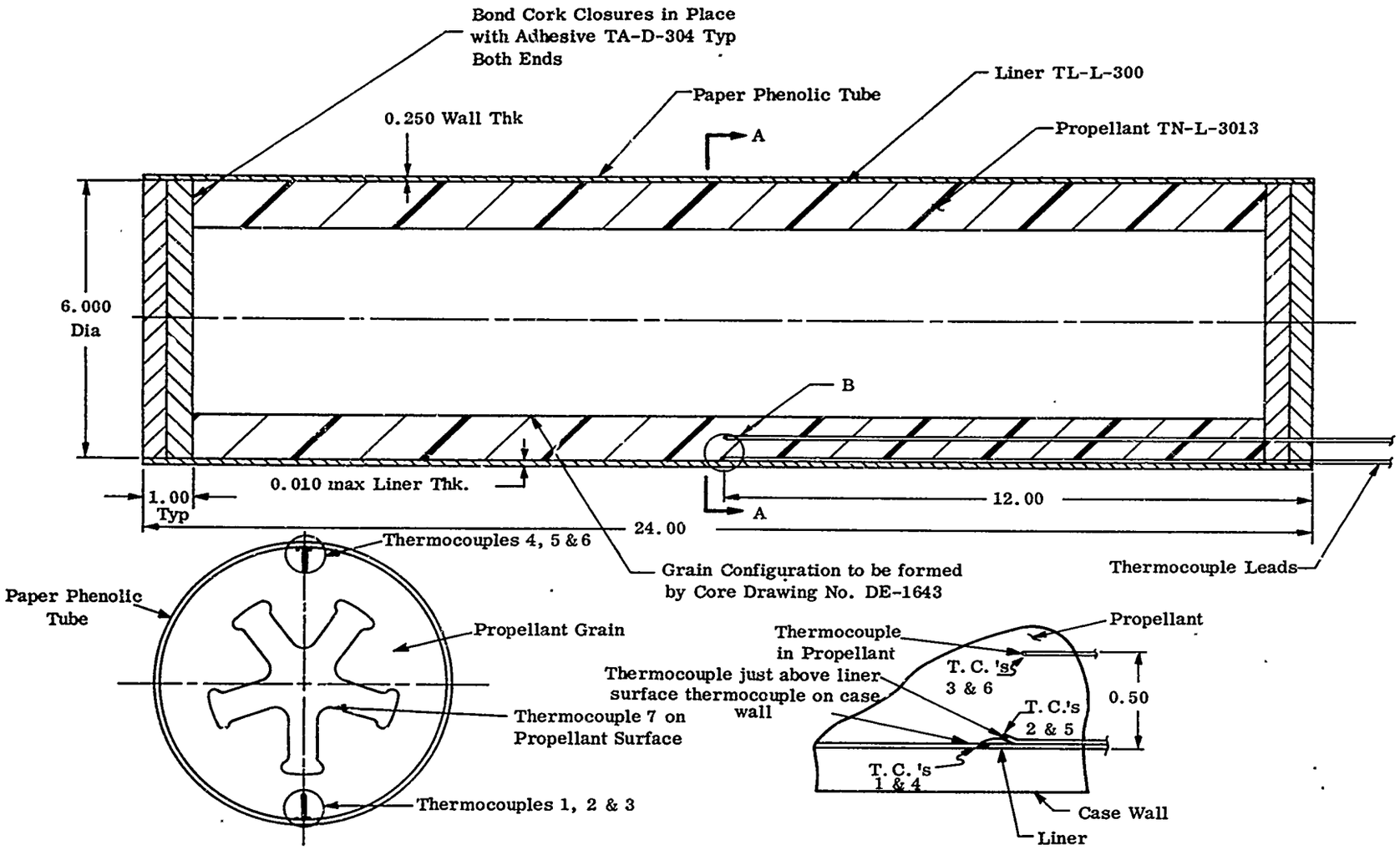


FIGURE 21. GRADIENT STUDY MOTOR

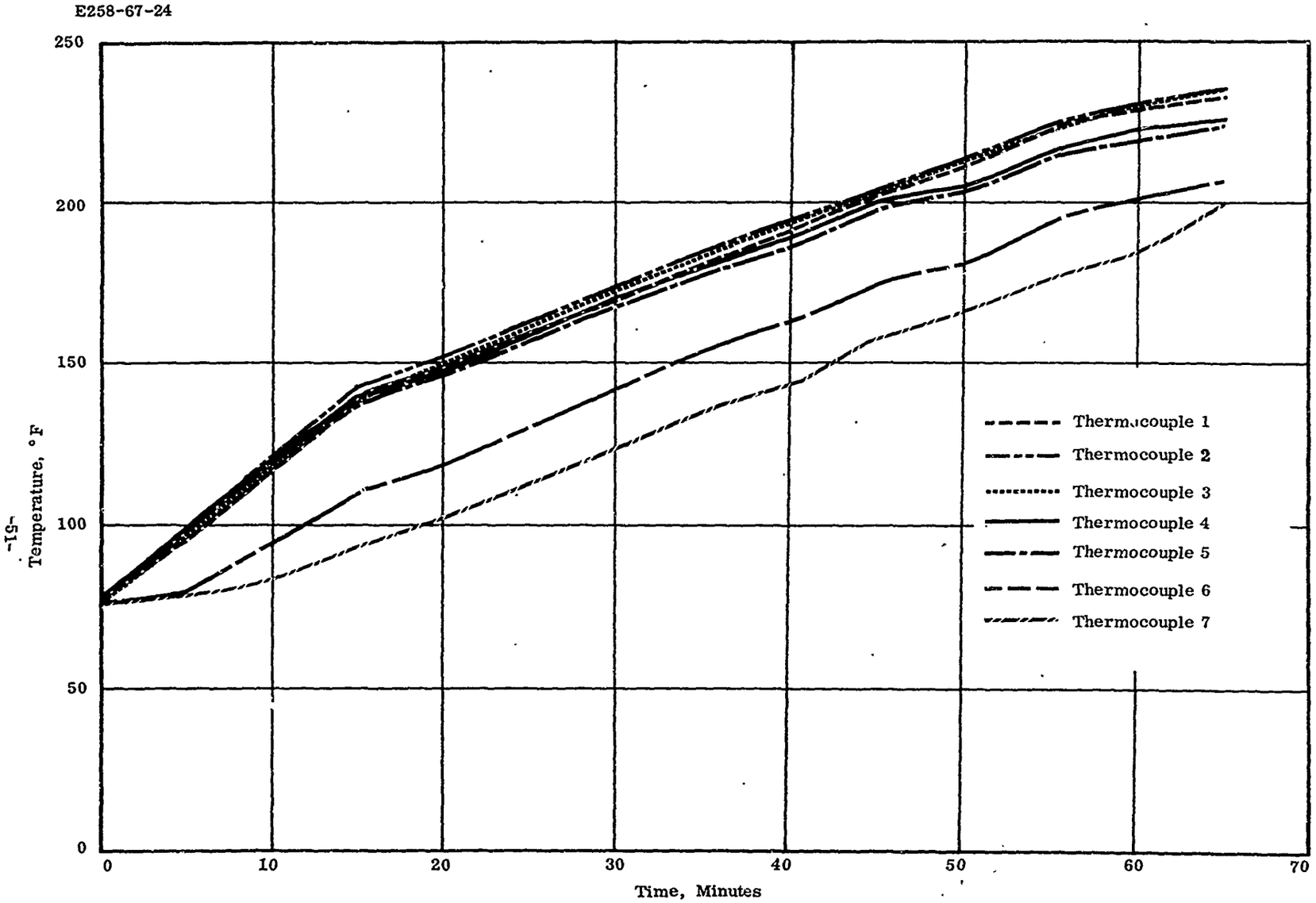


FIGURE 22. TEMPERATURE VERSUS TIME IN INERT PAPER PHENOLIC M58A2

Generally, however, the results appear consistent with the relative locations of the groups. As would be expected the three thermocouples located in a star point register lower temperatures than those in the star valley because of the larger heat sink in their immediate vicinity. It would be interesting to compare these results with similar results in a metal case M58A2 but we have been unable to locate any such data.

SECTION VIII

PRODUCTION TECHNIQUES FOR PAPER PHENOLIC COMPONENTS

SECTION VIII

PRODUCTION TECHNIQUES FOR PAPER PHENOLIC COMPONENTS

1. INTRODUCTION

As part of the requirements, we investigated fabrication methods for volume production of complex and conventional structural components. Our objectives were:

1) Determine cost factors for existing fabrication methods in consultation with material suppliers.

2) Evaluate cost effectiveness of high volume fabrication methods suggested by suppliers.

3) Evaluate strength-to-weight and cost factors for complex shapes with suppliers.

   a) Determine feasibility and estimate costs of molding with laminations parallel to spherical, elliptical, and other closure contours.

   b) Determine feasibility and estimate costs of reinforcing laminate materials to improve strength levels.

   c) Determine relative advantages of helical winding versus convolute winding.

   d) Determine estimated strength and cost factors for integrally fabricated metal attachments.

To accomplish these objectives, we had discussions with representatives of the Micarta Division of Westinghouse Electric Corporation and the Panelyte Division of Thiokol Chemical Corporation. The results of these discussions are presented in the following paragraphs.

Since we are primarily interested in the high strength, oriented fiber materials, our discussion is restricted to the production techniques and problems associated with these forms, except where discussion of other production techniques will provide general background.

2. PRODUCTION TECHNIQUES

a. Tubing

Paper phenolic tubing is produced by three general techniques; convolute wrapping, helical wrapping, and flash molding. Convolute wrapping appears to be the only desirable method for producing oriented fiber tubing. The flash molding process loses the advantage of the oriented fiber as the paper is crammed randomly into a split mold under pressure and the resulting tube has a random fiber orientation. Helical wrapping, as practiced in the paper tube industry, results in tubes of the form commonly used as spindles for rolls of paper. It is produced in the form of endless tubes of a single wrapping thickness with a slight overlap between adjacent wraps. The maximum wall thickness is severely limited as it is restricted to the thickness of a sheet which can be wrapped around a mandrel without wrinkling. The sheet is a laminate of several plies of paper that is formed just before it is wrapped on the mandrel.

Wall thickness is not the only disadvantage of the helically wrapped tube; it is also a poor structure for a pressure vessel. Pressurization loads would result in torsional stresses which would attempt to unwind the vessel, and the normal overlap between adjacent layers is inadequate for resisting these forces. Even if this overlap were increased to a point where it could resist these forces, the case would have a discontinuity at each overlap which would require additional wall thickness.

Variations of the helical wrapping technique which improve the structural properties of the tube were discussed with Micarta personnel. These variations included a layered vessel with the direction of the helix reversed in each successive layer, and a tape-wrapping technique. Each had one major drawback, a substantial increase in labor costs which would eliminate any cost advantage the material might have. No good estimates could be made for the first method but the tape wrapping should increase costs by about 10 to 15 percent based on Micarta's experience with a glass filament wound tube.

Convolute wrapping appears to be the most advantageous technique for producing tubing as it does maintain fiber orientation and it is a relatively low cost production technique. The process is quite simple, the fabrication takes four steps - treating, winding, curing and finishing. In the first step the fiber oriented kraft paper passes through a series of applicators rollers, wipers and heated drums which successively apply the resin, impregnate the paper under pressure, remove the excess resin and finally "B"-stage the resin. The treated paper then goes to the tube machine where it is convolutely wrapped on metal mandrels. Tension is maintained on the paper during rolling to prevent wrinkling and backlash and a single roller applies pressure to the tube as it is being formed to press the successive

layers together and prevent delaminations. When the desired wall thickness is reached, the wrapping is stopped, the mandrel with the uncured tube is removed from the machine, and the mandrel and tube are placed in a 150°C oven for curing. At the completion of the curing cycle, the mandrel and tube are removed from the oven, the mandrel is pulled from the tube, and the tube is centerless ground to the final outside diameter and trimmed to length.

The entire manufacturing process is a batch process and, consequently, the labor costs constitute the major portion of the production costs of a tube. Unfortunately, the process does not seem to be one which could be adapted to continuous operation but assembly line techniques can be developed quite readily if a sufficient quantity of tubes of a given size were required. Further savings can be realized by rolling as long a tube as possible, but here we are limited by the width of the paper available and, in turn, by the width of paper machines, 100 inches.

Batch processing, of course, restricts production rates and limits the cost savings that can be obtained by increasing volumes but using existing equipment. A typical (semi-automatic) tube roller can produce 230 tubes every 24 hours. Micarta has five machines which can produce 50-inch tubes up to 10 inches in diameter at this rate. They also have several older and slower machines which are used for tubes above 10 inches in diameter. Panelyte's equipment for the range of diameters we are concerned with is somewhat slower; each machine is capable of about 115 tubes per day. Their daily production is dependent on the size since Panelyte's individual machines are less versatile dimensionally than Micarta's, although Panelyte has many more machines and can produce much longer tubes. The data given in Section VIII-3 permits computation of daily volume for a given size. Generally speaking, both vendors have about the same total capacity. Costs are also quite competitive; typical values are shown in Table V.

Either of the vendors can obtain additional semi-automatic machines for about $15,000 each and the manual machines for about $6,000 each. Delivery lead time for the semi-automatic machines is on the order of 3 to 4 months and the manual machines a few weeks less.

The most exciting concept for high volume production which has been investigated by one vendor utilizes a fully automatic machine. This machine uses the same process as the standard and convolute wrapping machines but all steps, including curing and mandrel loading, have been automated. The result is a high-speed process which can produce between 6,000 and 7,000 tubes per day. Even the curing process has been accelerated by the use of quartz lamps. Development has advanced as far as preparing a preliminary design and cost estimate. A complete machine would cost about $500,000, but per-tube costs would be reduced by at least 25 percent as a result of 90 percent reduction in labor requirements.

TABLE V

BASIC COST DATA FOR PAPER PHENOLIC TUBING

PRODUCED TO NEMA STANDARDS

Number of Tubes Ordered			Unit Cost			
			100	500	1000	5000
Tube Dimensions						
Inner Diameter, in.	Outer Diameter, in.	Length, in.				
1	1-1/16	46	$ 3.25	$ 2.90	$ 2.70	$ 2.60
1	1-1/8	46	3.35	3.11	2.90	2.80
1	1-1/4	46	4.45	4.20	4.00	3.90
3	3-1/8	46	5.50	5.20	5.00	4.90
3	3-1/4	46	7.00	6.75	6.55	6.40
3	3-1/2	46	12.60	12.20	12.00	11.80
9	9-1/4	46	35.00	33.00	31.00	30.00
9	9-1/2	46	45.00	42.00	40.00	38.00
9	10	46	75.00	71.00	68.00	65.00

The automated machine is restricted in the range of diameters it can produce. No one machine can accommodate a variation in diameter greater than 10 inches, although the actual diameters can be any chosen 10-inch range within the limits of 1 to 24 inches. A machine could be modified to handle a different 10-inch span for about $25,000.

Since the mandrel cannot be removed until after the tube is cured, the number of mandrels available can be another limiting factor on production rates. In the present processes, one mandrel can produce about 4.5 tubes every 24 hours. No estimate has been made of the mandrel turnaround time for the automated process, but it would be expected to be several times faster than the present one. A mandrel can be purchased for $200 to $300 depending on size.

b. Sheet

Sheet is produced in a quite straightforward manner. Sheets of treated paper are cut from a roll and trimmed to the desired size. These sheets are then stacked in a frame to the desired thickness and pressure is applied with a flat plate press. The frame and press are then rolled into an oven for curing. After curing, the sheets are removed from the press and trimmed and finished as necessary. The density and, to some extent, the strength of the sheet can be regulated by the pressure applied by the press. Each individual sheet of paper can be oriented as desired with respect to grain direction so that desired strength orientation can be achieved in the finished plate.

c. Rod

Paper phenolic rod is produced by one of two techniques. The first is flash molding of unoriented paper in split molds. In the second technique, rods are made from convolute-wrapped tubes of small internal diameter. Intense external pressure is applied to the walls of an uncured tube from which the mandrel has been removed. This pressure collapses the walls of the tube and fills the center perforation of the tube with material from the walls. The resulting rod is then cured and ground to the finished diameter. Rod made in this last manner will not have the hoop strength associated with the tube from which it was made because the laminate contours are quite contorted.

d. Other Forms

Numerous other shapes are made of both oriented fiber and unoriented fiber paper phenolic. These include angles, channels, zees, and tubing of rectangular and elliptical cross section. Our interests were in techniques for fabricating hemispherical, elliptical, and dished domes for case and closures. Unfortunately,

the material does not seem to be adapted to fabricating components of complex shapes. The sheets of paper will not conform to the contours of domes without severe wrinkling and deformation of the material, resulting in degradation of the effective strength of the fibers. One possible method for fabricating these shapes would be with rosette layups; however, even with rosettes it might not be possible to close up a dome. There would probably be a small opening left at the pole, and this opening would then have to be filled with a plug. Although rosette layup offers the possibility of constructing complex shapes which would use the anisotropic properties to maximum advantage, it is a very costly process. Closures manufactured by this process would cost three to four times as much as equivalent metal closures.

None of the above is intended to eliminate the consideration of paper phenolic closures as they can be economically produced from rod or sheet stock. Gualillo successfully used closures machined from sheets in which the grain direction was rotated 90° in successive plies to obtain more desirable directional properties for a dome. This method can be quite competitive and even cheaper than metal under some circumstances, but it would not be wise to make a general comparison.

3. DIMENSIONAL LIMITATIONS

a. Convolute Tubing

As mentioned earlier, the length of the tubing is limited first by the width of the wrapping machine and ultimately by the available width of paper. Most machines are 50 inches wide, but material wastage at each end of the tube caused by uneven wrapping results in a usable length of 46 inches for tubes over a half inch in internal diameter. For tubes requiring mandrels of less than a half inch diameter, the length is further limited by the stiffness of the mandrel to lengths of 32 to 36 inches for tubes down to 1/4 inch and to 18 to 20 inches for tubes down to 1/8 inch. Micarta's 100-inch machine is capable of making tubes up to about 95 inches long in internal diameters from 1 to 3 inches.

The diameter of the tubing is limited only by mandrel size on Micarta's 50-inch machines. A practical upper limit seems to be about 72 inches and the lower limit is 1/8 inch. An additional restriction, though not a major one, is the centerless grinder used for finishing the outer diameter. Micarta's grinder cannot handle tubes greater than 9 inches in diameter and larger tubes must be turned on a lathe, a more expensive process. If necessary the larger centerless grinders probably can be obtained.

Thermal stresses generated during curing restrict the maximum wall thickness. These stresses are a function of the heat transfer rate into the tube; thus, the maximum thickness is a function of diameter. If the maximum thickness for a

given diameter is exceeded, circumferential cracks are produced in the wall of the tube by the thermal stresses. Typical values of wall thickness versus diameter are listed below for either vendor.

Tube ID, in.	Maximum Wall Thickness, in.
1	1/4
4	1/2
12	1

Panelyte's capabilities are generally similar. They can produce longer tubes in most sizes but are limited to a maximum outer diameter of 24 inches. As mentioned earlier, Panelyte's individual machines are not as versatile with respect to tube diameters but they have a much larger number of machines whose capabilities complement each other and result in more overall versatility. They have a total of 23 machines but 14 of these produce tubes of less than 1-1/2 inches in diameter and so are of little interest. The capabilities of the remaining machines are listed below:

Tube ID, in.	Tube OD, in.	Tube Length, in.	No. of Machines
1	8	50	3
1-1/4	6	65	1
1/2	8-1/2	100	2
2	18	50	1
8-1/2	24	72	1

Gross values are quoted for tube length and an allowance of 6 to 10 percent should be made for unusuable material at the tube ends.

Tubing is normally produced to dimensional tolerances established by the National Electrical Manufacturers Association (NEMA Standard LI-1-4.10 and LI-1-4.11). Similar tolerances are given in MIL-P-79C. Table VI is an extract from the NEMA standards. Our experience has shown that the standards are quite liberal, and tolerances of ± 0.005 inch on any dimension present no difficulties on tubes of up to 9 inches in diameter. The tolerance on the internal diameter is dependent on the tolerance on the metal mandrel, which can be held much tighter than ± 0.005. The outer diameter tolerance is restricted by the capabilities of centerless grinding, which is certainly better than reflected in the standards. Rough, unground tube is less than 0.050 inch oversize.

TABLE VI

NEMA STANDARDS FOR DIMENSIONAL TOLERANCES

ON ROLLED TUBES

Nominal Diameter, in.	Tolerances	
	Inside Diameter, in.	Outside Diameter, in.
2 to 4 incl.	± 0.008	± 0.008
4-1/8 to 12 incl.	± 0.010	± 0.025
12-1/8 to 18 incl.	± 0.030	± 0.030

b. Rod

Rod is available in standard sizes up to 2 inches in diameter and in special sizes up to 4 inches in diameter. Micarta makes only the molded rod while Panelyte makes both molded and the collapsed tube form. Rod standard dimensions and tolerances are in accordance with NEMA standards and MIL-P-79C. These standards permit ± 0.005 inch on diameters up to 1-15/16 inches and ± 0.008 inch on diameters from 2 to 4 inches. As in the case of tubes these tolerances appear to be liberal. The maximum diameter of the rod is limited by the thermal stresses induced during curing.

c. Sheet

The thickness of sheet is restricted to a maximum of 2 inches, again due to thermal stresses. Length and width limitations are dependent on the manufacturer. Panelyte can produce sheets up to 36 in. by 120 in. and Micarta, up to 50 in. by 120 in. In both cases, the restrictions are due to tooling dimensions but in any case one dimension cannot exceed 100 inches, the maximum width of the paper. On thicknesses above 1 inch, the tolerances are about ± 3 percent on the as-molded plate and about ± 1.1 percent on the sanded plate.

d. Integral Fabrication of Convolute Tubes and Metal Case Hardware

It appeared that cost savings could be obtained and joint efficiencies could be improved if the metal case hardware such as interface joints, launcher lugs, or head caps could be integrated into the tube structure during the wrapping process. This was investigated with several supplies and the results were discouraging. As mentioned previously, the ends of the tube are quite irregular and this material is normally trimmed off. The material in this area is of poor quality and is certainly not suitable for the transition section between a case and a metal component and so eliminates integration at the the ends.

With integration at points along the length of the case, another problem is encountered. Tubes are wrapped from a single width of paper and in order to incorporate fittings during the wrapping process, the paper would have to have cutouts at intervals to provide openings for the fittings or it would be necessary to use two or more spaced widths of paper to provide a circumferential groove for the fitting. With both of these techniques, we would encounter a variation of the "uneven ends" problem to some degree; and both techniques would introduce complexities and additional cost, particularly since they would require periodic halts in the wrapping process to change paper rolls. In addition, the second technique would result in a decrease in wall thickness over the entire circumference at the point of attachment.

A final problem with any of the schemes is the effect of cure shrinkage on the phenolic to metal bond. In general, integral fabrication does not appear to offer any advantages in bond efficiency or cost effectiveness.

SECTION IX

GENERALIZED DESIGN STUDIES AND COMPARISONS OF PAPER PHENOLIC WITH ALUMINUM AND STEEL

SECTION IX

GENERALIZED DESIGN STUDIES AND COMPARISONS OF PAPER PHENOLIC WITH ALUMINUM AND STEEL

1. WALL THICKNESS AND MASS FRACTION

In the selection of any structural material for a rocket motor two considerations are normally paramount. What effect will the material have on the dimensional envelope and what effect will the material have on the mass fraction? The first question can be rephrased as what will be the effect on the case wall thickness, and this dimension has been chosen as one parameter for comparing the capabilities of paper phenolic to aluminum and steel In our calculations we have used as the model a thin-walled, infinitely long cylinder subjected only to internal pressurization loads and have assumed that the limiting stresses would be results of hoop or meridian strains near the center of the tube. In the case of the metals, the thickness was controlled by hoop stresses and in the case of the paper phenolic, by the meridian stresses. It was assumed that the minimum yield strength was the maximum allowable stress. The results are shown in Figure 23A in terms of reduced wall thickness versus chamber pressure.

In order to determine the effect of a material on mass fraction it is merely necessary to determine its effect on inert weight. In our case this can be done by multiplying the reduced wall thickness by the material's density. These results are shown in Figure 23B.

It is obvious in both of the figures that the paper phenolic is generally quite inferior to the two metals. However, it should be pointed out that at the smaller diameters the metal case wall thickness may be limited by manufacturing limitations to a value several times the minimum required by stress considerations. In such a case, the paper phenolic tube may end up as the lighter unit.

The material properties used in these calculations are as follows:

Material	Minimum Tensile Yield Strength, psi	Density, lbs/in.^{3}
4130 Steel	179, 000	0.283
7075-T6 Aluminum	70, 000	0.103
HY-488 Paper Phenolic	8, 270*	0.048

*Usable strength or $\frac{\text{Minimum Ultimate Strength}}{1.3}$

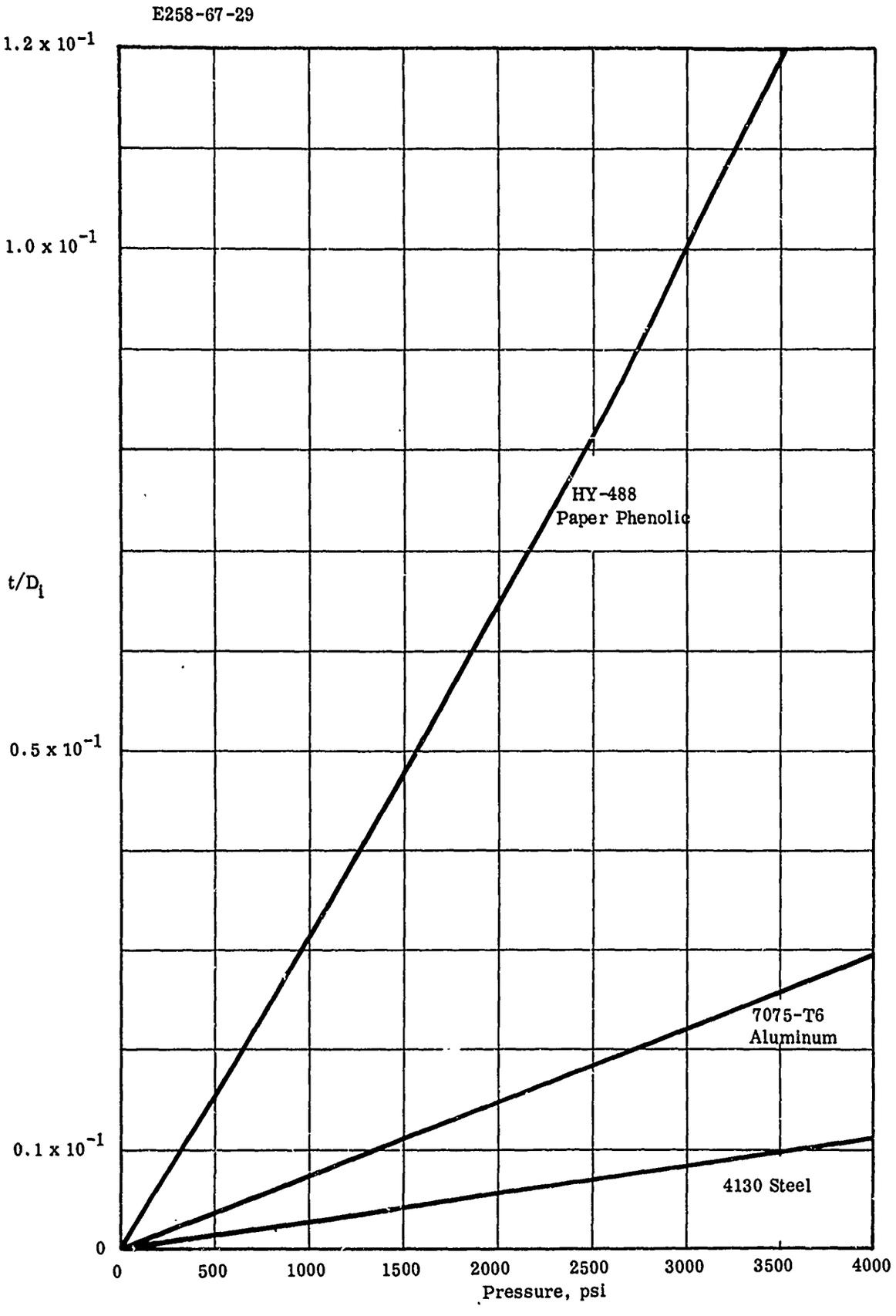


FIGURE 23A. REDUCED WALL THICKNESS VERSUS CHAMBER PRESSURE FOR PAPER PHENOLIC, ALUMINUM AND STEEL

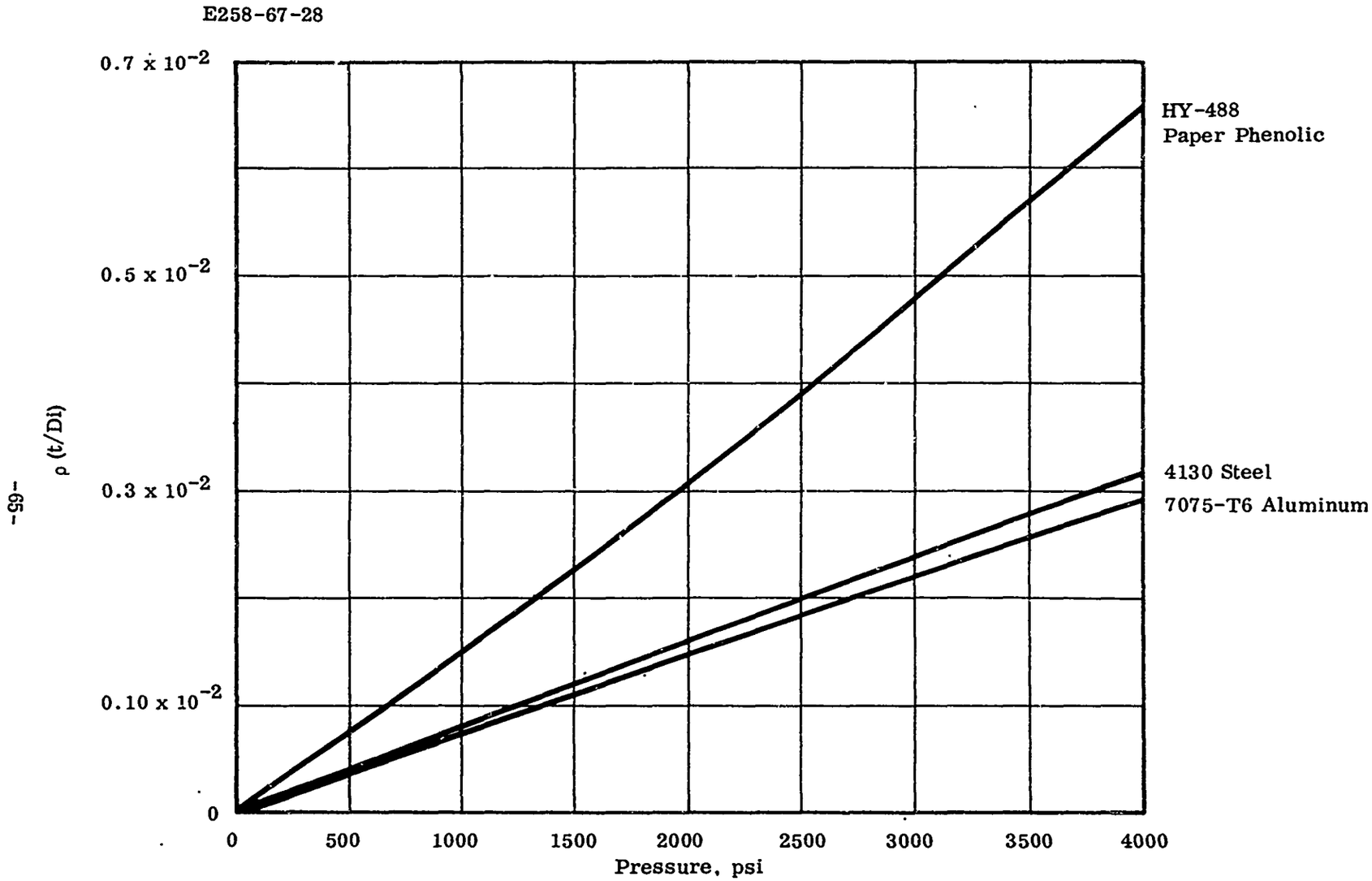


FIGURE 23B. REDUCED WEIGHT VERSUS CHAMBER PRESSURE FOR PAPER PHENOLIC, ALUMINUM AND STEEL

2. INTERNAL AND EXTERNAL INSULATION REQUIREMENTS

In order to evaluate the insulation requirements for paper phenolic in comparison to other materials we selected a quite simple model for the sake of generality. We performed a one-dimensional analysis of a slab or case material insulated with a 0.010-inch thick layer of V-44 rubber insulation. The insulation was exposed to a flame temperature of 4500° F for 1.5 seconds and we determined the temperature gradient in each case material at the end of this exposure time. A case wall thickness of 0.300 inch was assumed for the paper phenolic and the structural equivalents, 0.0711-inch thick 7075-T6 aluminum and 0.0332-inch thick 4130 steel (176, 000 psi ultimate) were assumed for the other materials.

The results of the analysis are presented in Figure 24 and show that the paper phenolic is superior to either of the metals because of its superior thermal properties and far greater thickness. Even though paper phenolic has the highest temperatures in the first 0.010-inch this is a much smaller proportion of the total thickness and the wall strength is decreased proportionally less in the paper phenolic than in the metals.

3. PROPELLANT-CASE INTERACTIONS

a. Introduction

The objective of this section is to assess the effect of propellant-case interaction as a function of temperature and pressure based upon the test data of Phases I and II, and to make a qualitative comparison between paper phenolic cases and those fabricated from steel and aluminum. For purposes of this study, it is sufficient to consider a model consisting of a long, hollow, right circular cylinder bonded to an elastic case and subjected to either a uniform temperature change or a uniform internal pressure. This model will provide a valid comparison of propellant-case interaction for case materials made from steel, aluminum and paper phenolic.

The geometry of the model under consideration is shown in Figure 25. Thermal and material properties of the materials studied are specified in Table VII. The properties of the propellant charge were selected as representative of state-of-the-art CTPB (carboxyl terminated polybutadiene) propellant compositions which are widely used in the propulsion industry today. D6AC steel and 7075 aluminum case materials were selected for use in the comparison. The Surveyor Main Retro (TE-M-364) case is fabricated from D6AC while the Tomahawk (TE-M-416) case is made out of 7075 aluminum.

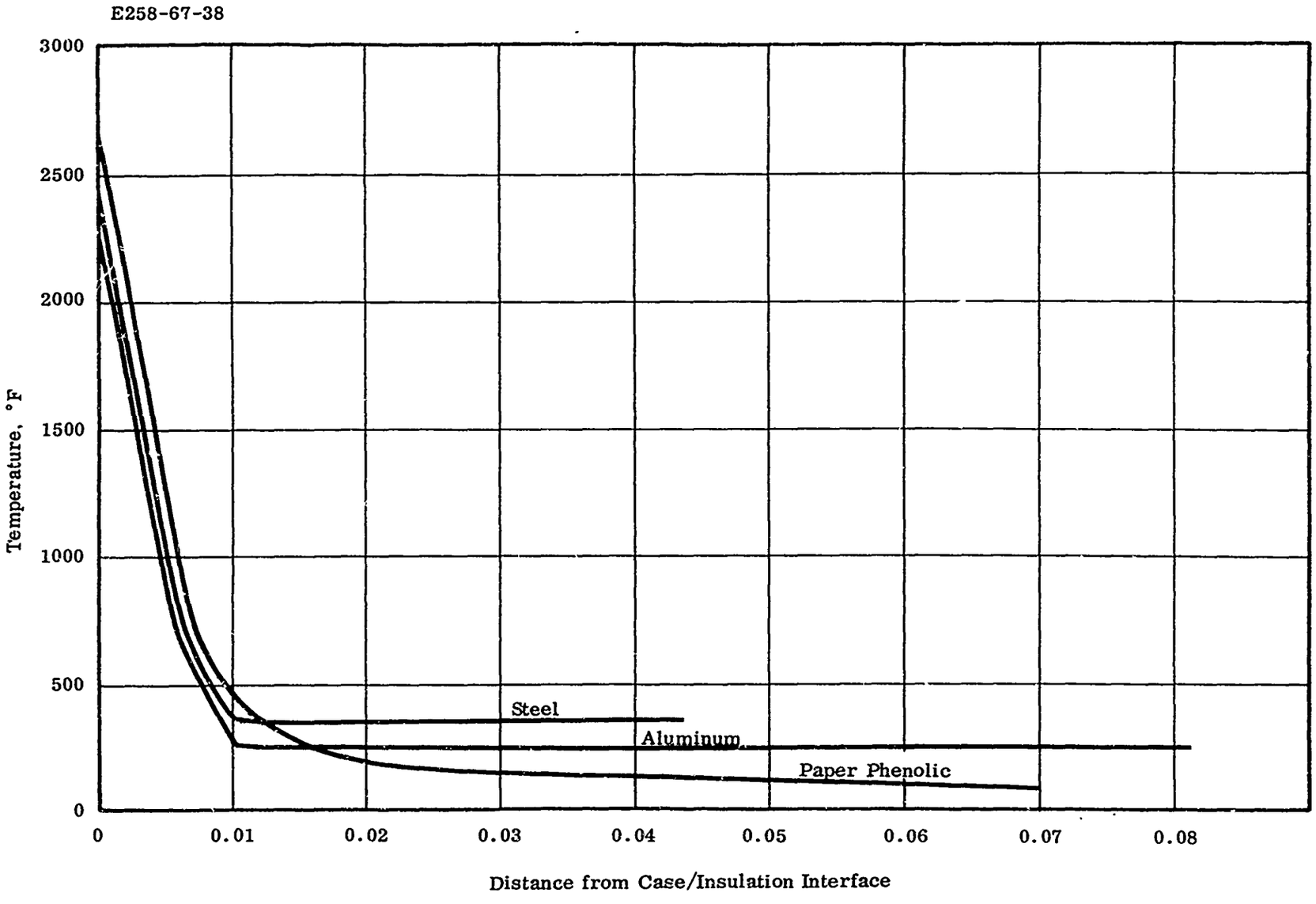


FIGURE 24. TEMPERATURE GRADIENT IN CASE WALLS OF VARIOUS MATERIALS

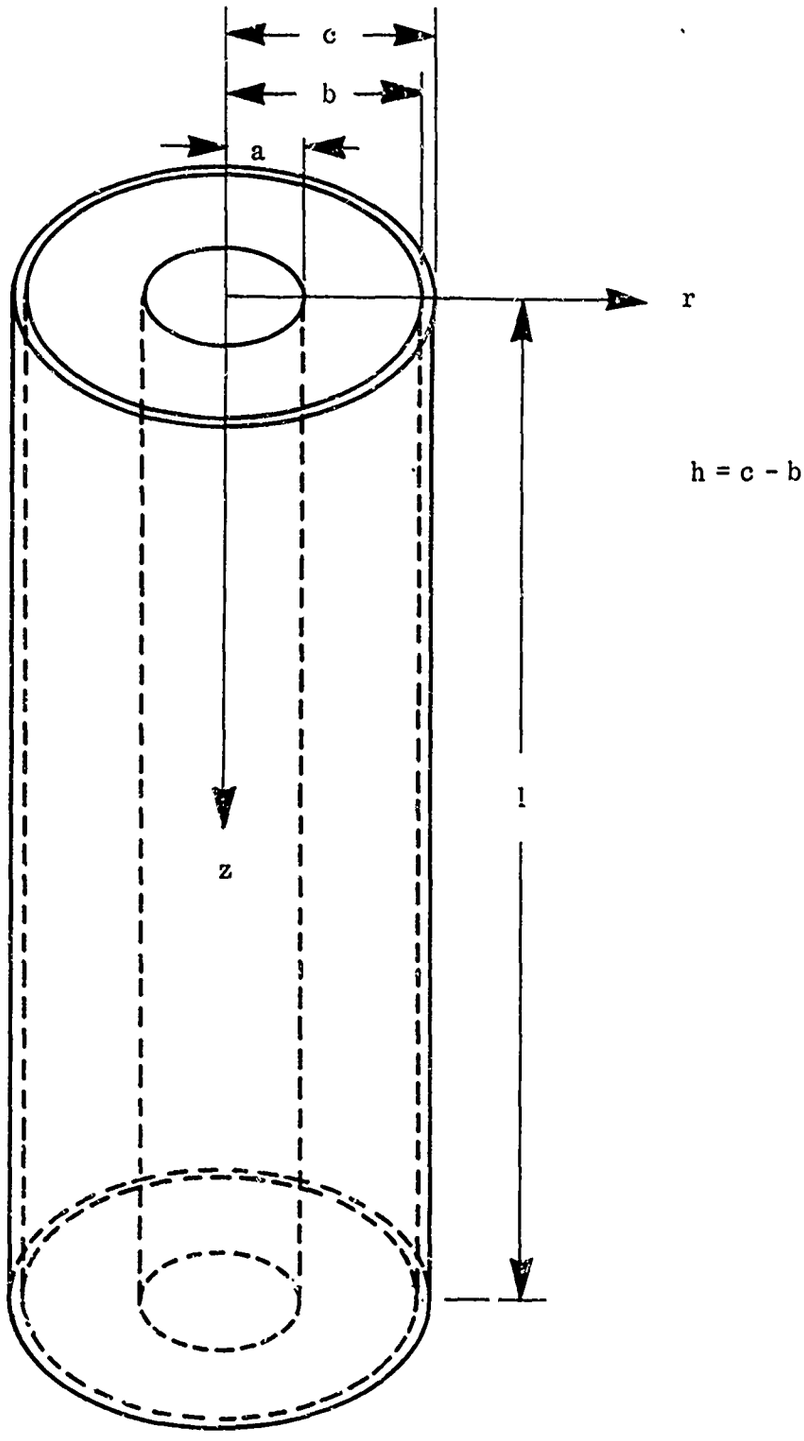


FIGURE 25. MODEL GEOMETRY FOR PROPELLANT-GRAIN INTERACTION ANALYSIS

TABLE VII

THERMAL AND MECHANICAL PROPERTIES FOR
PROPELLANT-CASE INTERACTION CALCULATIONS

	Micarta HY-488	D6AC	7075 Al
Density, lbs/in.^{3}	0.048	0.284	0.101
Thermal Expansion, in./in./°F		7.3×10^{-6}	12.9×10^{-6}
with grain	1.55×10^{-5}		
across grain	6.24×10^{-6}		
across plies	7.59×10^{-5}		
Modulus of Elasticity, psi		30×10^6	10.3×10^6
temperature cycling	3.5×10^6		
internal pressure	$2.8 - 3.7 \times 10^6$		
Poisson's Ratio		0.284	0.300
temperature cycling	0.500		
internal pressure	0.350		

CTPB PROPELLANT

Density, lbs/in.^{3}	0.065
Thermal Expansion, in./in./°F	5.5×10^{-5}
Equilibrium Modulus, psi	200
Glassy Modulus, psi	125,000
Poisson's Ratio	0.500

b. Thermal Loads

The Preliminary Grain Design Structural Analysis Program (E-40263) was used in the thermal stress analysis of the center perforate model shown in Figure 25. The program computes the resultant maximum tangential stress and strain in the bore and the interface bond stress caused by cure and temperature cycling. These quantities are obtained from the plane strain elastic solution corrected for finite length and finite straining (Ref. 4). The analytical expressions used in calculating the hoop strain and stress in the port and the bond stress at the case (as a function of temperature) are given by:

$$\varepsilon_{\varphi}(\tau) = \frac{3P\left[\mu_p - \frac{1+\nu_c}{1+\nu_p}\mu_c\right](\tau_0 - \tau)b^2}{2a^2\left(1 + \ln\left[1 + 3P\left(\mu_p - \frac{1+\nu_c}{1+\nu_p}\mu_c\right)(\tau_0 - \tau)\frac{R_o^2}{2R_i^2}\right]\right)} \tag{42}$$

$$\sigma_{\varphi}(\tau) = \frac{2b^2 P\left[\mu_p(1+\nu_p) - \mu_c(1+\nu_c)\right](\tau_0 - \tau)E_e}{(1+\nu_p)\left[(1-2\nu_p)R_o^2 + R_i^2\right] + (1-\nu_c^2)R_o E_e \frac{(R_o^2 = R_i^2)}{hE_c}} \tag{43}$$

$$\sigma(\tau) = \frac{P\left[\mu_p(1+\nu_p) - \mu_c(1+\nu_c)\right](\tau_0 - \tau)E_e}{\frac{(1+\nu_p)\left[(1-2\nu_p)R_o^2 + R_i^2\right]}{R_o^2 - R_i^2} + (1-\nu_c^2)\frac{R_o E_e}{hE_c}} \tag{44}$$

The end effect correction factor for finite length, P, corrects the predicted strain in the port for variations due to propellant charge length-to-diameter ratio.

The zero strain temperature, τ_0, is defined as that temperature above the cure temperature at which the grain inside diameter is equal to the core outside diameter. This parameter is a function of the volumetric cure shrinkage, μ_p, and the coefficient of thermal expansion, Φ_p. The inclusion of this term effectively corrects for the change in bore diameter caused by cure shrinkage and thus allows the accurate prediction of the actual port strain at any given temperature, τ

c. Pressure Loads

The Preliminary Grain Design Structural Analysis Program (E-40263) was also used in the pressurization stress analysis of the center perforate model shown in Figure 25. The program computes the resultant tangential strain in the bore for a specified operating internal pressure (Ref. 4). The expression used in calculating the strain (as a function of pressure) is given by:

$$\varepsilon_{\varphi}(P) = \frac{3.4\, r_o \lambda^2 P}{E\,(3+\lambda^2)} + \frac{(\lambda^2-1)}{2}\,\frac{P}{E_B} \qquad (45)$$

where:

$$\lambda = r_o/r_i$$

d. Discussion of Results

A comparison of the results obtained for thermal loadings can be made by examining the curves plotted on Figures 26, 27 and 28. It is quite evident that for this loading condition the Micarta HY-488 results in lower stresses and strains in the port and at the case interface. This is to be expected since the paper phenolic case-propellant linear coefficent of thermal expansion difference, the stress inducing reaction of the thermal load, is relatively small.

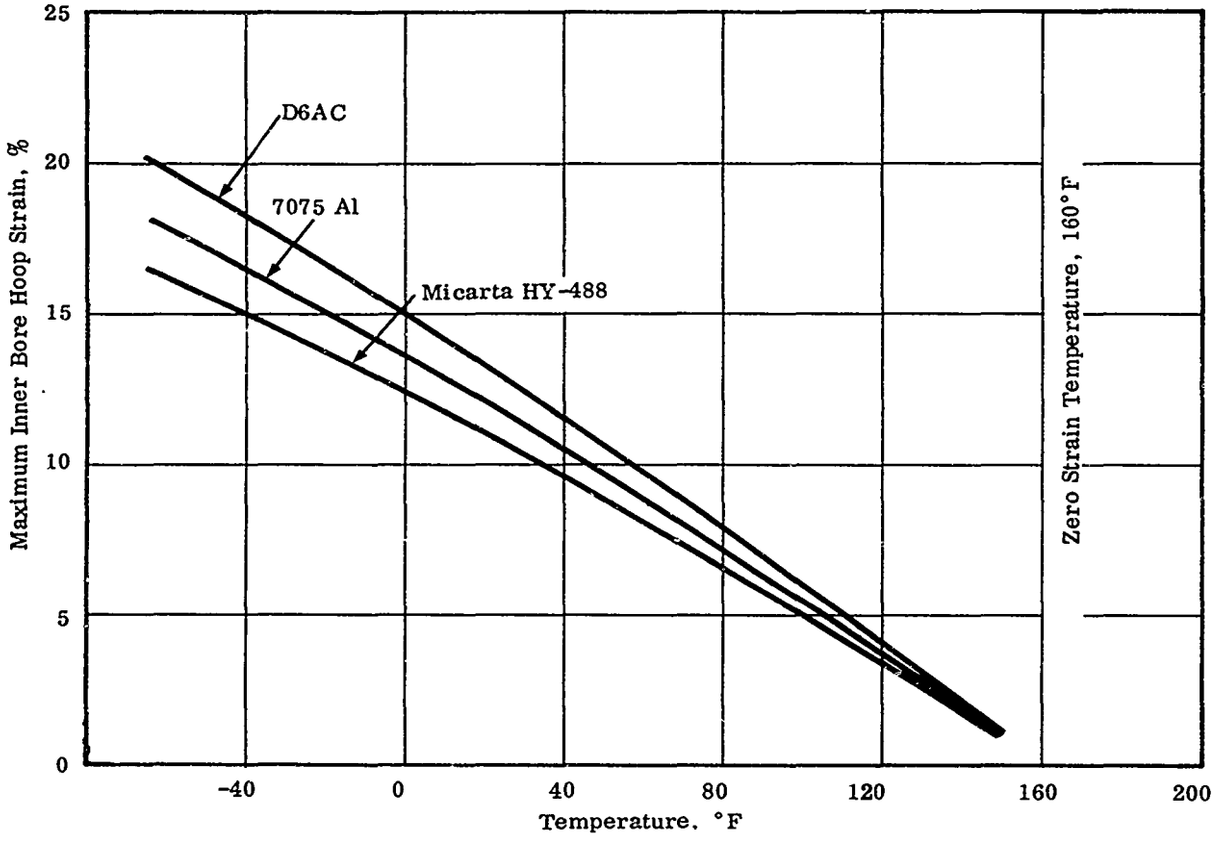
The results of the pressurization analysis are shown in Table VIII. It is readily evident that the use of a paper phenolic case as opposed to steel or aluminum does not result in higher imposed strains.

TABLE VIII

INNER BORE HOOP STRAINS (%) DUE TO INTERNAL PRESSURIZATION

Case Thickness (in.)*	Micarta HY-488	7075 Aluminum	D6AC Steel
0.490 (3000 psi)	1.50		
0.060 (300 psi)	0.14		
0.150 (3000 psi)		1.67	
0.040 (300 psi)		0.63	
0.050 (3000 psi)			1.72
0.040 (300 psi)			0.21

*These are design case thicknesses for the operating pressures specified. All computations were made using a propellant bulk modulus of 350,000 psi/in.^{3}.

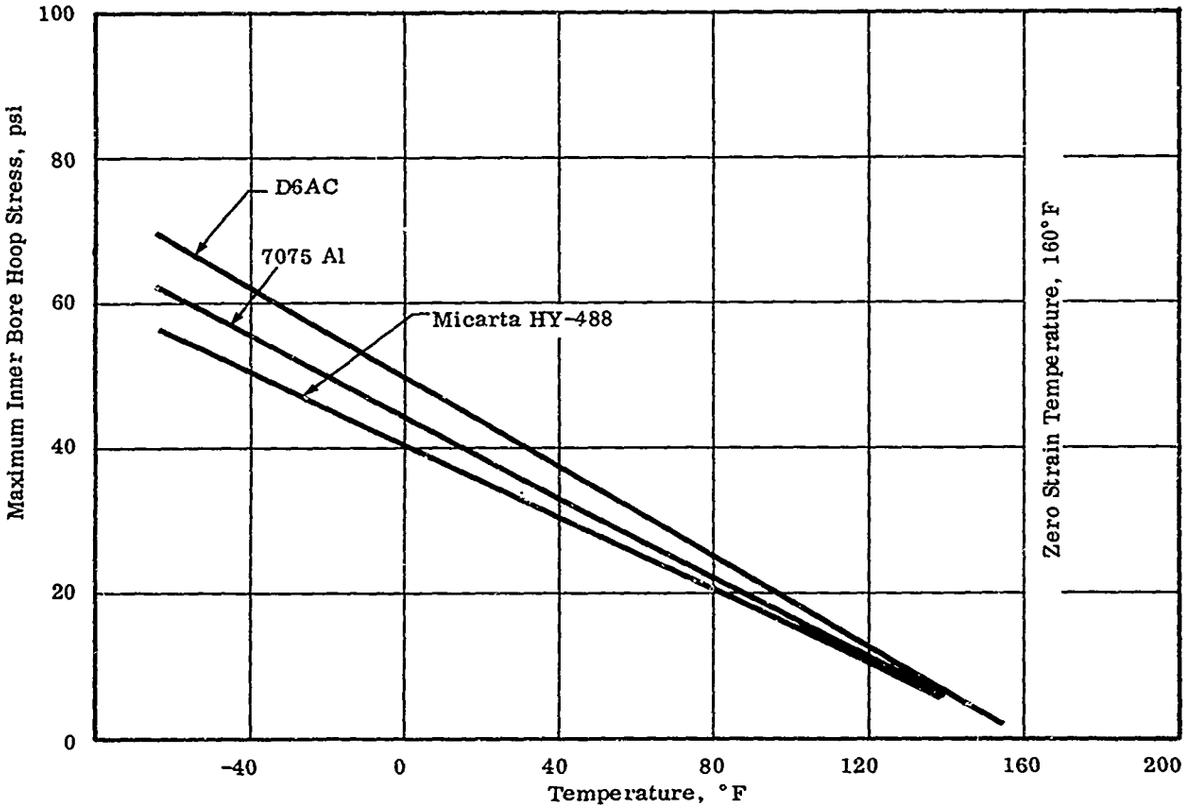


Cure Temperature = 135.0°F
Zero Strain Temperature = 160.0°F
Length to Diameter Ratio = 6:1

ν_p = 0.5
a = 0.750 in.
b = 3.000 in.
μ_p = 5.5×10^{-5} in./in./°F
E_e = 200 psi

FIGURE 26. MAXIMUM INNER BORE HOOP STRAIN VERSUS TEMPERATURE

E258-67-26

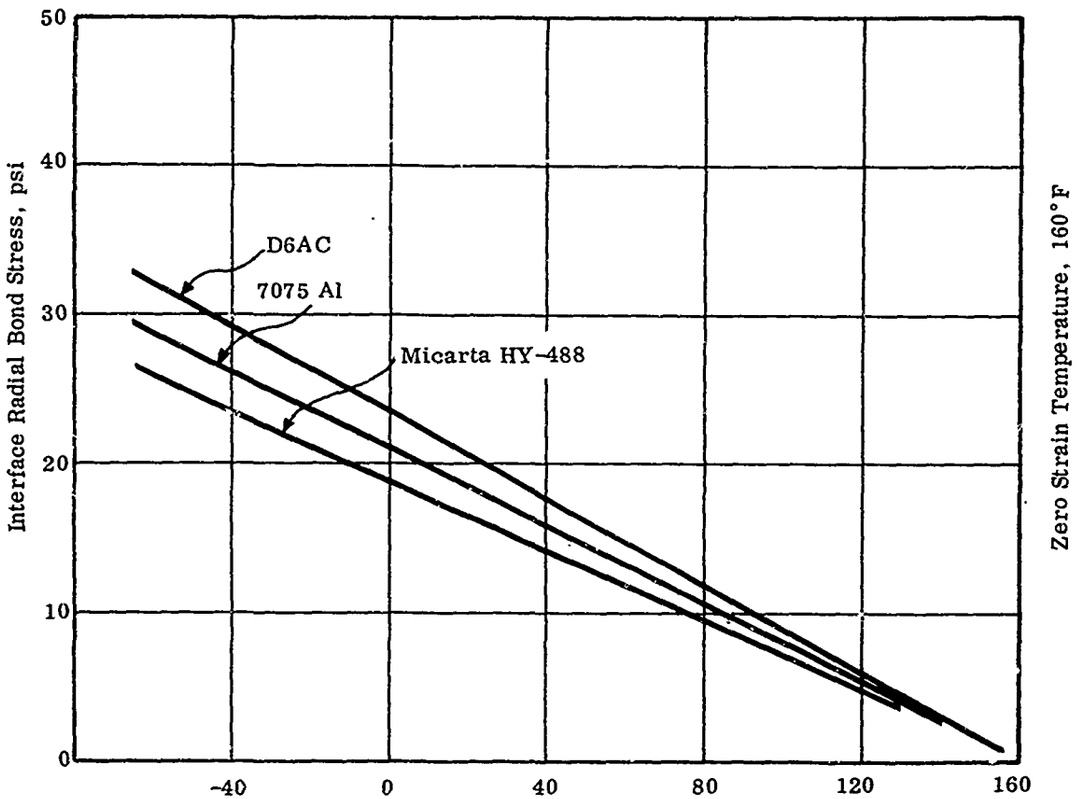


Cure Temperature = 135.0 °F
Zero Strain Temperature = 160.0 °F
Length to Diameter Ratio = 6:1

ν_p = 0.5
a = 0.750 in.
b = 3.000 in.
μ_p = 5.5×10^{-5} in./in./°F
E_e = 200 psi

FIGURE 27. MAXIMUM INNER BORE HOOP STRESS VERSUS TEMPERATURE

E258-67-25



Cure Temperature = 135.0 °F
Zero Strain Temperature = 160.0 °F
Length to Diameter Ratio = 6:1

ν_p = 0.5
a = 0.750 in.
b = 3.000 in.
μ_p = 5.5×10^{-5} in./in./°F
E_e = 200 psi

FIGURE 28. INTERFACE RADIAL BOND STRESS VERSUS TEMPERATURE

4. AEROELASTIC BENDING

A simple rocket configuration consists of a nose section, a cylindrical body and a tail section. At small angles of attack at hypersonic speeds this configuration is acted on by normal forces only at the nose and the tail (Fig 29). Normal forces on a cylindrical body section at hypersonic speeds are proporational to $\sin^2 \alpha$. The following discussion is an evaluation of aeroelastic bending effects on aerodynamic stability, under the influence of normal forces on the nose and tail only. Thrust force will be considered to be zero, as will the spin rate of the rocket.

It is assumed that the rocket has reached a trim condition in which the angle of attack, α, and the deflection angle, θ, of the rocket body are constant (Figure 29). The force on the nose is F_N, and that on the tail, F_T. Since the equilibrium values of θ and α would be zero for a perfectly symmetric rocket, we let the nose be misaligned by a very small angle δ. Then the nose force is:

$$F_N = q(C_{N\alpha}S)_N \left(\alpha + \frac{\theta}{2} + \delta\right) \tag{11}$$

$$F_T = q(C_{N\alpha}S)_T \left(\alpha - \frac{\theta}{2}\right) \tag{12}$$

$(C_{N\alpha}S)_N$ = lift coefficient slope of the nose times reference area of the nose (ft^2/radian)

$(C_{N\alpha}S)_T$ = lift coefficient slope of the tail times reference area of the tail (ft^2/radian)

α = angle of attack (radians)

θ = deflection angle (radians)

δ = misalignment angle (radians)

$q = \rho/2\, V^2$ = dynamic pressure (lb/ft^2)

ρ = atmospheric density ($slugs/ft^3$)

V = rocket velocity (ft/sec)

To simplify the computations, the center of mass of the rocket will be assumed to be at the center of the body section and the coordinate origin will be at the center of mass. The point of action of F_N will be $L/2$, and that of F_T will be $-L/2$, where L is the length of the rocket vehicle. The condition that α is constant means that the sum of the moments due to applied forces is zero, or

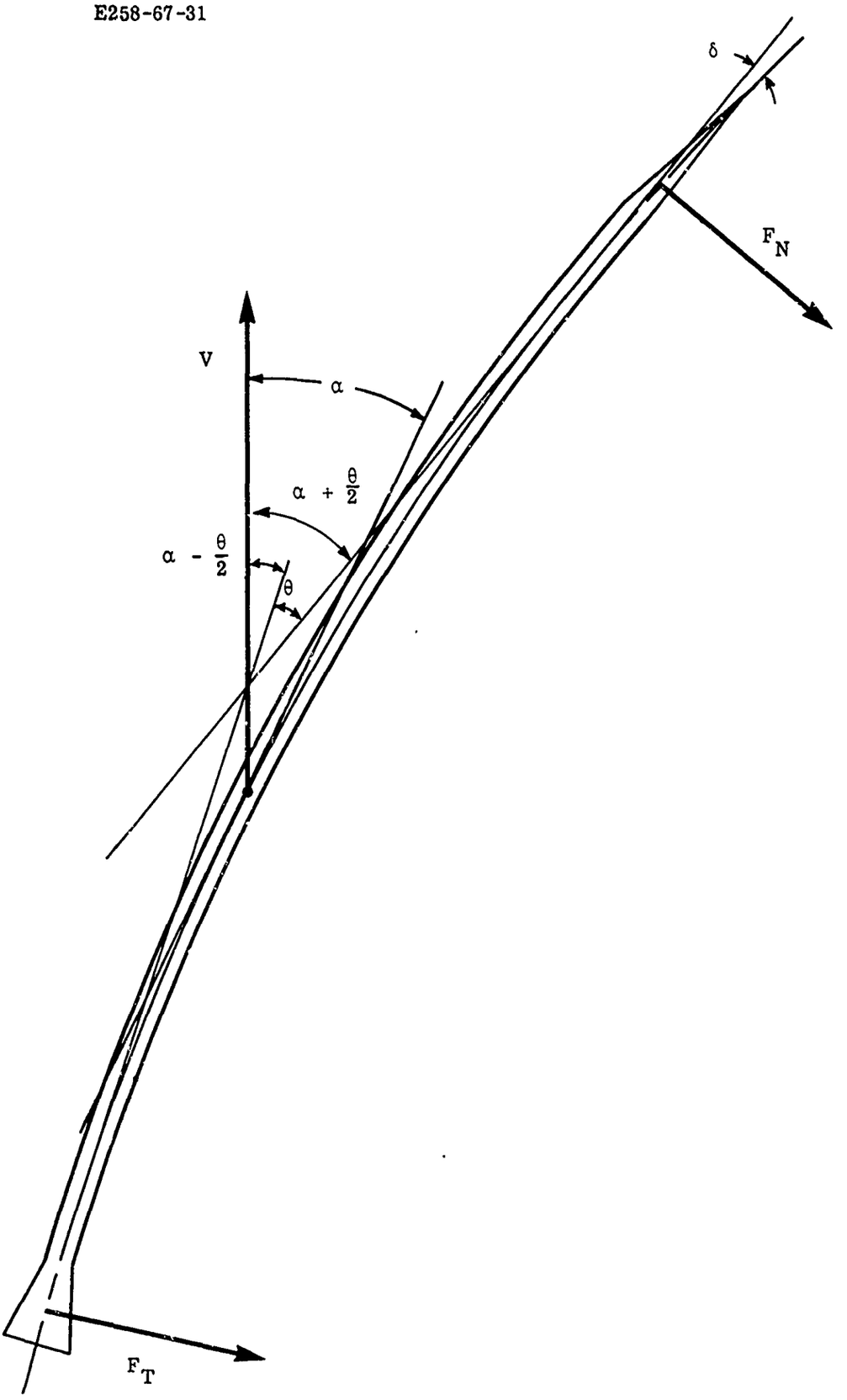


FIGURE 29. AEROELASTIC BENDING ANALYTICAL MODEL

$$F_N \cdot \frac{L}{2} + F_T \cdot \left(\frac{-L}{2}\right) = 0,$$

so that

$$F_N = F_T \tag{13}$$

The bending moment on the rocket is the sum of the moments due to the applied forces, F_N and F_T, and the inertial force distribution $f_I \cdot f_I$ is distributed along the rocket length with the magnitude

$$f_I = -\rho a \text{ (lb/ft)} \tag{14}$$

ρ = mass distribution along the length of the rocket (slugs/ft)

a = normal acceleration of the rocket (ft/sec^2)

$$a = \frac{F_T + F_N}{m} \tag{15}$$

m = mass of the rocket (slugs)

If the mass of the rocket is uniformly distributed:

$$\rho = m/L \tag{16}$$

Equation (12), with ρ and α substituted from Equations (15) and (16), is

$$f_I = -\frac{F_T + F_N}{L} \tag{17}$$

and using Equation (13) for F_T,

$$f_I = -\frac{2F_N}{L} \tag{18}$$

The bending moment at any distance x from the center of gravity is

$$M = F_N \left(\frac{L}{2} - X\right) - \int_X^{L/2} f_I (\xi - X) d\xi \tag{19}$$

$$M = \frac{F_N}{L} \left(\frac{L^2}{4} - X^2\right) \tag{20}$$

The deflection angle is

$$\theta = \int_{L/2}^{L/2} \frac{M}{EI} \, d \, X$$

$$\theta = \frac{F_N L^2}{6 \, EI}$$

Where:

EI = flexural rigidity of the body (lb ft^2) (21)

I = $\pi \left(\frac{d}{2}\right)^3 . T$ for a cylindrical shell of diameter d and thickness t.

Substituting F_N from Equation (11) into Equation (21) yields

$$\theta = \frac{q \, L^2}{6 \, EI} \quad (C_{N\alpha} S)_N \quad (a + \frac{\theta}{2} + \delta) \tag{22}$$

Substituting F_N anf F_T Equations (11) and (12) into Equation (13) yields

$$q(C_{N\alpha} S)_N \quad (\alpha + \frac{\theta}{2} + \delta) = q \quad (C_{N\alpha} S)_T \quad (\alpha - \frac{\theta}{2}) \tag{23}$$

Equations (22) and (23) are the conditions for equilibrium, or trim, for α and θ. Rearranging, they become

$$[K - 1] \quad \frac{\theta}{2} - \alpha = \delta \tag{24}$$

$$- [r + 1] \quad \frac{\theta}{2} + [r - 1] \quad \alpha = \delta \tag{25}$$

Where

$$K = \frac{12 \, EI}{q \, L^2 (C_{N\alpha} S)_N} \tag{26}$$

and

$$r = \frac{(C_{N\alpha} S)_T}{(C_{N\alpha} S)_N} \tag{27}$$

A simultaneous solution of Equations (24) and (25) for

θ and α yields

$$\frac{\theta}{2} = \frac{r\,\delta}{K(r-1) - 2r} \tag{28}$$

$$\alpha = \frac{(K+r)\,\delta}{K(r-1) - 2r} \tag{29}$$

Equations (28) and (29) give the equilibrium or trim values of deflection angle and angle of attack for a simple rocket body at hypersonic speeds. The maximum bending moment under these conditions can be found by substituting into equation (20) for X = 0

$$M_{max} = q(C_{N\alpha}S)_N \left(\alpha + \frac{\theta}{2}\right) \frac{L}{4} \tag{30}$$

It is then a simple matter to calculate tensile stress in the material at the outer edge of the cylindrical shell using Equation (31).

$$f_t = \frac{M}{I}\,\frac{d}{2} \tag{31}$$

For each value of r, there is a value of q which cannot be exceeded because the rocket becomes unstable. This value of q is that for which the denominator in Equations (28) and (29) becomes zero. When this condition exists,

$$K = \frac{2r}{r-1}$$

Substituting for K from Equation (26),

$$\frac{6\ EI}{q\ L^2(C_{N\alpha}S)_N} + \frac{r}{r-1} \tag{32}$$

The critical value of q is given by

$$q_{crit.} = \frac{6\ EI}{(C_{N\alpha}S)_N\ L^2}\ \frac{(r-1)}{4} \tag{33}$$

For a thin cylindrical shell

$$I = \pi R^3 T \tag{34}$$

R = radius of shell

T = Thickness of shell

For a slender body at hypersonic speeds, the normal force coefficient slope is 2/radian, and

$$(C_{N\alpha} S)_N = 2\pi R^2 \tag{35}$$

Assume that in order to maintain aerodynamic stability, the center of pressure is located aft of the center of gravity, a distance 0.1 L. Then $0.6\ L(C_{N\alpha} S)_N = 0.4\ L(C_{N\alpha} S)_T$

and

$$r = 1.5$$

$$\frac{r-1}{r} = \frac{1}{3} \tag{36}$$

then

$$q_{crit.} = \frac{6E\pi R^3 T}{2\pi R^2 L^2} \cdot \frac{1}{3} \tag{37}$$

or

$$q_{crit.} = \frac{E R T}{L^2} \tag{38}$$

For the paper phenolic material under study, the effective longitudinal modulus is

$$E = 10^6 \text{ lb/in.}^2$$

$$= 1.44 \times 10^8 \text{ lb/ft}^2$$

The thickness of the case wall can be considered to be proportional to case pressure and to case radius.

In the current design

$$T/R = \frac{1}{6}$$

and assuming that the case pressure is the same for all designs, let

$$T = R/6$$

and

$$q_{crit.} = 1.44 \times 10^8 \frac{R^3}{6L^2} \tag{39}$$

Letting R = D/2, where D is the case diameter

$$q_{crit.} = \frac{6 \times 10^6}{\left(\frac{L}{D}\right)^2} \tag{40}$$

Equation (40) gives the condition for aeroelastic instability in the simplified model discussed. As a design practice, an acceptable limitation is that the dynamic pressure should not exceed one half the value given by Equation (40)

$$q_{design} = \frac{3 \times 10^6}{\left(\frac{L}{D}\right)^2} \tag{41}$$

For a typical sounding rocket application, q(Design) = 10, 000 lb/ft^2. For this condition,

$$(L/D)^2 = \frac{3 \times 10^6}{1.0 \times 10^4} = 300$$

$$(L/D) = 17.4$$

For a high performance, low altitude hypersonic vehicle q = 75, 000 lb/ft^2

$$(L/D)^2 = \frac{3 \times 10^6}{7.5 \times 10^4} = 40$$

$$(L/D) = 6.2$$

A hypersonic vehicle with L/D ratio of 6.2 is probably not feasible, because of high drag. A sounding rocket with L/D = 17.4 is reasonable, and merits further investigation.

For the condition in which $q = q_{crit/2}$, from Equation (32)

$$K = \frac{4r}{r-1}$$

and from equations (28) and (29)

$$\frac{\theta}{2} = \frac{\delta}{2}$$

$$\alpha = \frac{r+1}{r-1} \cdot \frac{\delta}{2} = 5 \frac{\delta}{2}$$

Since δ, the misalignment angle is measured in radians, and is of the order of magnitude of .001 radian, the angles of attack and stresses induced by the steady state response to a misalignment are negligible, so long as the dynamic pressure does not exceed one half of the critical value given by Equation (40).

In order to interpret these results, it is necessary to examine critically the assumptions made.

First, the assumptions that normal forces act only on the nose and tail, and that the forces are linearly dependent on local angle of attack, are valid only for small angles of attack. A body normal force exists and is proportional to $\sin^2 a$. Further, the normal force on the nose is a linear function of $\sin 2\alpha$ rather than simply α. This means that as the angle of attack increases, and the body bends, the nose, which sees a greater angle of attack than the tail, will experience forces smaller than those given above. At the same time, the normal forces acting on the body will tend to decrease the bending moment from the value computed above. From these two effects, we can assume that the rocket, instead of becoming completely unstable at the critical value of dynamic pressure, will experience large angles of attack and deflection angles, but will not necessarily break up immediately.

It is probable that aerodynamic heating resulting from large angles of attack at high velocity will cause degradation of physical properties sufficient to cause failure, if the flight continues long enough.

The assumption that the normal force coefficient slope of the nose is 2/radian, based on cross section area, is valid for every condition except a blunt body.

If the thrust is not zero, the equation for trim condition of the angle of attack, Equation (13), must contain a term for the moment of the thrust force about the center of mass of the bent rocket This moment will be destabilizing, tending to increase the angle of attack and thus the bending.

If the spin is not zero, the completely valid equations will have to be in three dimensions, including gyroscopic and coning effects. The effect of any large spin will be to increase bending, since the deflected body will experience inertial forces due to spin, tending to increase the deflection. This effect is negligible for spin rates less than 10 rps which is the rate usually used for rocket vehicles.

SUMMARY

Using a set of simplified assumptions, an equation was derived relating the length/diameter ratio of a rocket vehicle and the maximum dynamic pressure required to initiate catastrophic aeroelastic bending.

The assumptions are reasonable for rocket vehicles with high length/diameter ratios, such as sounding rocket vehicles.

The analysis showed that for cases made of the paper phenolic material being analyzed, the critical dynamic pressure, $q_{crit.}$, is related to the length/diameter ratio (L/D), by

$$q_{crit.} = 6 \times 10^6/(L/D)^2 \ (lb/ft^2)$$

So that if the design factor of safety is 2,

$$q_{design} = 3 \times 10^6/(L/D)^2 \ (lb/ft^2)$$

For a typical sounding rocket vehicle, with a maximum q of 10,000 psi, a design L/D of 17.4 is possible.

5. EFFECTS OF VEHICLE INTERFACE ATTACHMENTS ON CASE STRUCTURE

a. Introduction

Study of the impact of the nature of the paper phenolic material upon potential solutions to interface problems leads inevitably to ideas of an artistic or architectural character. A structural concept that is a fitting and effective expression in some given structural material could easily be quite ludicrous in another. As an example, we would have to recognize the igloo as an elegant solution for a temporary structure using an available material with poor tensile properties; the thought of a wooden igloo,

however, is funny because it is incongruous with the character of the material. Similarly, rocket structural concepts that would be elegant in metal are likely to be neither effective nor appropriate for paper phenolic. If the structural configuration of an entire paper phenolic rocket system were conceived to properly reflect the nature of the material, a fitting and even elegant structure might well result, which then could be analyzed in comparison to alternative solutions using alternative materials.

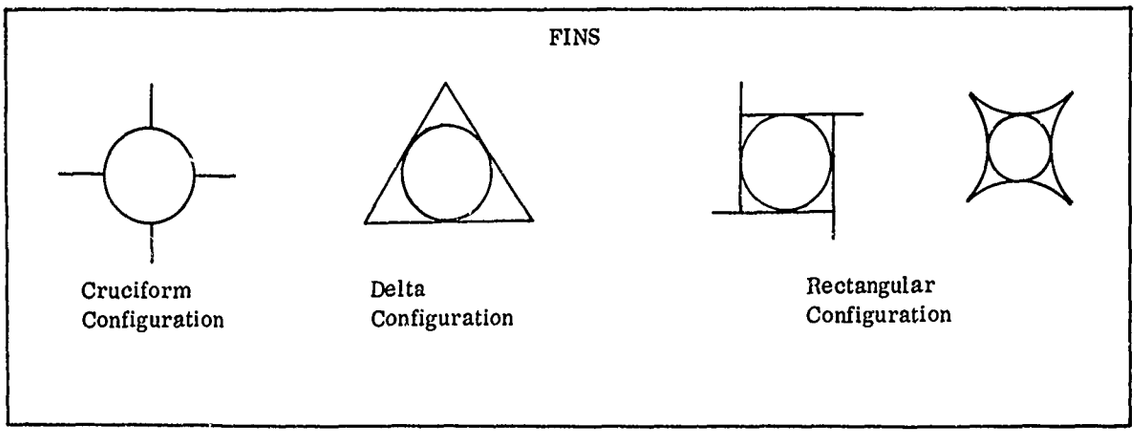
b. Closure Configurations

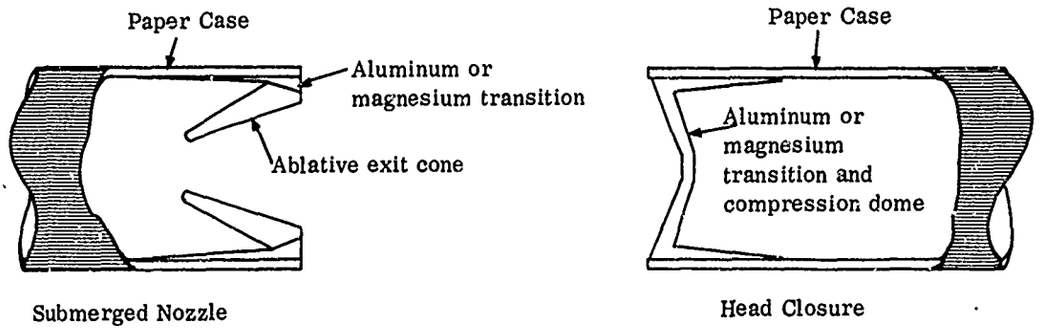
Because of the expected low ratio of longitudinal-to-hoop strength of the paper laminate, the design of vessels of this material is governed by stresses in the longitudinal direction. Thus the effect of geometric discontinuities in such a vessel, and the coincident internal bending moments in the longitudinal direction, is to reduce the pressure capability of the vessel far more than would obtain in an isotropic material. Moreover, prior experience suggests that the shearing strength of a bonded surface, or the interlaminar shear strength of the material, are severely affected by the state of stress normal to the shearing surface. Normal compression, or at least the absence of normal tension, leads to much higher strength values. Accordingly, considerable attention is appropriate to the design in closure regions of configurations which act by development of through thickness compressions (for greater bond effectiveness) and in which the internal pressure applied to the paper cylinder is afforded a very gradual transition along the cylinder length (for control of longitudinal bending moments). In Figure 30 head and aft attachments which employ a tapering aluminum or magnesium internal transition the inner surface of which would be subjected to the full case pressure are shown. Such a transition, together with a compression dome in the head end, assures the existence of an interface compression across the bond surface.

Figure 30 shows a nozzle concept wherein the ablative insert is slotted almost through its thickness, with the slots filled with a low modulus material. The intended function of the slots is to effectively eliminate the hoop stiffness of the ablative insert so that the case will be subjected to the gradually changing pressure throughout the length of the nozzle. Admittedly, this presents an erosion problem but this could be overcome with a more complex adaptation of the same concept.

c. Fin Configurations

For configurations with the case cylinder carried out to the nozzle exit plane, the difficult connection problem of cantilevered fins of cruciform configuration — Figure 30 — can be effectively avoided through the use of a delta or rectangular configuration. Here, the connection could easily be accomplished by bonding the fin to a machined flat-land on the cylinder or alternatively, machining a cylindrical





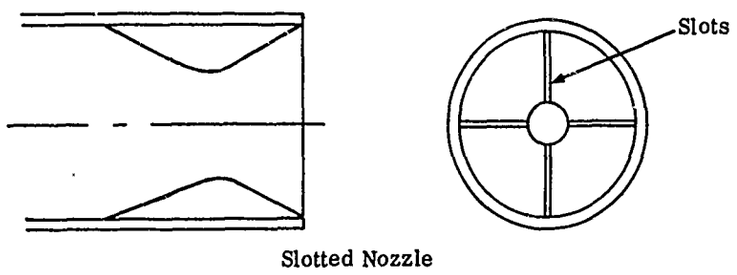


FIGURE 30. STRUCTURAL CONCEPTS FOR FIN AND CLOSURE INTERFACES

depression on the fin. These configurations lend themselves well to the use of either metal or paper for fin material.

Fin configurations where the case cylinder is not carried this far aft present fin connection problems as in the usual metal rockets and are soluble in the usual manner. In effect, such configurations trade the fin connection problem for a more-severe closure problem.

d. Payload and Launcher Attachments

For the attachment of payloads and for the attachment of the rocket to the launcher device it is always necessary to have some type of mechanically fastened joint or to provide suspension points. The various types of mechanically fastened joints, bolted, threaded, shear pins and various types of shear rings all require mechanical properties beyond the capabilities of paper phenolic. Suspension points, whether they be slots, trunnions or clevises, also require mechanical properties and dimensional stability which necessitate the use of metals. In either case it is necessary, in general, to provide metal payload and launcher attachments which must in turn be attached to the case. For reasons concerned with limitations on dimensions of various forms of paper phenolic materials and the general structural limitations which make it almost impossible to obtain efficient closure designs, it would generally be advantageous to have a metal closure. This then presents the closures, or their prolongations, as the optimum locations for payload and launcher interfaces. An interesting payload configuration could evolve from the compression dome by making use of the concave cavity as part of the payload compartment and then making all the necessary interface attachments on the diameter of a prolongation of the dome.

Unfortunately, systems designers do not always want their interfaces at the ends of the motor. Sometimes they want them somewhere along the length of the motor. It is then necessary to mount some form of external ring on the outer diameter of the paper phenolic case resulting in severe stress concentrations caused by the difference in the modulii of the metal ring and the paper phenolic case. These stresses are not necessarily any more severe than those at the closure and additional case thickness might not be necessary. But, it must be remembered that the mounting ring would generally be attached to the case with an adhesive bond and thus the ring must provide adequate surface area for a structurally sound bond. This concern combined with manufacturing limitations would necessitate that the ring be larger and hence heavier than the equivalent built-up area and transition zone that would be required to take out the interface loads in an analagous metal case.

6. EFFECT OF EXPECTED HANDLING AND STORAGE ENVIRONMENTS ON PAPER PHENOLIC MOTOR STRUCTURAL INTEGRITY AND PERFORMANCE(1)

TABLE IX

EFFECT OF EXPECTED HANDLING AND STORAGE ENVIRONMENTS
(Per MIL-R-25534)

	Environment	Conditions	Effect
1.	Temperature	-75° F to +170° F	See Note 2
2.	Vibration	30 hours of ± 5 g @ Resonant Points or 500 mile Rough Road	Better (5)
3.	Shock	Packaged & Unpackaged Drop	Equivalent
4.	Humidity	360 hours @ 120° F 95% R. H.	Equivalent (3)
5.	Rain	2 hours @ 4 in./hr @ 60° F	Equivalent (3)
6.	Salt Spray	20% NaCl spray for 50 hrs	Better (3) (4)
7.	Sand & Dust	Dust Velocity of 100-500 ft/min for 6 hrs. Sand & Dust density @ 0.1-0.5 gms/ft^3.	Equivalent

NOTES:

1. Effects are judged relative to the effect on an equivalent metal case.

2. Material strength diminishes rapidly at temperatures above 100° F and at 170° F the strength has decreased by about 16% from the room temperature value. Fortunately, there is no permanent degradation and full strength returns when the case is brought to room temperature, thus storage at high temperature in itself is not deleterious. Operating temperatures, however, are a necessary consideration for structural design.

3. The material must be coated with a suitable waterproof coating such as TA-D-311.

4. Salt spray has no more effect than that of any other form of moisture.

5. The internal damping of the paper phenolic is substantially greater than that of a metal and would result in a diminished effect of a vibration environment.

SECTION X

METHODS OF IMPROVING PHYSICAL PROPERTIES

SECTION X

METHODS OF IMPROVING PHYSICAL PROPERTIES

1. INCREASE STRENGTH

Approaches in this area seem to be limited to improvements in the phenolic resin since improvements in the cellulose fibers can not be made easily. Micarta is conducting a development program with a new resin system which seems to produce a significant increase in the strength of paper phenolic laminates. Improvements in the resin system would be most noticeable in the axial (across-grain) direction of tubes made of oriented fiber papers.

2. ANISOTROPY

Tubing fabricated from HY-488 has a hoop strength approximately 2.5 times its meridian strength. This is not exactly optimum since the hoop stresses in a cylindrical pressure vessel are only twice as large as the meridian stresses; in a rocket motor case, this ratio is even less because of the throat opening. As a result, we must design a vessel which is more than 1.25 times as thick as it needs to be for hoop stresses in order to withstand the meridian stresses. This is the converse of the situation with a vessel made of an isotropic material; however, in the case of the paper it appears that something might be done to optimize the ratio of the strengths.

The paper used in making oriented fiber tubing is ordinary kraft paper that has been subjected to controlled viscous shearing forces during processing which orient the fibers parallel to the length of the paper. This operation can be performed only on "cylinder" paper machines but most paper manufacturers have these machines. By controlling the intensity of the shearing forces, the degree of orientation can be controlled and varied over a range which provides ratios of with-grain to across-grain strengths from 2:1 to 9:1. When the paper is laminated, the impregnated resin reinforces the fibers but its effect is much more significant in the across-grain direction, resulting in a reduced ratio. For example, Panelyte uses a paper having a ratio of 6:1 in their Grade 6004 tubing, but the finished tube has a ratio of about 2.7:1. The strength ratio of the Micarta paper stock is apparently of the same order as the Panelyte material.

The magnitude of the shearing force is a function of paper thickness. The paper presently used is 3 mils thick and has a ratio of about 6:1, but a paper 5 mils thick, made under the same conditions would have a lower ratio and perhaps optimum properties for a pressure vessel. This thicker paper is available commercially, but we could not arrange to have any tubes fabricated from this material.

It is quite evident from the information now available that it would be desirable to optimize the strength ratio of paper phenolic material used in rocket motor cases, and from the preceding discussions, it does not appear that this would be very difficult. By a proper choice of fiber orientation and resin system, it would be possible to obtain the optimum strength ratio for any given rocket motor. Economics would probably dictate a compromise on the optimum ratio for a conventional pressure vessel, i.e., a hoop strength twice the meridian strength.

3. TEMPERATURE DEGRADATION

The major problem here is with the thermosetting phenolic resin which softens with increased temperature. Although the cellulose fibers degrade at high temperature, they are not the major factor at temperatures below 220°F. At about 220°F, the cellulose will degrade after 1000 hours of exposure. At higher temperatures it degrades after shorter exposures and at lower temperatures, there is no detectable degradation. Again it appears that the problem can be alleviated by the proper choice of impregnating resin, and we understand that resins are available which increase the resistance of the cellulose fibers.

4. COMPOSITE STRUCTURES

One method of improving the overall strength or of improving the strength in a particular direction would be to use composite laminates of paper phenolic and some compatible materials such as glass cloth. Micarta has used this technique to produce convolute-wrapped tubes from a composite sheet made up of one ply of paper phenolic and one ply of glass cloth. This composite does not appear to be cost effective because of the high cost of glass cloth and increased fabrication costs.

5. TESTS

Samples of an improved paper phenolic tubing were obtained from Micarta and meridian tensile specimens were prepared from the tubes. Six of these samples were pulled and the tensile strengths ranged from 9,780 psi to 11,750 psi. The sample at 9,780 psi was isolated with all other samples falling above 10,500 psi. It does not appear that this improved tubing offers any meridian improvement over the HY-488.

These tubes were custom fabricated from a special paper and resin with the intent of obtaining a hoop strength approximately twice the meridian strength. In addition, they were cured under pressure to produce a higher overall strength. Since there was no improvement in meridian strength we did not bother to evaluate the hoop strength and for our purposes the experiment was a failure.

SECTION XI

PRELIMINARY DESIGN STUDIES

SECTION XI

PRELIMINARY DESIGN STUDIES

1. INTRODUCTION

We prepared preliminary designs of several rocket motors and one incendiary device using paper phenolic laminates as a major structural material. The objective of this phase of the program was to provide data for specific comparisons of the effect of paper phenolic on the dimensional envelope, external and internal insulation requirements, center of gravity, vehicle performance and cost effectiveness. All of the units were selected because they were generally representative of a particular class of rocket motors with respect to design requirements, and in most cases they were units with which TCC/Elkton had specific design and production experience. Because of its significance to the conclusions of the study, the cost effectiveness studies for each unit are presented separately, in Section XIII. One of the selected units, the M58A2, was also selected as the design to be used for loading and firing a feasibility demonstration round. Because of the extensive effort involved in this design and the implications of the tests that were performed it too has been treated in a separate section (Section XII). This leaves us, in this section, with the designs of the 2.75 inch FFAR, Tomahawk igniter, XM165 Parachute Flare, and the 1.0-KS-25 Spin Motor.

In preparing each of the designs our objective was to provide only the minimum detail required to make a valid comparison on each of the points cited above. The designs are preliminary designs in all respects that the term preliminary design implies with one exception. The Tomahawk igniter discussion is a comparison of units that have actually been produced and are considered operational.

2. 2.75-INCH FOLDING FIN AIRCRAFT ROCKET

This unit was selected as being generally representative of the category of inexpensive, unguided, rocket propelled weapons. Our objective was to make a direct substitution of paper phenolic and other plastics for the present all-metal hardware of the 2.75 inch FFAR. The design is shown in Figure 31. One unique feature of the design is the method of retaining the head closure. A simple flat metal disc forms the head closure and it is retained against the pressure load by a cylindrical sleeve bonded to the internal wall of the case. The edges of the disc are bonded to the case with an elastomeric adhesive which serves as a pressure seal yet allows the edges of the flat plate to rotate and the case to expand locally. Such a design minimizes the discontinuities at the closure joint and takes advantage of the warhead compartment space to obtain the necessary shear area for the adhesive structural bond.

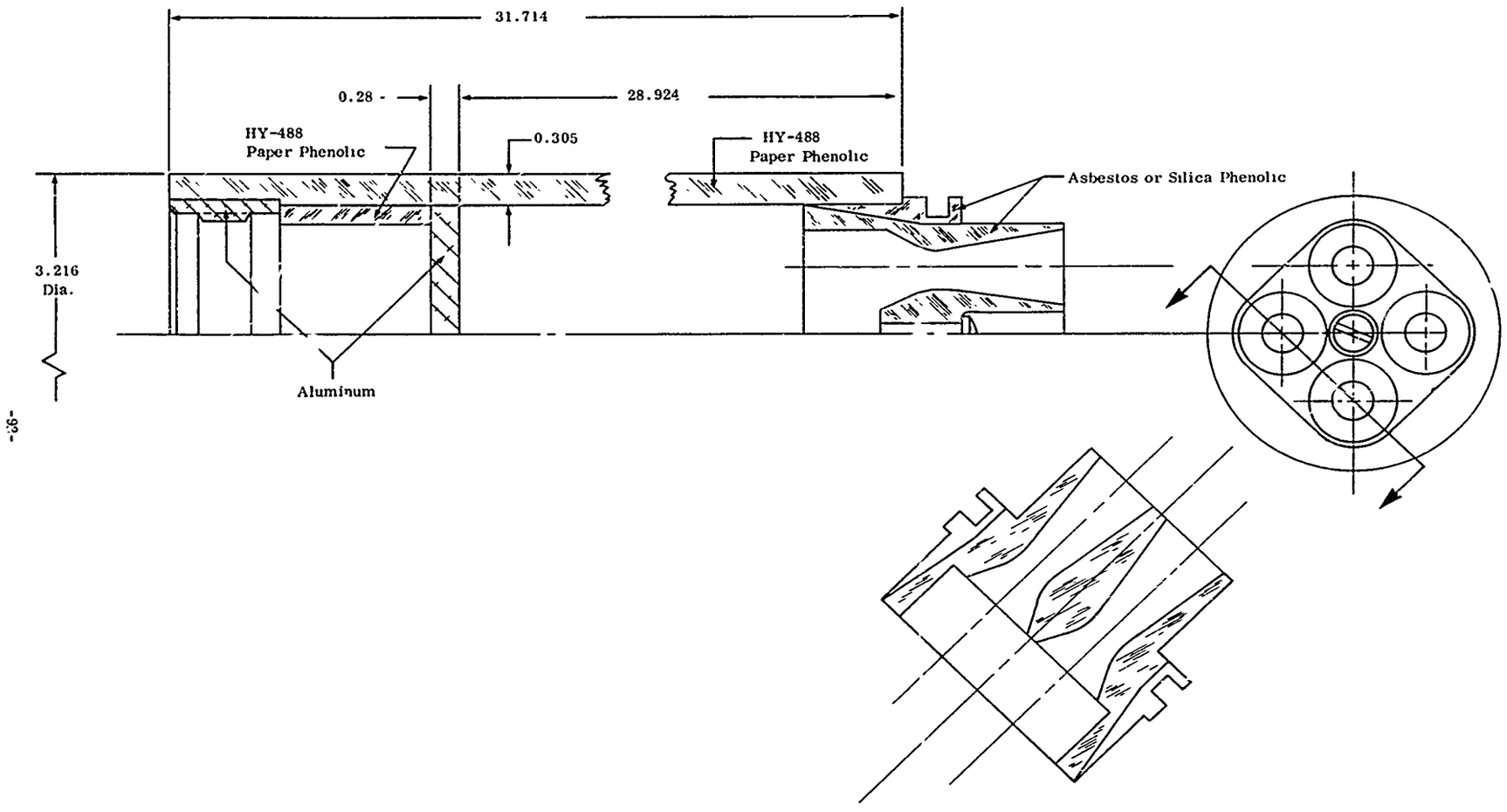


FIGURE 31. PAPER PHENOLIC 2.75 INCH FAIR

TABLE X

WEIGHT COMPARISON OF METAL AND PAPER CASE 2.75 FFAR

	MK 4 Mod 8 2.75 FFAR	Paper Phenolic 2.75 FFAR
Case	2.375	4.64
Nozzle and Fin Assy.	1.870	1.28
Misc. Inert Parts	0.316	0.27
Igniter	0.045	0.045
Propellant	6.40	6.400
	11.006	12.635

From the performance standpoint the paper phenolic unit does not compare favorably with the existing unit. The paper phenolic unit is 0.466 inches greater in diameter, 0.30 inches longer, and 1.629 pounds heavier than the MK 4 Mod 8 unit. All of these deficiencies are due to the low strength to weight ratio of the paper phenolic and the large bond areas required to overcome the low shear strength of the paper phenolic. Both the increase in diameter and the increase in weight will decrease the burnout velocity of the round with the result that the burnout velocity of the paper phenolic round will be about 15% lower than that of the existing 2.75 inch rocket. There does not appear to be any significant effect on C. G. location due to the change in case materials. The change in materials had no significant effect on internal or external insulation requirements.

The limiting material properties for this design were the meridian tensile strength and the interlaminar shear strength. At 150°F, the maximum operating temperature of the motor, the minimum expected strengths were 8,000 psi and 1100 psi respectively. A 1.25 safety factor was applied to each value to take into account the effect of defects and cyclic loading and an additional 2,000 psi were subtracted from the available meridian strength to account for discontinuity effects.

3. TOMAHAWK IGNITER

Both a metal case and paper phenolic case Pyrogen igniter for the Tomahawk rocket motor have been produced by Thiokol and are in service. Several versions of each are in use, and one of each type is shown in Figure 32. All of the units have the same ballistic performance and meet the same interface requirements. It is impossible to give a direct comparison of weights and costs between a paper phenolic and a metal igniter because other differences exist beside the case material. These differences are primarily in the squibs and ignition circuitry and effect both weight and cost. The two depicted are the most nearly similar units of each type.

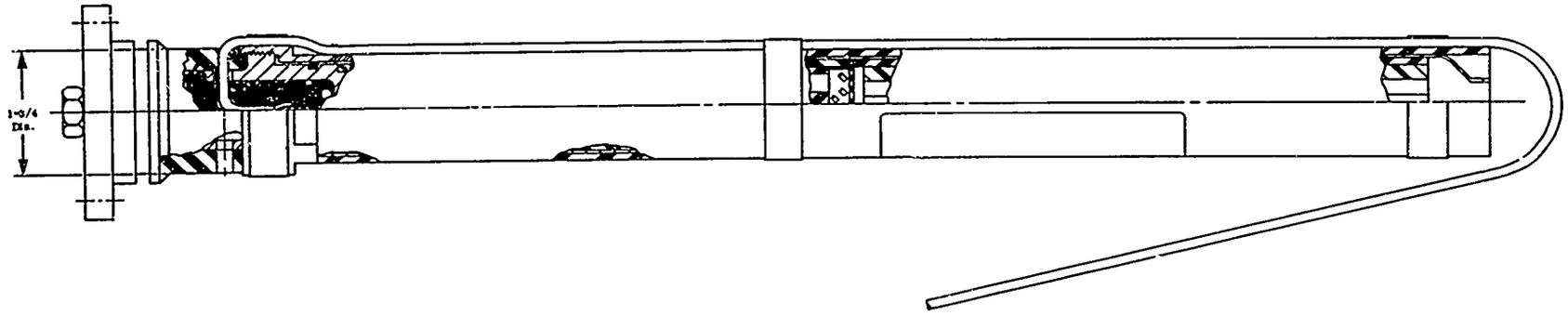
The metal parts of the metal igniter must be well insulated to prevent a breakup of the igniter case during motor operation and the resulting possibility of damaging the motor throat when the metal parts are ejected through the nozzle. However, the paper phenolic igniter requires extensive insulation only over the aft portion of its case to prevent this problem. All components forward of this point are of paper phenolic. Most of the material of these parts is consumed in the combustion process and those which are ejected are of such low mass as to constitute no hazard to the throat.

At the case diameters and chamber pressures of this application, the metal tube wall-thickness is limited by manufacturing limitations to about twice the thickness required by stress considerations. This restriction offsets the superior strength to weight ratio of the steel and, because of the decrease in insulation requirement, the paper phenolic igniter is about 0.5 pounds (16%) lighter than the metal igniter. The center of gravity is inconsequential in this application and was not determined.

4. XM165 PARACHUTE FLARE

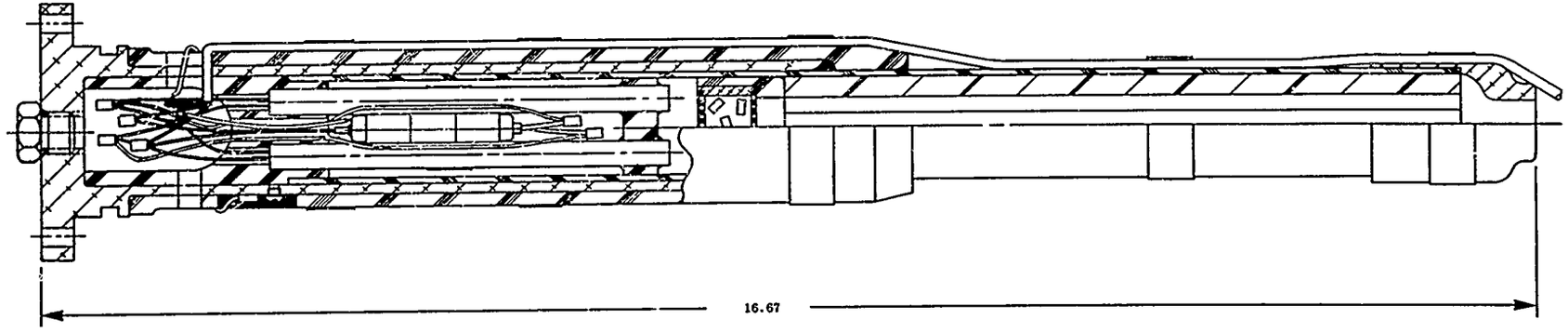
This design presents an application in response to a rather unique requirement. The tube shown in Figure 33 serves as a casing and launching tube for an aircraft-launched parachute flare. After being dropped from the aircraft, a fuze inserted in the metal base pressurizes the tube, ruptures the "MYLAR" diaphragm and ejects the parachute flare. The specific requirements for the tube are that the diaphragm not burst below 50 psi and the case not burst below 150 psi. In the present design, the tube is made of aluminum and is brazed to the aluminum aft closure. The forward closure is formed by a crimp and wadding somewhat similar to a shotgun shell. Although the present design functions satisfactorily and was very cheap to produce, the peculiarities of the Vietnamese Conflict have imposed a new requirement. It was feared that the Viet Cong were salvaging the expended casings and using them as a ready source of supply for metal for use in fabricating weapons. In order to deny the Viet Cong this source of supply, the Army wished to minimize or eliminate the metal in the casing.

E258-67-37



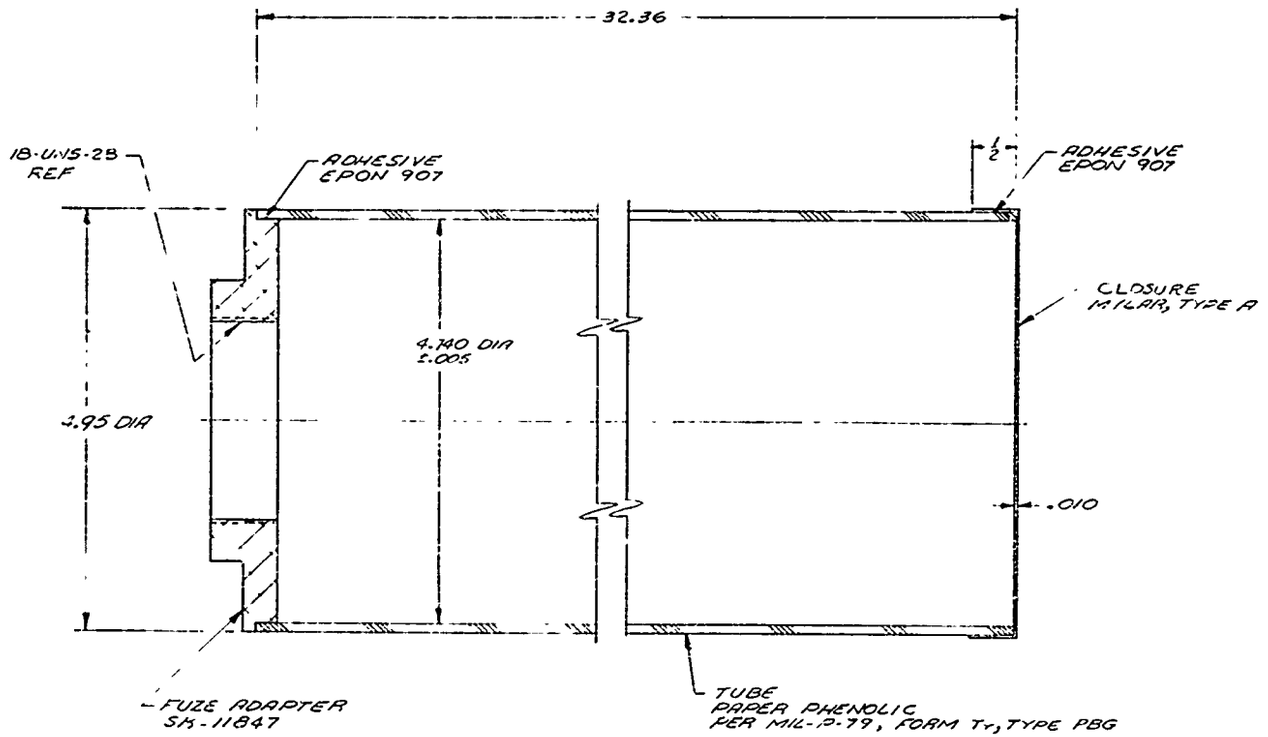
A. STEEL PYROGEN IGNITER

E258-67-36



B. PAPER PHENOLIC IGNITER

FIGURE 32. TOMAHAWK IGNITERS



QTY REQD PER DASH NO.	ITEM NO.	CODE IDENT	PART OR IDENTIFYING NO.	NOMENCLATURE OR DESCRIPTION	MATERIAL	SPECIFICATION

LIST OF MATERIAL OR PARTS LIST

UNLESS OTHERWISE SPECIFIED.
DIMENSIONS ARE IN INCHES
TOLERANCES
.XX=± 030 .XXX=± 010
ANGULAR ± 30' FRACTIONS ± 1/16
BREAK SHARP EDGES .003-.015
ALL SMALL FILLETS .020-.040 R
THREADS PER FED. HNDBK H-28 AND SUPPLEMENTS
DIMENSIONING PER MIL-STD-8
WELD SYMBOLS PER JAN-STD-19
SURFACE ROUGHNESS SYMBOLS PER MIL-STD-10
ALL FINISHED SURFACES 125

DRAWN	R.D. NESTER	5 MAR 63
CHECKED	C. JOHNSON	6 MAR 63
ENGR		
ENGR		6 MAR 63
ENGR		
USER		
STRESS	N/A	
SAFETY		
APPD		

DESIGN ACTIVITY APPROVAL

Thiokol. CHEMICAL CORPORATION
ELKTON DIVISION ELKTON, MARYLAND

INERT PARTS ASSY
FLARE, AIRCRAFT, PARACHUTE, XM164
FOR
PICATINNY ARSENAL

CODE IDENT NO	SIZE	
07299	C	LO-2327

SCALE	WEIGHT	CALC ACTUAL	SHEET

FIGURE 33. XM165 PARACHUTE FLARE

Two prototypes of this design, with metal rather than Mylar closures, were fabricated for design evaluation. The first was hydroburst at Elkton and failed at 300 psi. The second was shipped to Picatinny Arsenal for their evaluation. It was not feasible to fabricate Mylar closures for either of these units because of high costs for molds and schedule.

The design shown uses a metal aft closure similar to that used in the current XM165 Flare. It is felt that with some evaluation testing we could find a suitable nonmetallic material for the aft closure but at that time we did not have adequate design data to select a completely satisfactory material. Further, Picatinny Arsenal was not very concerned about metal in this portion of the casing. It was not necessary to make any changes in the metal aft closure to adapt it to the paper phenolic case. The adhesive joint geometry is identical to the existing brazed joint geometry.

The tube used in this application was made of Panelyte Grade 550 paper phenolic. This material is significantly less expensive than HY-488 and, although its strength is also less than HY-488, it is adequate for this application. The minimum meridian tensile strength of Grade 550 is 8,000 psi at 70°F. A design safety factor of 3.0 on ultimate was used to take into account uncertainties of environmental effects and the expected storage and handling conditions. There would be no appreciable gain in reducing this margin as neither envelope nor weight are very critical in this application.

The substitution of paper phenolic had the effect of increasing the case diameter by about 0.10 inches. The effects on insulation requirements, and center of gravity are irrevelant in this application.

5. 1.0-KS-25 SPIN MOTOR

This motor, depicted in Figure 34, is used to impart a spin force to a classified experimental device and is typical of the structural design techniques used in very small rocket motors. Only one change was made from the original design: a paper phenolic tube is used for the case rather than an aluminum tube. This substitution had the effect of reducing the weight by an insignificant amount, due to manufacturing limitations on the minimum thickness of metal tube. There were no changes in the dimensional envelope, insulation requirements, center of gravity or performance.

The case design is very conservative with a safety factor of 1.6 on ultimate meridian stress at 150°F. This factor should be adequate to take into account both fatigue effects and discontinuities.

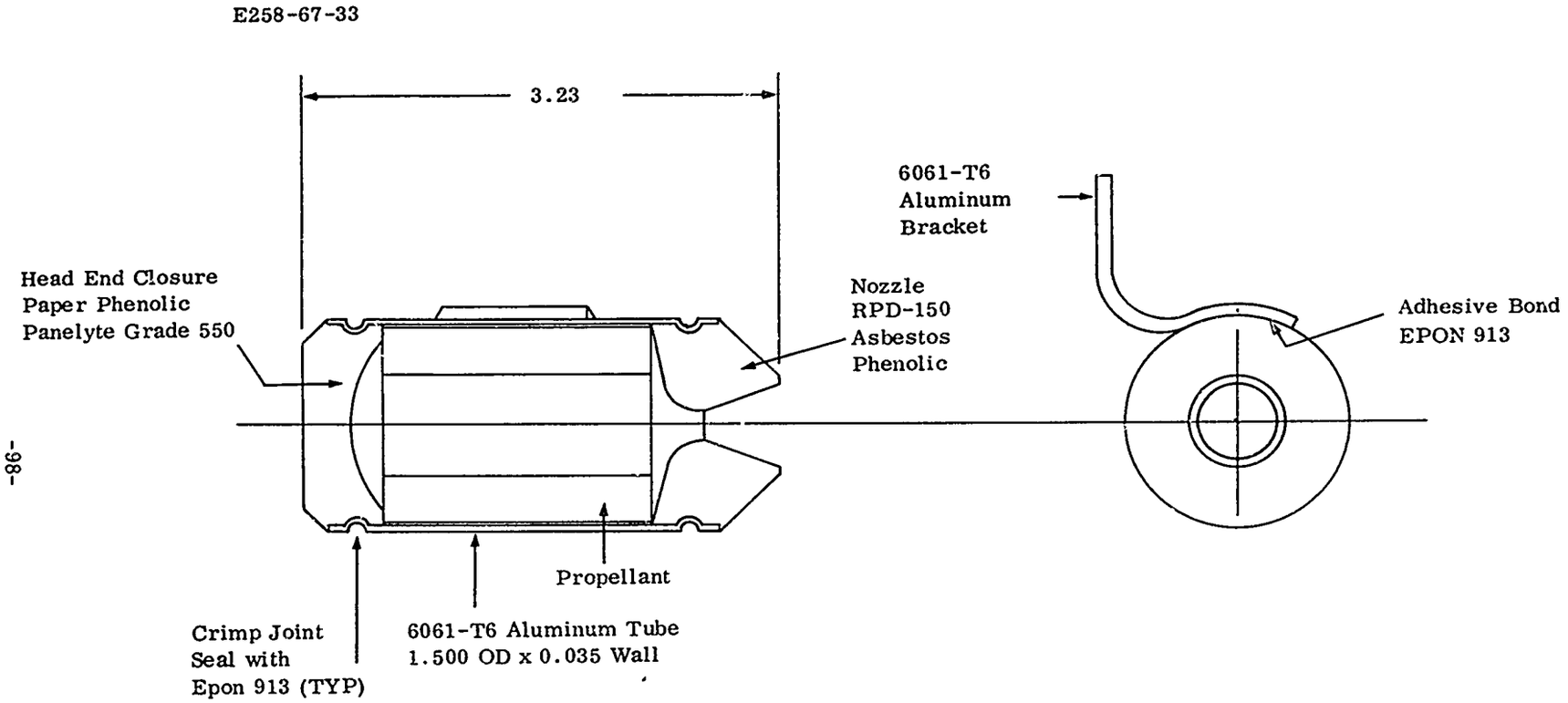


FIGURE 34A. METAL CASE, 1.0-KS-25 SPIN MOTOR ASSEMBLY

E258-67-32

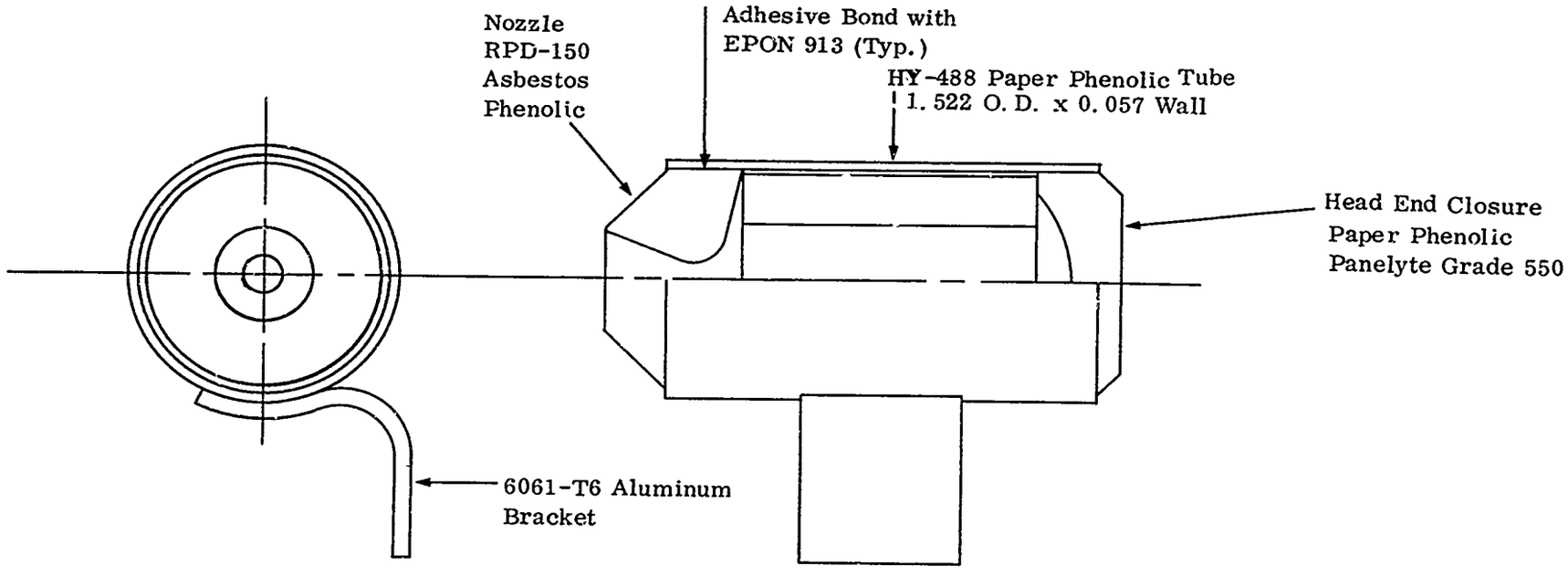


FIGURE 34B. PAPER PHENOLIC CASE

SECTION XII

DESIGN AND DEMONSTRATION OF A PROTOTYPE PAPER PHENOLIC M58A2

SECTION XII

DESIGN AND DEMONSTRATION OF A PROTOTYPE PAPER PHENOLIC M58A2

1. INTRODUCTION

As the culmination of the program it was our objective to successfully static test fire a prototype M58A2 to demonstrate the feasibility of utilizing paper phenolic laminates as the principle structural material for a rocket motor case. A successful demonstration was performed on November 13, 1967.

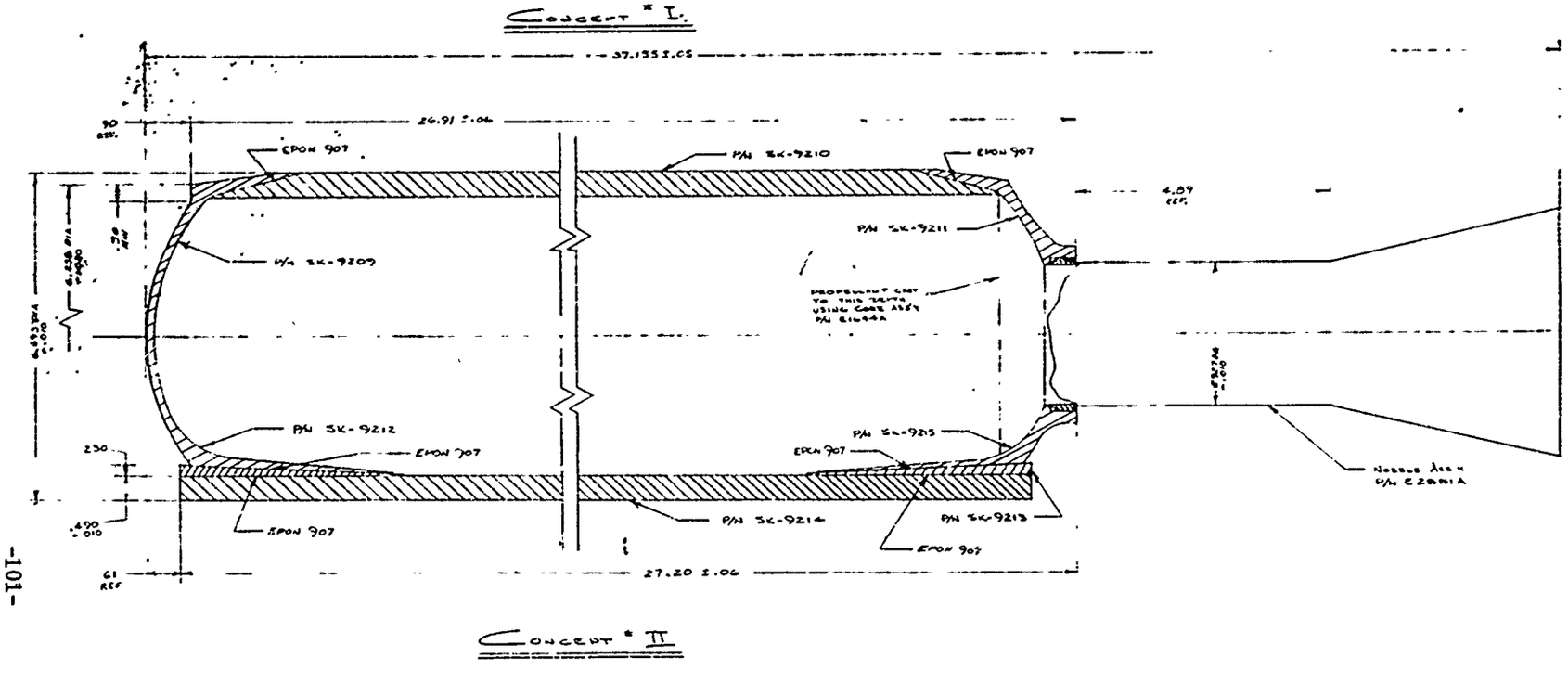
Our design criteria for the prototype paper phenolic M58A2 were simple. They were to build a motor to the same specifications as the original, metal case M58A2. Originally our interpretation of these criteria was quite literal in that we used the safety factors that were used in the original motor. Later, however, this interpretation was liberalized to permit the use of safety factors that would give a design with the same reliability that the M58A2 was originally designed to provide. This change was to take into account advances in the art of solid propellant rocketry since 1957, the year the M58A2 was designed.

It was decided, with the concurrence of AFRPL, that it would only add unnecessary expense and difficulty, without any meaningful gain, to duplicate the thrust skirt interface and the external configuration of the headcap. Consequently these geometries were optimized for compatibility with test and production tooling and for ease of fabrication.

A second major decision involved the use of metal end closures. It is not possible to obtain either paper phenolic rod or sheet in the dimensions necessary to fabricate the M58A2 end closures from a single rod or sheet. It would be necessary to piece the closures together from four or five concentric, thick wall cylinders by nesting each cylinder inside the next larger one. Our studies convinced us this technique was necessary and that it could never be more cost effective than a one piece metal closure. Consequently, since any motor of this size would probably use metal closures, there was nothing to gain by using paper phenolic closures in our demonstration motor. Aluminum closures were therefore used in all the designs discussed below.

2. DESIGN AND PROOF TESTS

During the first stages of this phase our objective was to design and hydroburst two cases, each case using a different design concept for the closure to case joint. One of these concepts was then to be selected for the demonstration unit. The two concepts depicted in Figure 35 were the first two developed and will be identified as



ITEM NO	CODE IDENT	PART OR IDENTIFYING NO	NOMENCLATURE OR DESCRIPTION	MATERIAL	SPECIFICATION
			LIST OF MATERIAL OR PARTS LIST		

Thiokol. CHEMICAL CORPORATION
ELKTON DIVISION ELKTON, MARYLAND

INERT PARTS ASS'Y

TC-M-49-1

07299 DLO-2282

FIGURE 35. CONCEPT I AND CONCEPT II CASE DESIGNS

Concepts I & II. Both of the joints used a tapered adhesive joint to minimize discontinuities caused by difference between the modulii of the metal closure and the paper phenolic tube. The major difference in the two is that in one closure the metal closure forms the male portion of the joint and in the other the female portion.

Both of the cases were designed for a proof pressure of 2, 650 psi and a minimum burst pressure of 3, 100 psi using a design factor of 1.3 on the minimum ultimate strength at 150° F. Both the proof pressure and minimum burst strength requirement had to be demonstrated at 70° F. It was only necessary to demonstrate analytically that the minimum burst pressure requirement could be met at 150° F. These requirements for proof and minimum burst pressure are the model specification requirements for the M58A2 (Ref. 7). A safety factor of 2.0 was used on the manufacturer's listed values for the adhesive tensile shear strengths.

A structural analysis of the two cases was performed using the technique described in Section VI. This analysis indicated that the designs were adequate and, strangely, showed that because of compensating changes in the ultimate strength and modulus, the minimum burst strength was nearly the same, and above 3, 100 psi, at both 70° F and 150° F.

Efforts to perform a successful proof test and burst test of the Concepts I and II designs were uniformly unsuccessful. Three Concept I units and one Concept II unit were hydrotested and in every instance, the case failed in a case-to-closure joint at a pressure considerably below the proof pressure, as is detailed in Table XI.

TABLE XI

SUMMARY OF HYDROTEST RESULTS

	Burst Pressure, psi	Failure Location	Surface Preparation
Concept I	900	Nozzle End	Surfaces lightly abraded with emery cloth and cleaned with trichloroethylene.
	650	Head End	Surfaces cleaned with MEK and primed with Grip Cald. Primer cleaned with MEK before adhesive was applied.
	1250	Nozzle End	Surfaces lightly grit blasted. Aluminum etched with chromic acid followed by rinse with distilled water. Paper phenolic cleaned with MEK.

	Burst Pressure, psi	Failure Location	Surface Preparation
Concept II	1200	Head End	Surfaces lightly abraded with emery cloth and cleaned with trichloro-ethylene.

Only one test has been performed with the Concept II design. In this test the failure was due to a combination of poor fit and poor adhesion of the adhesive to the aluminum (Figures 36-38). Further tests on this design were canceled in order to devote more time to the resolution of the problems with the Concept I design. The Concept I configuration is easier to case and was thus preferred for the demonstration firing. Since available case materials were in limited supply, the Concept I design was given priority.

In the first test with Concept I, the failure resulted from a single unbonded area representing about 25 percent of the total bond surface (Figures 39 and 40). In this area the adhesive had not adhered to the aluminum closure. For the second test, both the closure and case surfaces were coated with "Grip Clad" (TM of Sherwin-Williams) primer before the adhesive was applied. This reduced rather than improved the adhesion strength as was evidenced by the fact that failure occurred over the entire surface of the bond. The closure neatly and cleanly separated from the case, without damage to either (Figure 41). There were only faint traces of "Grip Clad" on the closure, whereas the bond surface of the case was uniformly coated with adhesive topped with the primer that had been applied to the closure.

Elaborate procedures and precautions were followed in preparing for the third test of Concept I. Each closure was individually fitted to a particular case end to ensure a good fit and the desired bond line thickness (0.005 inch), new surface preparation techniques were used (Grit blasting followed by a chromic acid etch), and great care was taken to prevent contamination of the cleaned surfaces. Even then, however, we were not successful in obtaining a satisfactory bond. The adhesive did not satisfactorily adhere to 15 percent of the total bond area (Figure 42).

Since the previous failures were due to imperfections in the adhesive bond and since it did not appear that these imperfections could ever be reduced to a level consistent with the present design safety factor, the design safety factor for the adhesive shear strength was increased from 2.0 to 4.0. It was also decided to change the joint configuration to minimize the manufacturing problems associated with maintaining the proper glue line thickness. A tubular lap joint was substituted for the tubular scarf joint used in the previous designs but the case wall thickness was not changed.

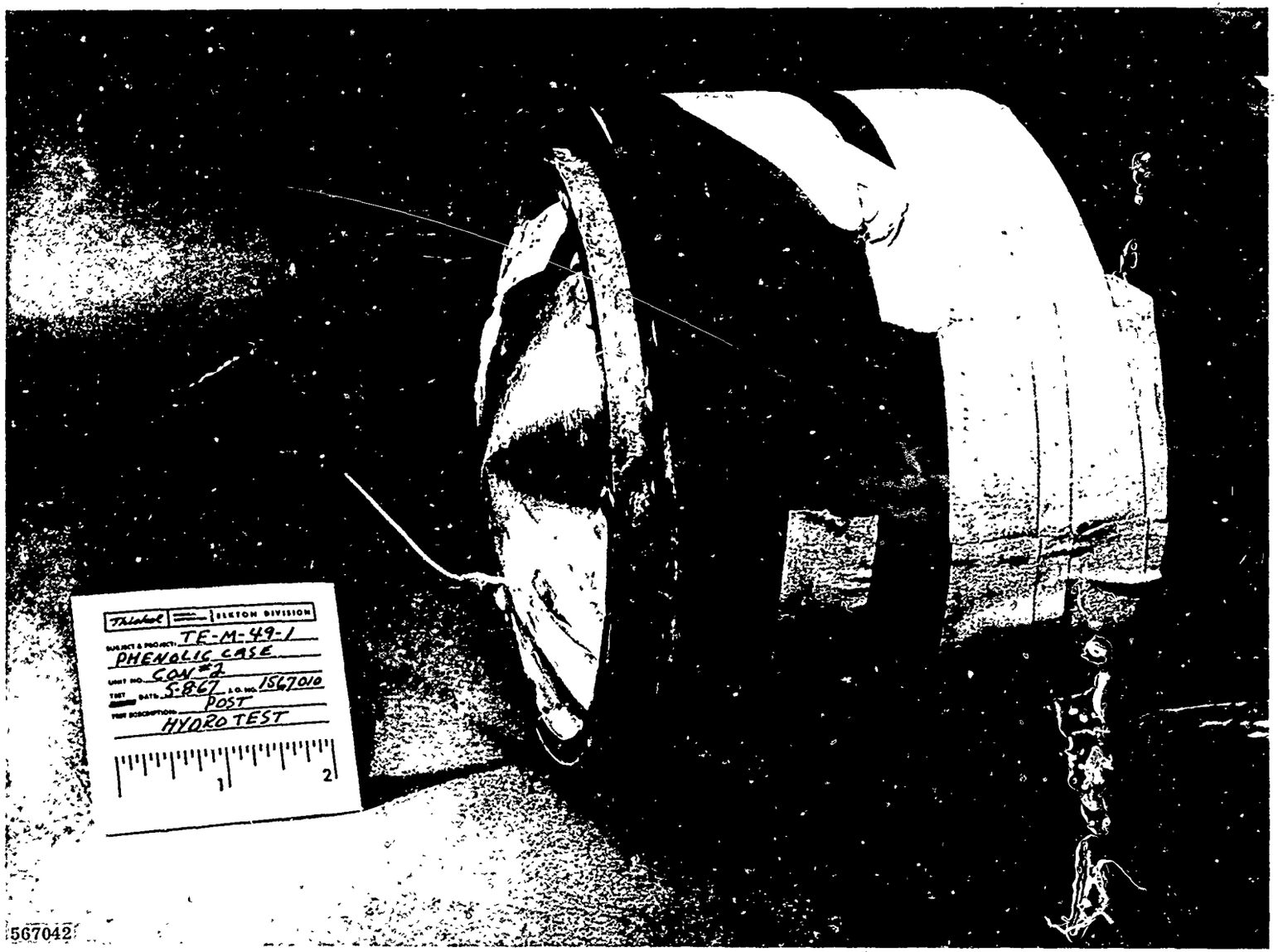


FIGURE 36. AREA OF FAILURE, CONCEPT II HYDROTEST

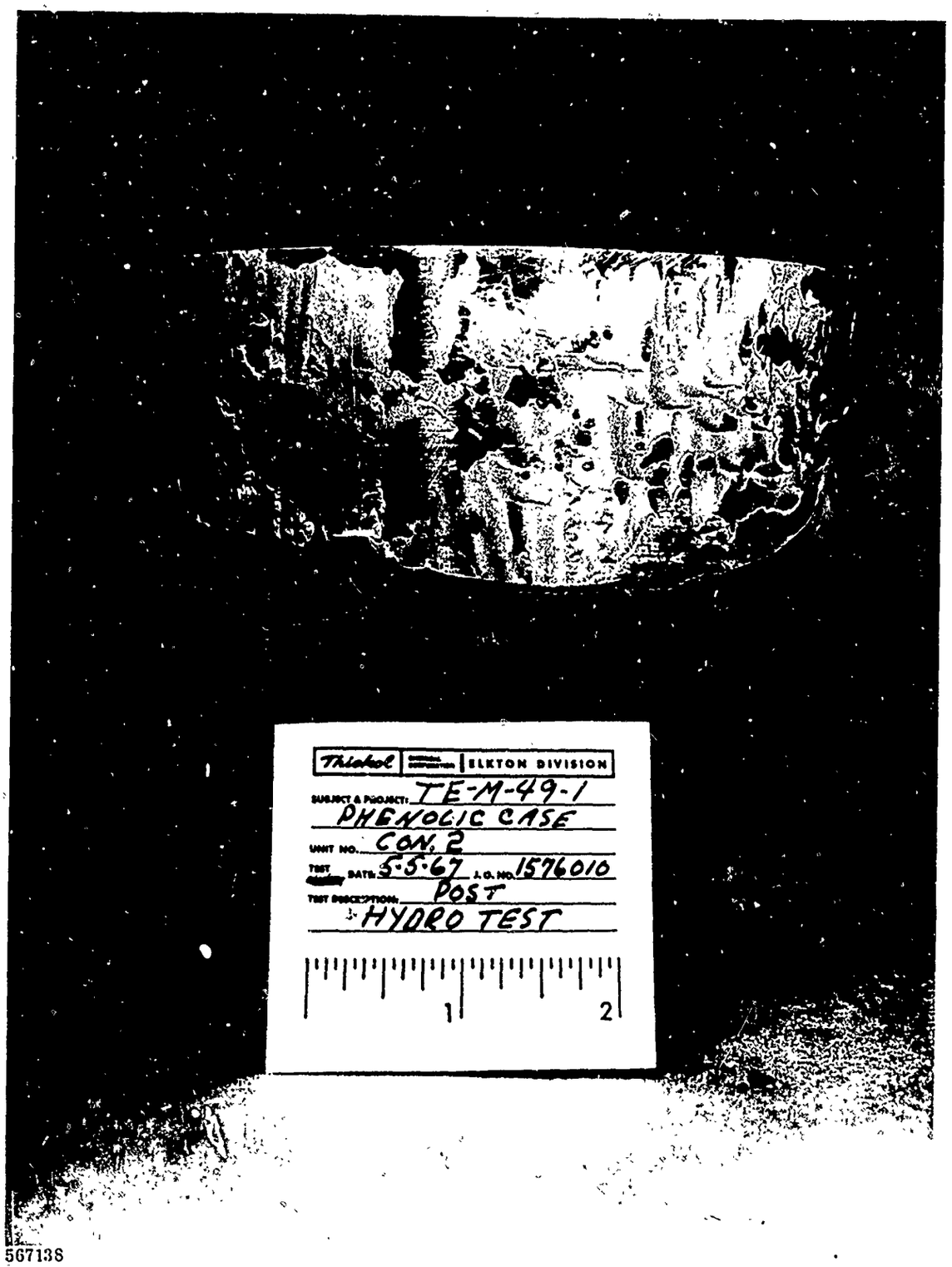
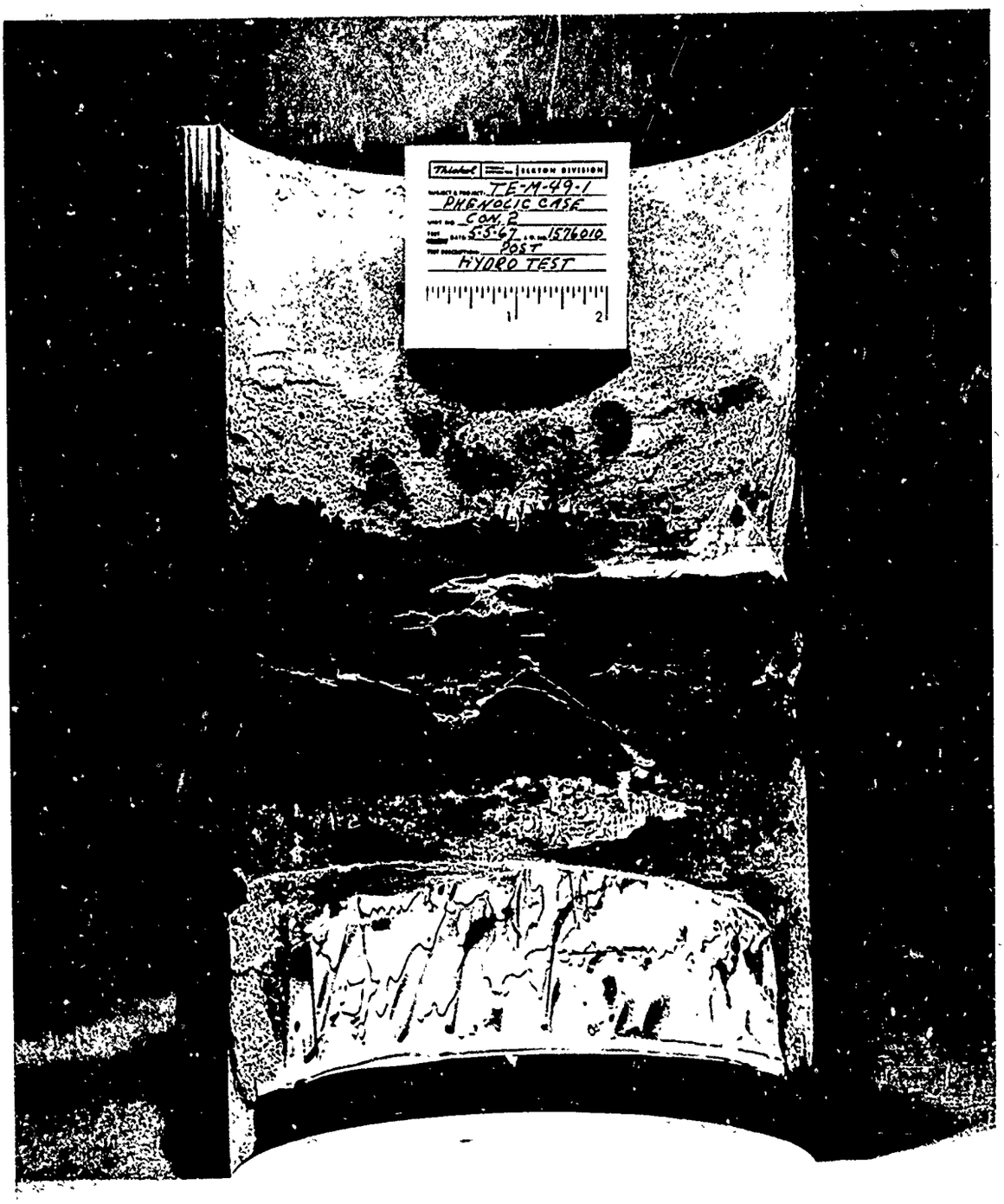


FIGURE 37. ADHESIVE BOND IN AREA OF FAILURE, CONCEPT II HYDROBURST



567137

FIGURE 38. ADHESIVE BOND IN AREA OF FAILURE, CONCEPT II HYDROTEST

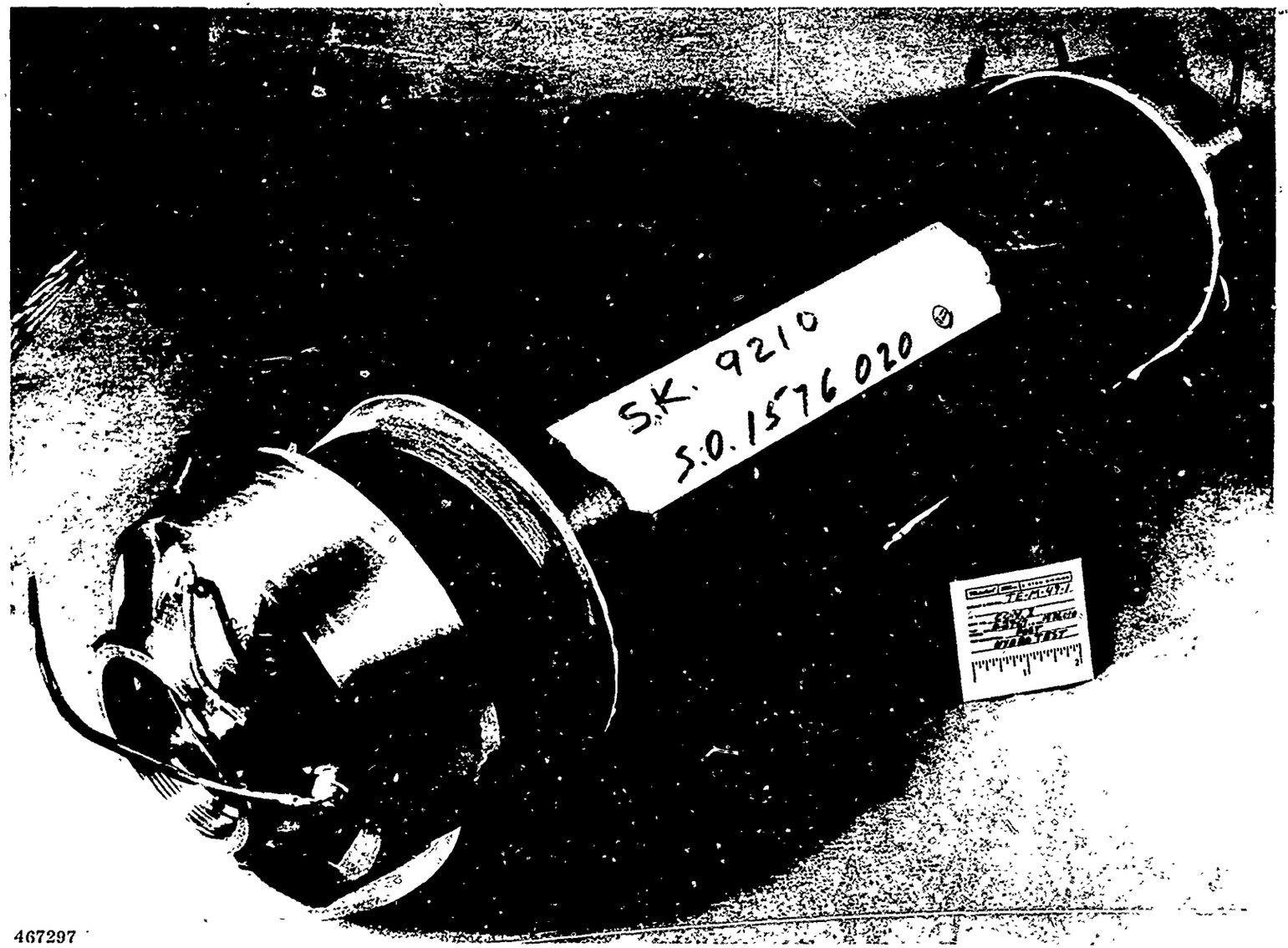


FIGURE 39. BURST CASE, CONCEPT I, TEST I

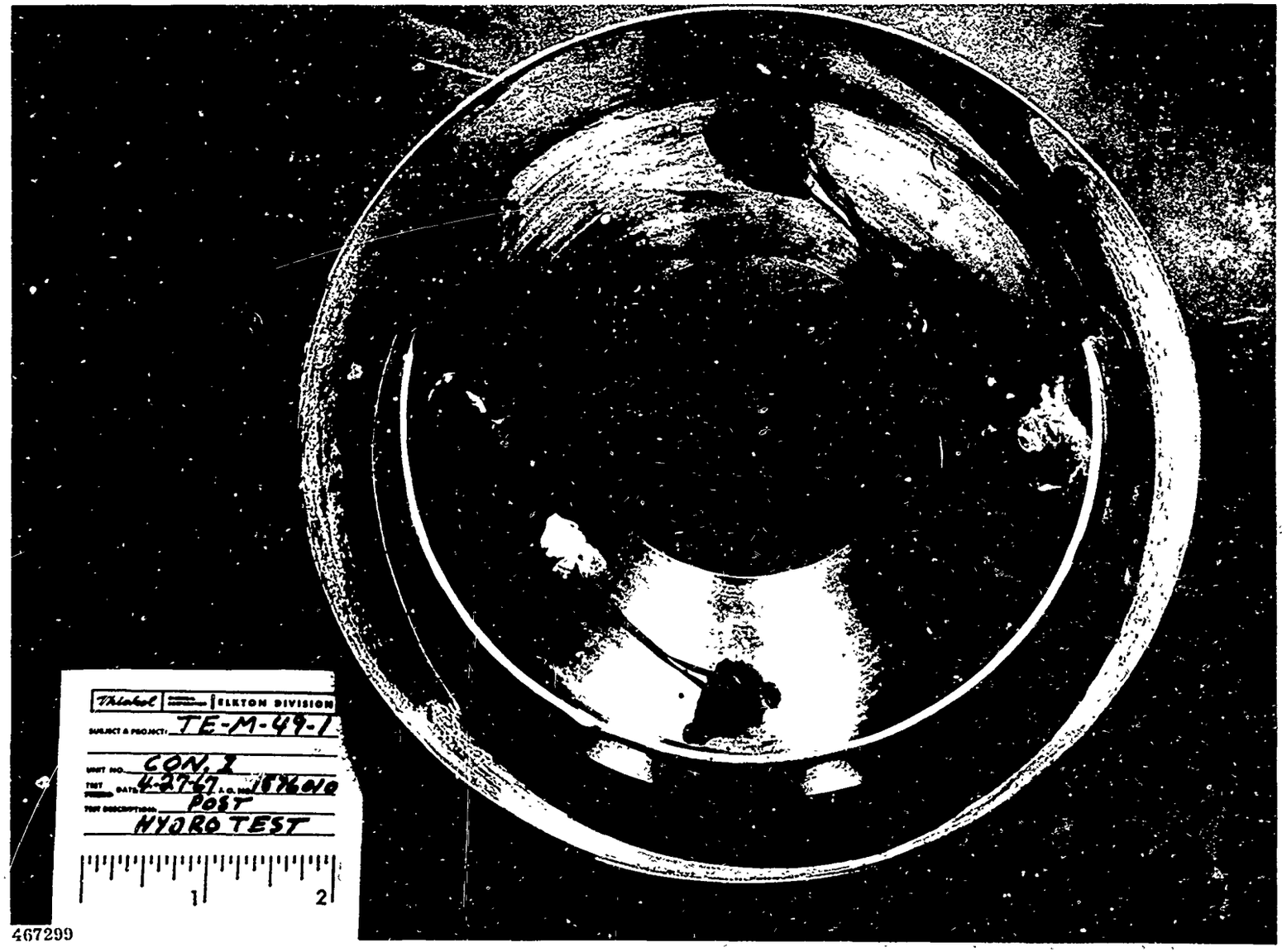
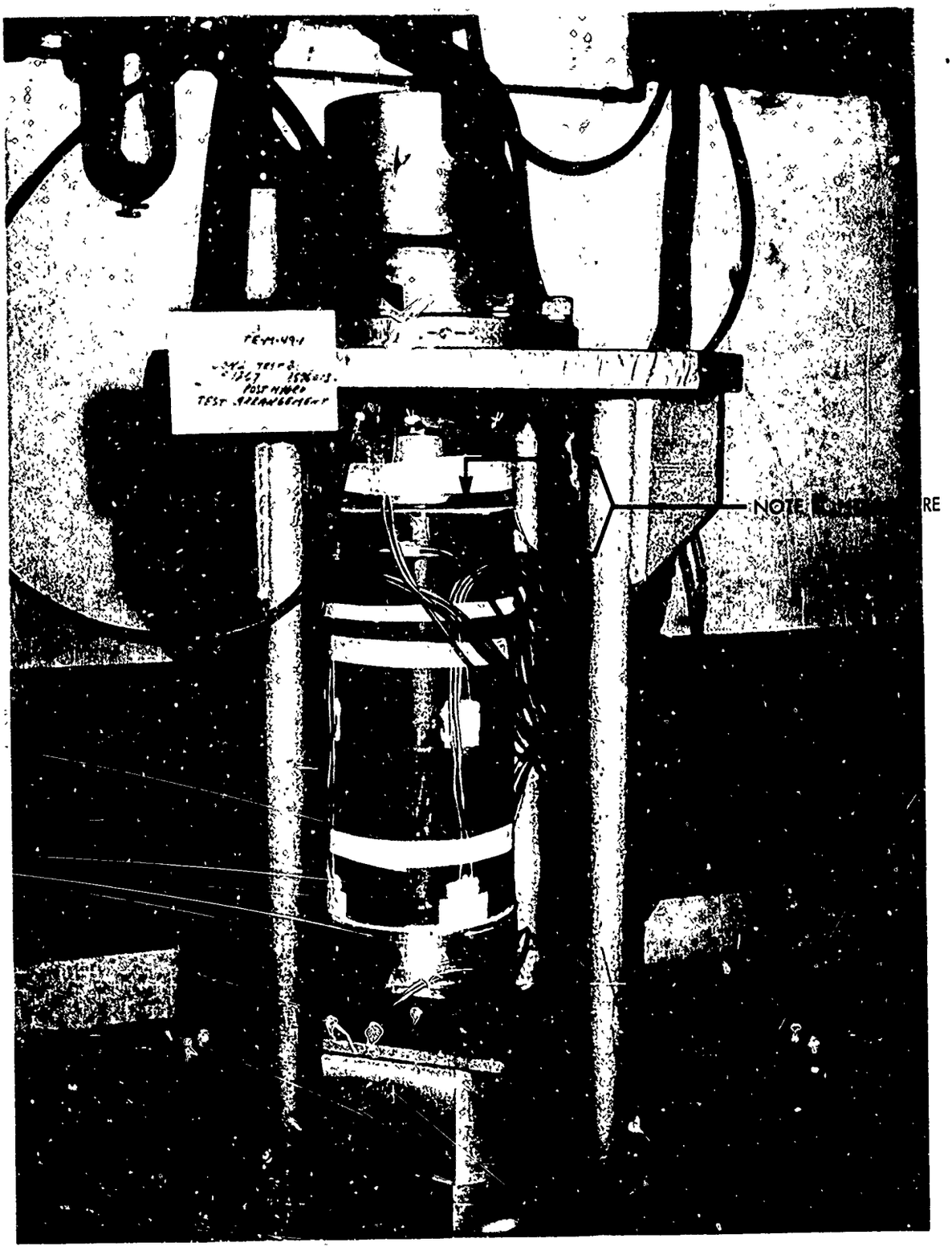


FIGURE 40. ADHESIVE BOND IN AREA OF FAILURE, CONCEPT I, TEST I



567132

FIGURE 41. BURST CASE. CONCEPT I, TEST II

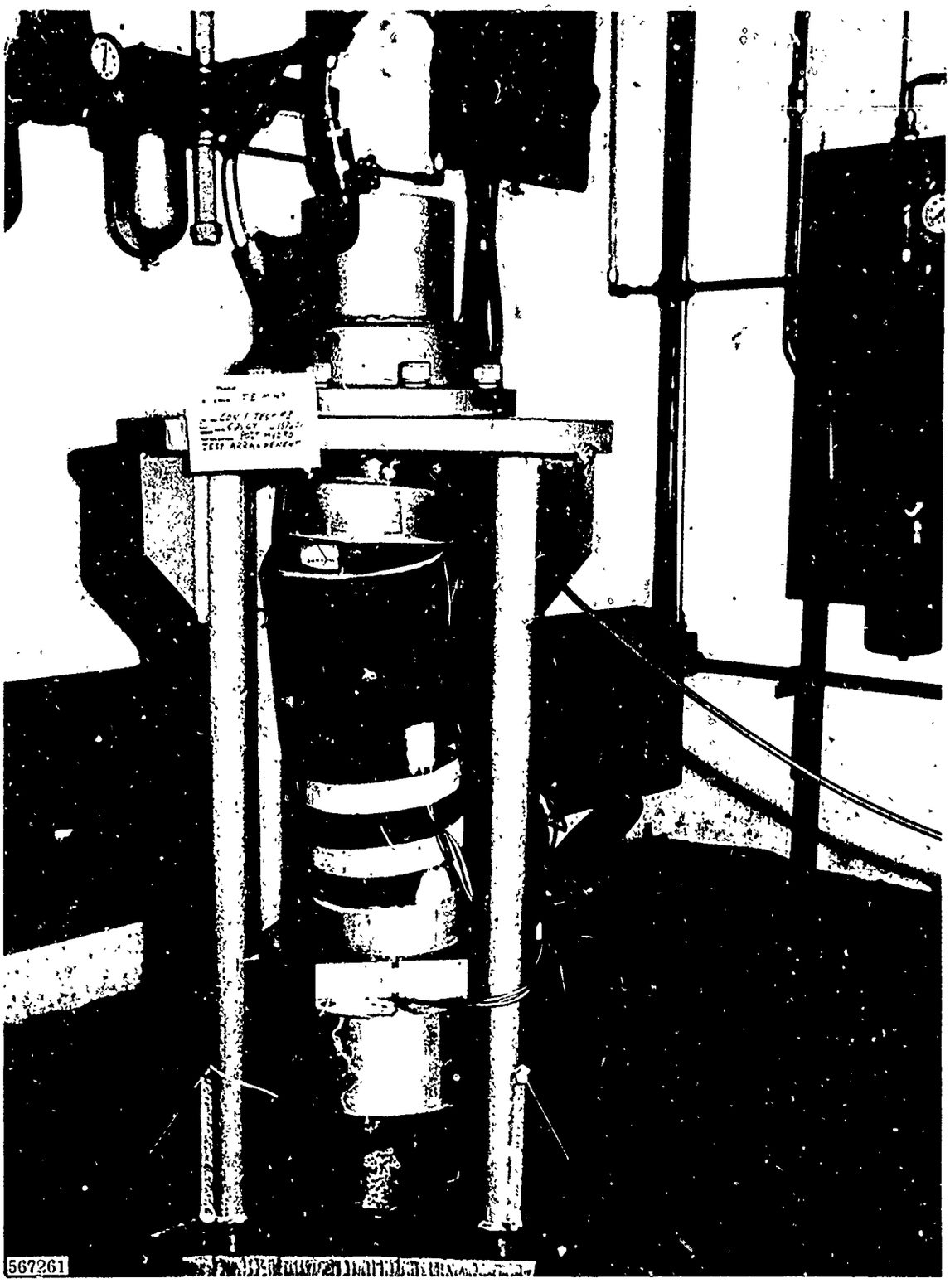


FIGURE 42. BURST CASE, CONCEPT I, TEST III

During the period of redesign, Mr. S. P Gualillo of the Huntsville Division visited Elkton to discuss the design and the adhesive bonding problems. He suggested that the adhesive be rubbed into the surface with either the hand or a spatula to remove air bubbles and to ensure penetration of the adhesive into the pores and crevices on the surface. This technique was adopted.

A prototype paper phenolic M58A2 of the new design (Figure 43) was successfully hydrotested on July 28, 1967. The case was pressurized to 2, 650 psi and held at this pressure for one minute. Subsequently, the pressure was released and the case was then repressurized until it burst. The burst pressure was 3, 200 psi, whereas the minimum required burst pressure for the M58A2 is 3, 100 psi.

This case apparently failed at two independent points (Figure 44). One failure was due to meridian stresses at a point in the paper phenolic tube approximately 1/8 inch forward of the adhesive joint at the aft end of the case and propagated throughout the phenolic tube in both hoop and longitudinal directions. The other failure occurred in the aluminum nozzle adapter in the longitudinal direction in the region of the thread relief; it is not known if the metal failure occurred before, or after, or simultaneously with the failure in the phenolic tube.

The adhesive bonds of this case had been inspected with an ultrasonic tester and there were no indications of voids or unbonded areas.

A second case of the same design was then fabricated for use in the demonstration firing. This case was hydrotested on August 30, 1967, and burst at 2, 200 psi, while we were attempting to pressurize the case to the intended proof pressure of 2, 650 psi. As in the previous case, the failure originated in the paper phenolic tube in the region of the joint discontinuity (Figure 45). There was no evidence of failure in the adhesive bond.

The case fragments were subjected to a detailed visual examination and compared to fragments from the case which had burst at 3, 200 psi. There was only one noticeable difference between the fracture zones in the two cases. In the case which burst at 2, 200 psi, there was a resin-rich area at the origin of the failure approximately 1/4 inch long in the hoop direction and 1/32 to 1/16 inch wide. From examination of other pieces of the two cases, it appears that resin-rich areas are not uncommon in the material, however, we could not determine if there were any such areas located in the highly stressed region around the joints of either case.

The following tensile data were obtained from three NOL Ring Specimens that were cut from the material of each of the cases.

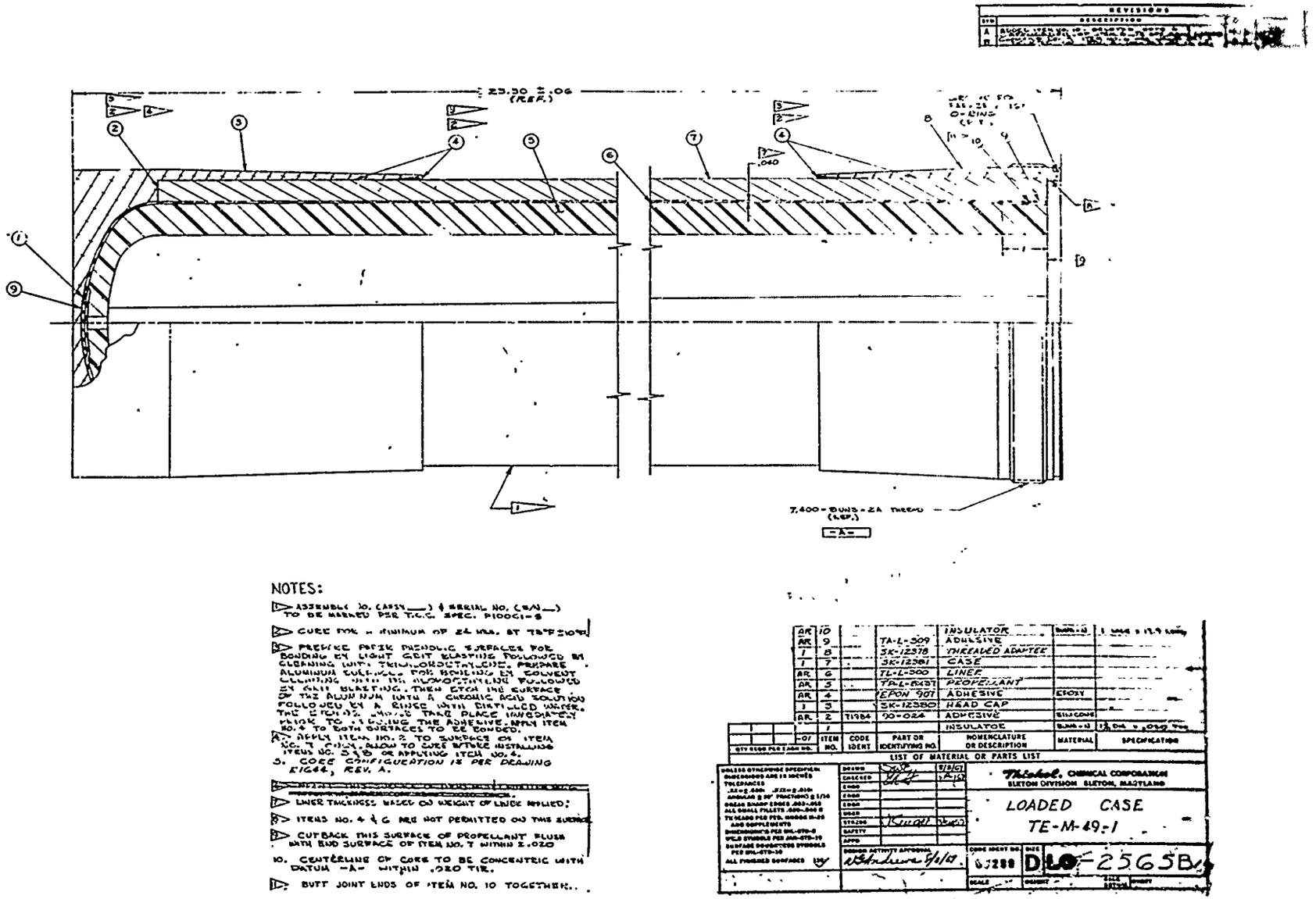


FIGURE 43. CONCEPT III LOADED CASE

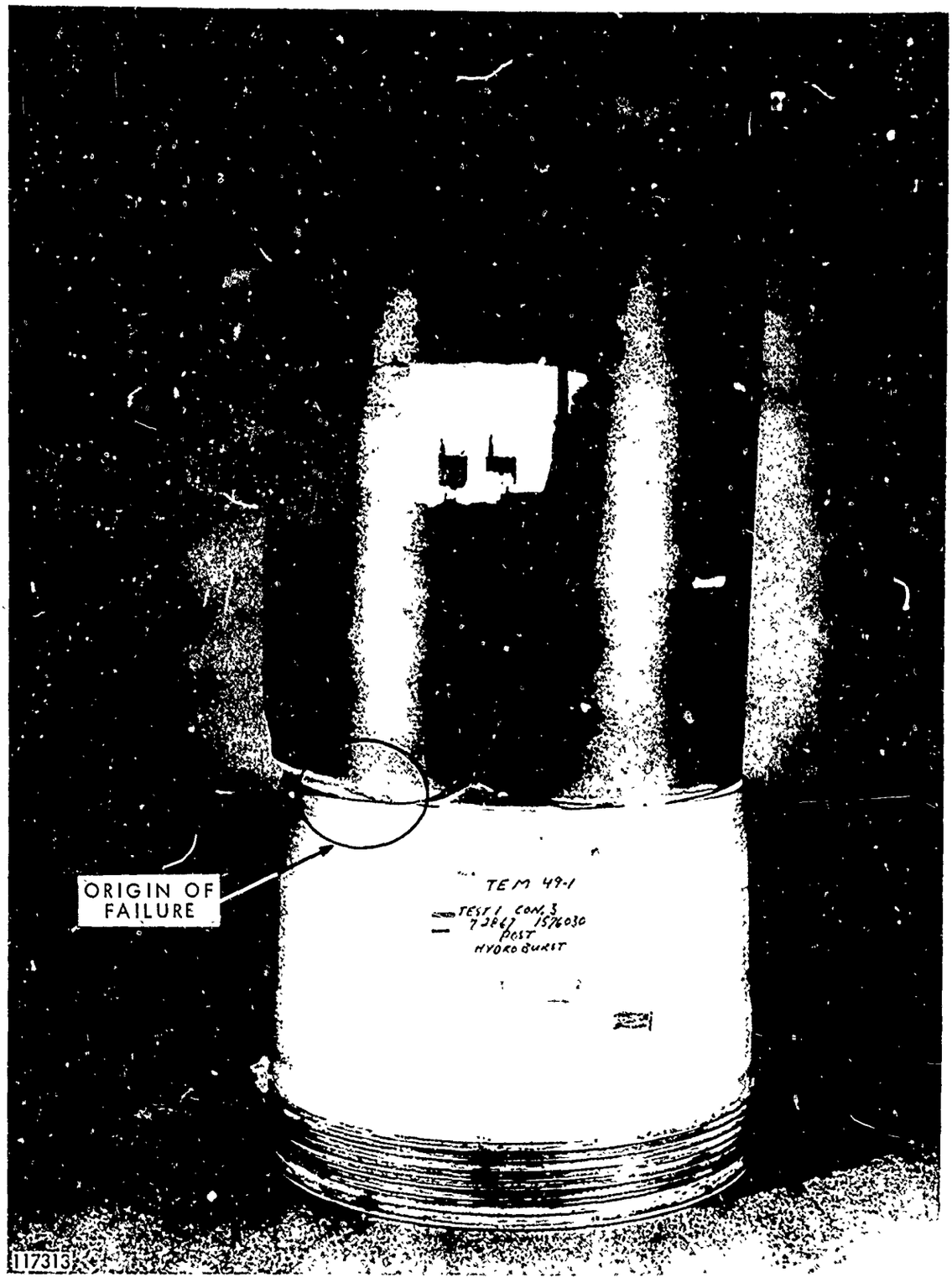
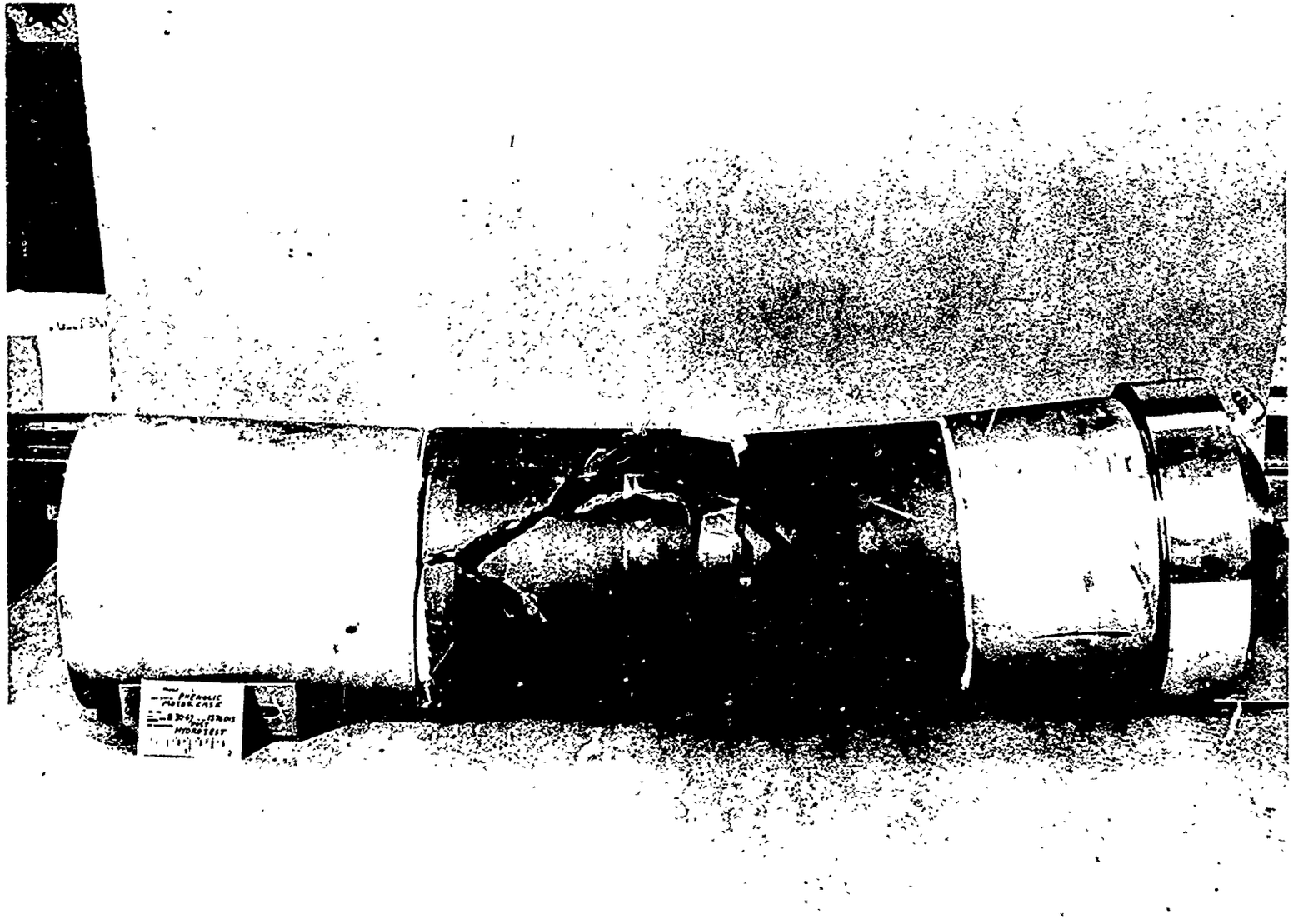


FIGURE 44. BURST CASE, CONCEPT III, TEST I



967030

FIGURE 45. BURST CASE, CONCEPT III, TEST II

TABLE XII

HOOP TENSILE RESULTS FROM FAILED CASES

Case Burst Pressure, psi	Hoop Tensile Strength, psi
3200	30,730
	35,500
	33,800
2200	33,450
	34,570
	34,100

These values, with one exception, are higher than any we have obtained previously. The one low value, 30,730 psi, was obtained with a specimen whose mode of failure indicated that some bending had been induced at the point of failure.

We have attempted to establish a correlation between the high hoop strength of these tubes and the low meridian strength. The fiber orientation dependence of the hoop and meridian strengths leads to speculation that any increase in hoop strength would be at the expense of a proportional decrease in meridian strength. Unfortunately, meridian tensile specimens could not be obtained from either case, therefore, we can only make logical speculations as to the probable differentiation in meridian properties of this material and the effect of these differences on case burst pressure.

Unfortunately the facts do not support this hypothesis. Any reasonable estimate of the degradation in meridian strength resulting from the observed increase in hoop strength leads to a value only 11% below the design value (The design value is the minimum expected meridian strength divided by a safety factor of 1.3) and it is difficult to believe that this would result in a 30% decrease in burst pressure.

The most convincing argument against attributing the failure to a below-par tensile strength is the similarity of the hoop tensile strength results for the two cases. Two cases whose hoop properties correspond so closely would hardly be expected to have meridian properties sufficiently different to account for the difference in burst pressures. Since material strength cannot be blamed, it appears that the cause must be a material defect. It cannot be determined if the resin-rich area at the origin of failure is alone a defect of sufficient magnitude to cause the failure, or if it was necessary for it to be combined with other unknown defects. It can be said that all tubes can be expected to have similar defects and that we have no way of defining

critical defects, no way of detecting the defects, and no way of predicting the probability of a critical defect occurring at a highly stressed region of the case.

The usual procedure in dealing with a problem of this nature is to increase the safety factor to provide for the defects and then perform tests to determine if the new safety factor is adequate. Of course, some assumptions as to the actual minimum burst pressure must be made in establishing the new safety factor. In this case, with only two data points, the selection of the safety factor had to be an educated guess and to ensure success the factor had to be highly conservative.

Another approach is to not change the design, but to lower the proof pressure by whatever amount is required to give the desired ratio between the proof pressure and the anticipated minimum burst pressure. This route is normally closed of course; however, in this instance, it was a promising alternative because of the antiquated safety factors used in establishing the ratio of proof pressure to MEOP for the existing M58A2. The proof pressure, 2, 650 psi, is 1.49 times the 3 sigma MEOP at the maximum service temperature, 150° F, and 1.73 times the 3 sigma MEOP at 60° F. In contrast, contemporary practice for similar applications is a proof pressure of at least 1.1 times the MEOP. Strangely, the minimum burst pressure requirement for the M58A2 is only 1.17 times the proof pressure, whereas current practice generally calls for a factor of 1.25.

To satisfy our requirement of firing a demonstration motor, a demonstration of structural integrity suitable for a firing of the prototype at 60° F could be obtained with a proof test at 1, 690 psi (1.1 times the 3 sigma MEOP of 1535.3 psi at 60° F). This provides us with a factor of 1.3 between the observed minimum burst pressure of 2, 200 psi and the proof pressure. Although this change in structural standards precludes any direct comparison between the paper phenolic and present case designs, by current design standards the two cases are both suitable for the original mission. We can thus fulfill our principal objective of demonstrating the feasibility of fabricating and firing a prototype motor with a paper phenolic case.

A third case of the same Concept III design was fabricated and successfully hydrotested at 1, 690 psi. The case was then loaded with propellant and prepared for static test (Figures 46 and 47) and on November 13, 1967 the unit was successfully static tested. Although there was an obturation failure in the nozzle threads (Figures 48 and 49) that lead to a burn through of the aft closure, the failure was in no way associated with the use of paper phenolic and occurred very near the end of the web burn time. As can be seen in the pictures the failure was non-catastrophic. It was initiated at about 70% of normal web burn time and there was a gradual release of pressure somewhat similar to the normal tailoff. Since the ballistic performance of the M58A2 is classified, the pressure versus time plot has not been included in this report. Copies of this record may be obtained from TCC/Elkton. Performance of the motor was completely normal until the time of failure.

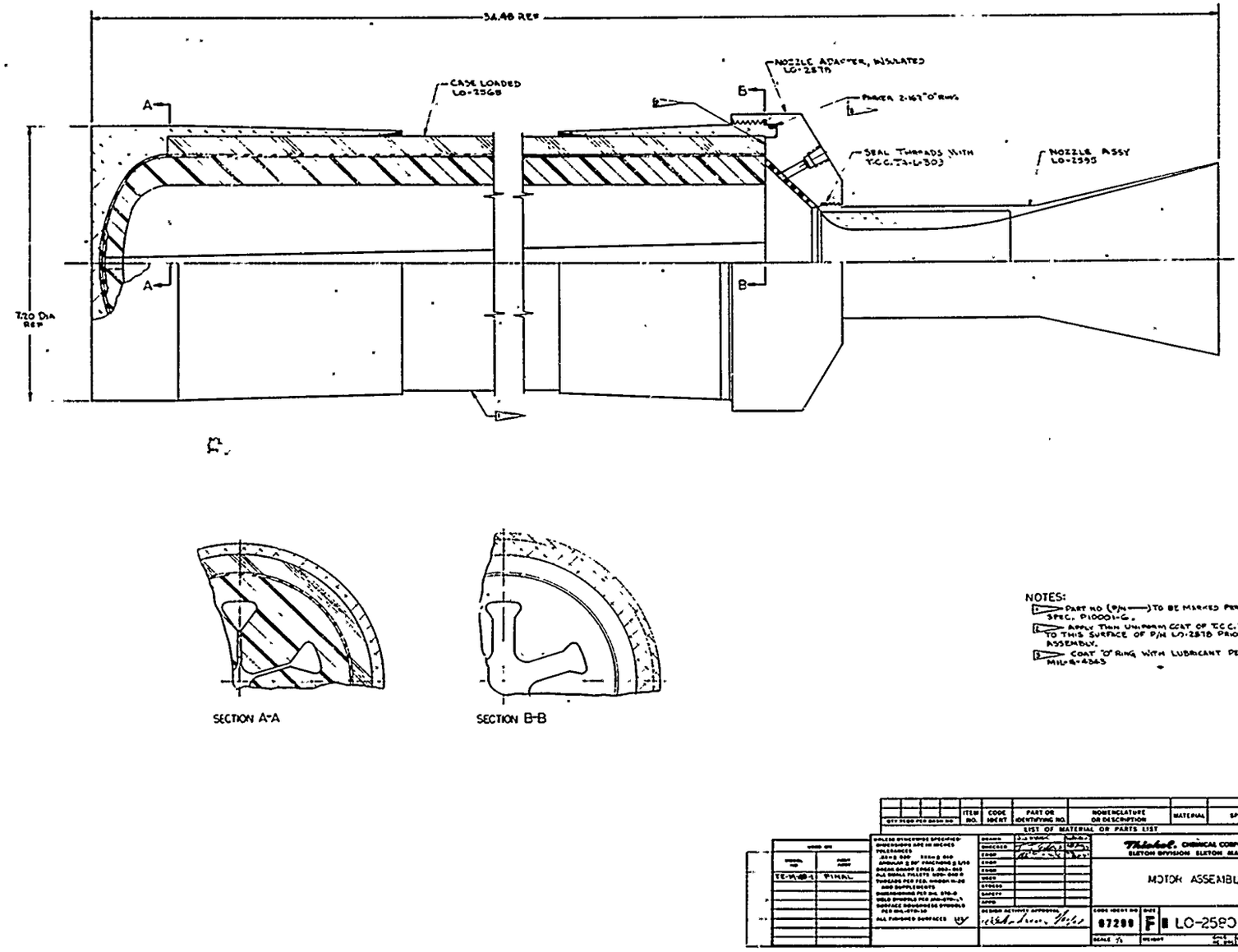


FIGURE 46. MOTOR ASSEMBLY, CONCEPT III

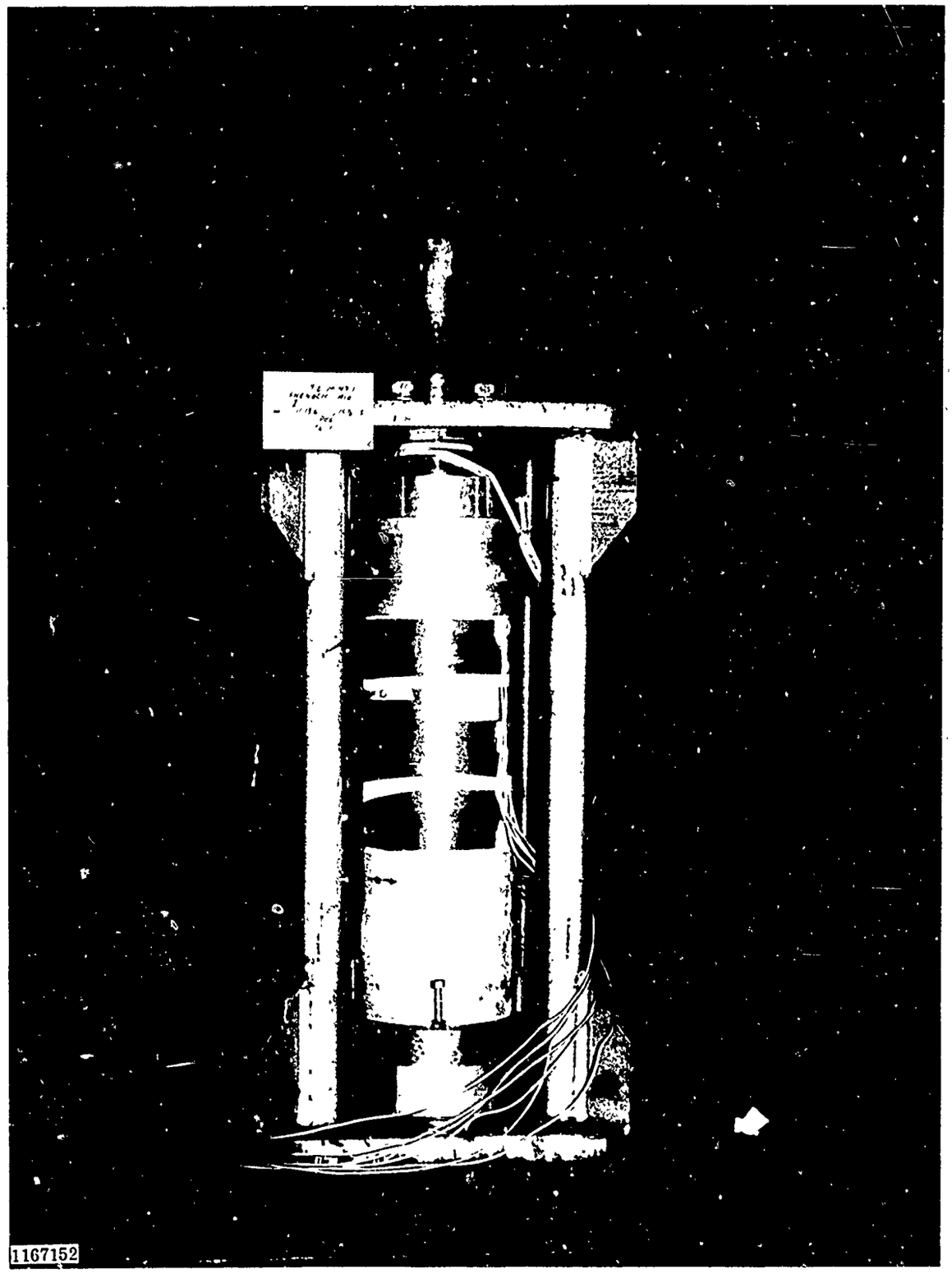


FIGURE 47. STATIC TEST ARRANGEMENT, CONCEPT III

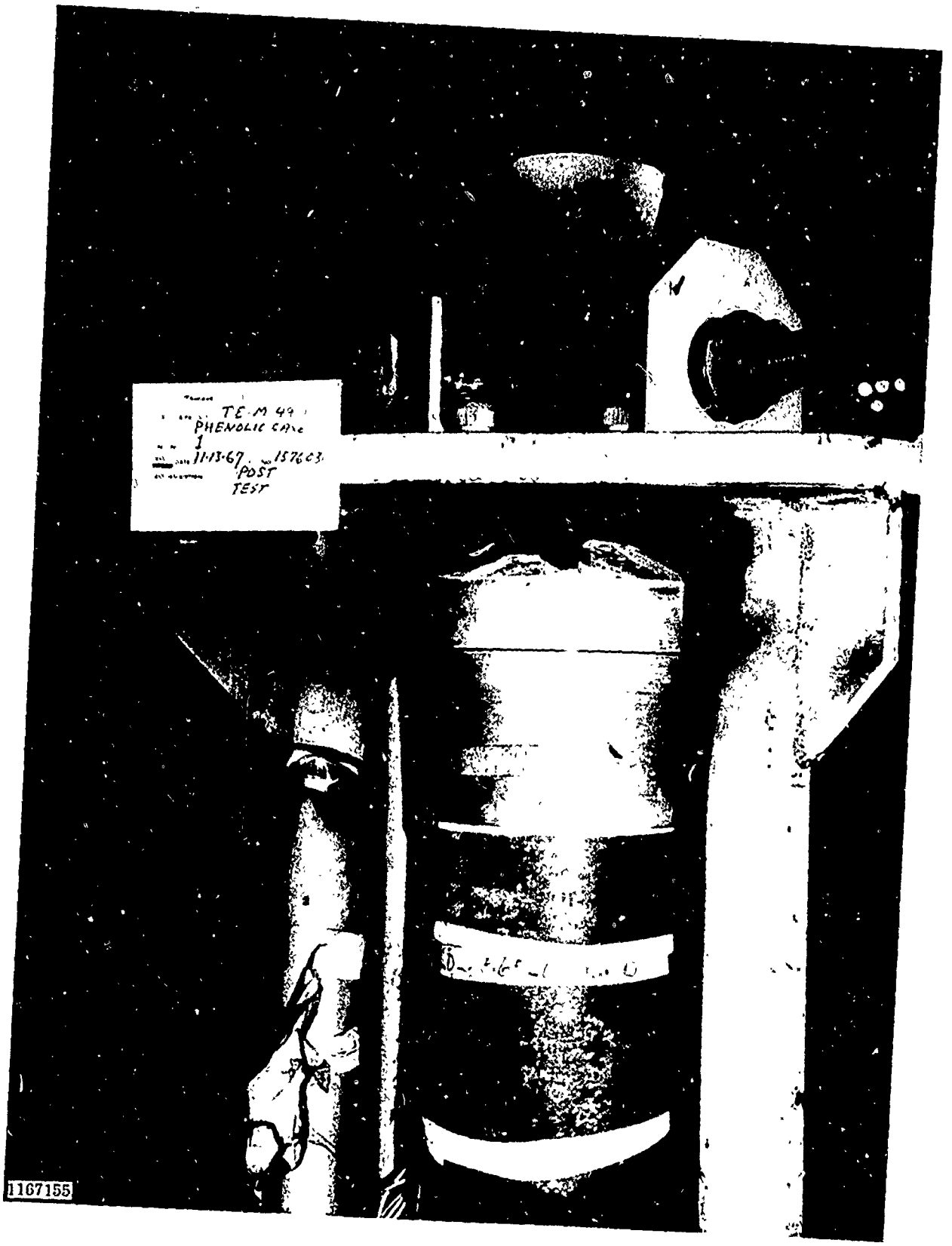


FIGURE 48. POST STATIC TEST, CONCEPT III



FIGURE 49. FIRED COMPONENTS, CONCEPT III

Portions of the case were sectioned and examined for evidence of charring (Figure 50). The section at the bottom of the figure was taken about 1/4 inch from the nozzle end of the case, in the area protected by a 0.020 inch thick strip of Buna-N insulation. The other section was taken at the end of the case near the closure joint at the nozzle end of the motor. In this area the only thermal protection was about 0.030 inches of liner. In neither case was there any evidence of charring or other degradation that extended below the surface. The charred material visible on the surface is almost entirely liner and insulation. It appears that the insulation at the aft end could be safely eliminated and the liner thickness throughout the case could be reduced to the minimum to assure a good bond.

The use of the paper phenolic had a severe impact on mission performance and dimensional envelope but no effect on internal or external insulation requirements. It is estimated that the weight would increase by twelve pounds, the loaded motor C.G. would shift forward by 107 inches and the post-fire C.G. would shift forward by 5.5 inches, these estimates being based on the design shown in Figure 44. If it is assumed that with a more sophisticated design we could reduce the weight by 10%, it is estimated that the burn out velocity of missile using the paper phenolic motor would be about 8% lower than that of a missile using the present steel case M58A2.

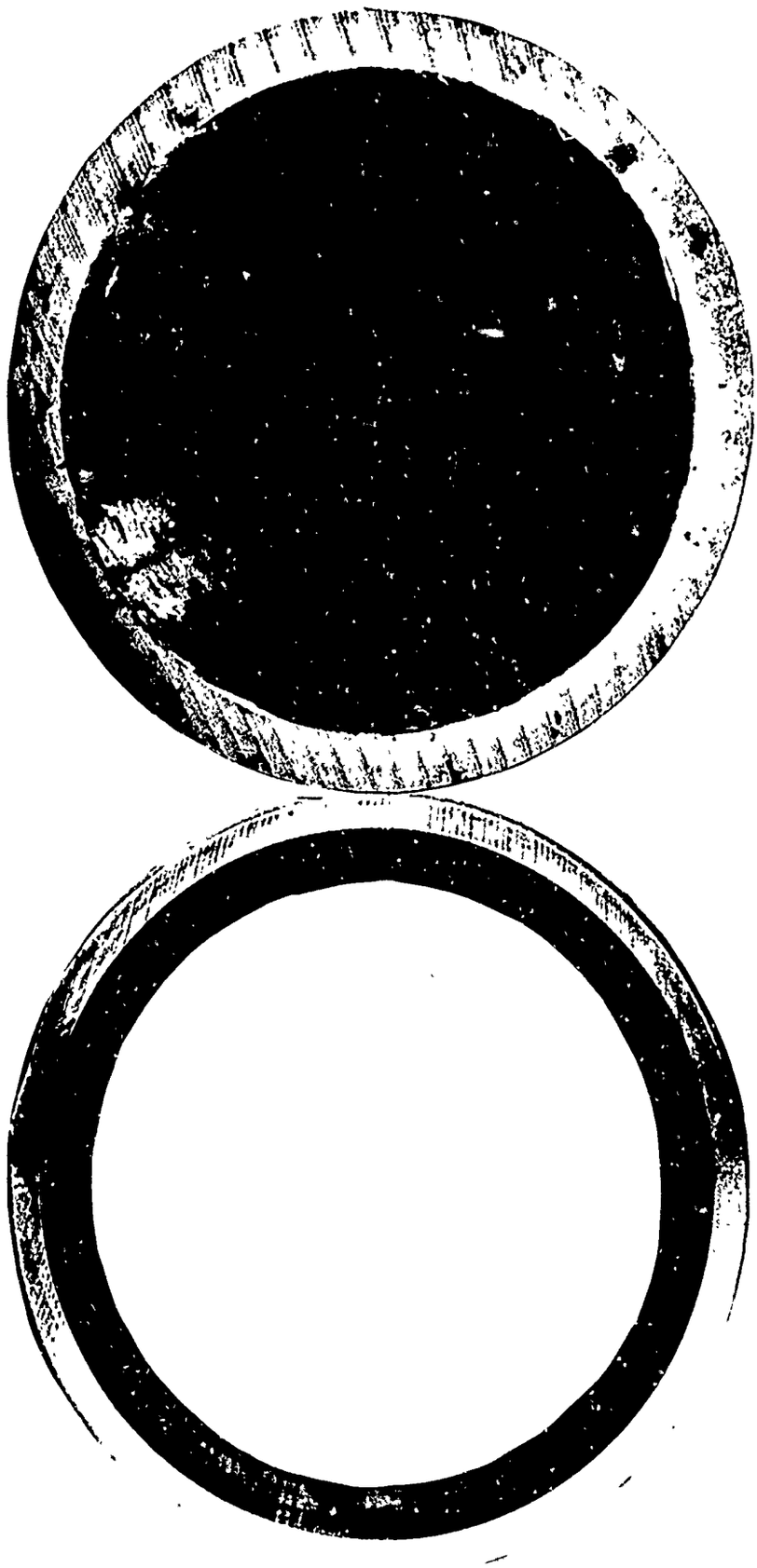


FIGURE 50. SECTIONED CASE, CONCEPT III

SECTION XIII

COST EFFECTIVENESS STUDIES

SECTION XIII

COST EFFECTIVENESS STUDIES

1. MEASURES OF MERIT

While it is easy to evaluate any rocket case material in a specific application, it is much harder to derive a general measure of merit. Any such yardstick should consider the material weight, density, and cost, fabrication costs and resulting system performance.

Most of the likely applications for the paper-phenolic material are volume limited. A lower density case material may usurp a greater share of the envelope, displacing fuel or payload. For this reason, the common stress-to-density (strength-to-weight) factor must be applied with care to any material evaluation.

Fabrication costs vary dramatically with the production technique used. Paper phenolic cases now require a lot of labor for tube rolling and production of quality adhesive joints. In very large-scale production, greater tooling costs and process development costs can be eliminated and hard-labor reduced to a minimum.

In an earlier study for Edwards Air Force Base (Ref. 9), we concluded that system effectiveness tends to be a function of the square of burn out velocity.

In designing a motor for the Falcon missile configuration using paper phenolics, we determined that the loss of envelope to inert material results in 8 percent lower final velocity. System performance is thus 85 percent (0.92 squared) of that achieved with the present design.

If fabrication cost can be neglected, an estimate of relative cost effectiveness for a candidate case material may be derived in the following manner.

Wall Thickness

$$T = \frac{PD}{2\sigma} , \qquad (46)$$

Case Weight

$$W = k_1 \pi \, DTL \, \rho, \text{ where:} \qquad (47)$$

W = case weight;

k_1 = end closure, weight factor;

L = motor length;

ρ = density of candidate material.

System Effectiveness

$$e = k_2 V^2, \text{ where:} \qquad (48)$$

k_2 = proportionality factor;

V = motor burn out velocity.

Cost Effectiveness

$$(CE) = \frac{e}{CW} = \frac{2}{\pi} \left(\frac{k_2}{k_1} \right) \left(\frac{L}{D} \right)^{-1} D^{-3} P^{-1} \left(\frac{\sigma}{\rho} \right) V^2, \text{ where:} \qquad (49)$$

C = Delivered material cost per pound.

For any operating pressure and envelope definition, the relative cost effectiveness of a candidate case material reduces to:

$$(CE)_R = \frac{V^2 \left(\frac{\sigma}{\rho} \right)}{C}$$

On this basis, the relative cost effectiveness of paper phenolics in the Falcon-type configuration is 38 percent of that for steel.

2. ACTUAL FINDINGS

The limiting assumption in developing the measure of relative cost effectiveness in the previous section lies in neglecting fabrication costs. When we consider relatively small numbers of motors, we are forced to accept present production technology and any new candidate material is placed at an additional cost disadvantage.

a. Falcon Motor

We have surveyed several suppliers to develop realistic costs for paper-phenolic components for the Falcon motors in quantities of 1,000 and 5,000 units. The unit costs for motors are given below:

Total Units	1,000	5,000
Paper Phenolic	$ 520	$ 438
Present Design	$ 535	$ 439

It is clear that the cost advantage for the paper phenolic design is only marginal, and when the 8 percent velocity degradation is considered, all advantage is lost.

b. 1.0-KS-25 Motor

We assembled similar data on a small 1.0-KS-25 spin motor and reached the same conclusions:

Total Units	1,800	200,000,000
Paper Phenolic	$ 72	$ 12
Competitive Aluminum	$ 85	$ 10.50

In very small motors of this type, material costs become negligible in the total price and fabrication costs become the principal criteria.

c. XM-165 Flare

The present design for the XM-165 flare uses an aluminum launcher tube which must withstand about 500 psi of internal pressure when fired. We have studied production methods for producing such units from paper phenolic tubes and find that the idea is feasible.

In quantities of 1,000 in 10,000 units, the paper tubes would add between $2 and $3 to the estimated unit price of $14. However, the paper tubes have the advantage of not leaving debris which an enemy can use for bombs. In limited-war situations such as in Southeast Asia, every effort is made to deny the guerilla any possible bomb components. Since such flares are used in large numbers in Viet Nam, this advantage seems to balance out the cost disadvantage.

d. Pyrogen Igniter

We are now using paper-phenolic cases in many pyrogen igniter motors for still larger rocket motors such as the TE-P-415 device in the TE-M-416 Tomahawk motor. Design engineers associated with these projects tell us that the selection of the material was made on a technical basis, rather than on one of cost. The device must survive inside the motor during operation without creating harmful debris. The paper-phenolic case is partially consumed during motor burning but does not produce damaging debris.

The cost of the pyrogen device is about $600 in a rocket motor costing $5, 500. Substitution of cheaper case materials might make $3 difference in total cost. Since we typically make only 100 such units a year, the total possible savings are trivial relative to the cost of redesign and requalification.

SECTION XIV

CONCLUSIONS AND RECOMMENDATIONS

SECTION XIV

CONCLUSIONS AND RECOMMENDATIONS

Paper phenolic laminates can best be used in those applications where the requirement for their unique characteristic, e.g., consummability, overcomes their low strength to weight ratio. In missile systems where high terminal velocity is a prime criterion, their low strength to weight ratio gives them a low cost effectiveness rating. However, in some special applications, such as those where structural efficiency is relatively unimportant and where other factors, such as denying an enemy guerrilla force a supply of scrap metal, are more important, paper phenolic laminates have a potential application.

We examined two applications in which the paper phenolic was used to form the pressure vessel of a high performance rocket. In one case, the M58A2, there was no significant decrease in cost and an 8% decrease in burn out velocity, resulting in a 15% reduction in cost effectiveness. In the other case, the 2.75 FFAR, although no actual cost analysis was performed, it is doubtful that the paper phenolic could be produced more cheaply than the present case. In this instance the reduction in burn out velocity is about 15% and it appears the reduction in cost effectiveness would be even greater than for the M58A2. It must be pointed out that both of these comparisons were unfair to the paper phenolic in that both motor and weapon system had been optimized for a metal case and it was necessary to work within these restraints which were not optimum for the paper phenolic when designing the equivalent motors. As stated earlier in the report, the nature of the material to be used must be considered in the total system design. If paper phenolic were considered from the beginning in designing a weapon system equivalent to the Falcon and the 2.75 FFAR, the material would certainly fare better than it has in the present cost effectiveness analysis. This is not to say that it would prove to be more cost effective: there are too many structural disadvantages to overcome to expect that result. Additional, but still not offsetting improvements could be expected if the manufacturers would modernize their circa 1917 production facilities. However, this change cannot be expected without high volume requirements.

In applications where velocity and weight are not critical it is possible that paper phenolic can offer other advantages. It is possible that it could be a competitive structural material for low velocity weapons such as those used by the Army against fixed and slow moving targets. Here, other specific non-structural criteria, such as unusable debris in the case of XM165 Flare, might give the material an inherent overriding advantage. As cited in some of the specific examples we studied, the cost is frequently equivalent to that of other materials so if weight and envelope are not critical, it is directly competitive. A final case where it can present advantages are those similar to the igniter example where the consummability of the igniter was the technical criterion for selecting the material.

Our investigations of the material, while far more definitive than any others ever performed, have certainly not resolved all the questions concerning this highly complex material. There are many problems remaining before any reliable stress analysis of efficient designs can be performed. If applications of these material to any great extent are contemplated, further investigations are warranted, particularly of flexural effects, the effects of temperature on tensile and compressive properties, and the definition of defect criteria.

Additionally, before extensive applications are made, extensive efforts must be made on the part of manufacturers to improve the reproducibility of the material and the general level of quality control. These are definite limiting factors on current design standards.

To summarize our conclusions and recommendations, paper phenolic laminates offer potential as a competitive structural material in systems insensitive to strength to weight ratios, particularly where the other unique characteristics of the paper phenolic offer specific advantages. The paper phenolics are not suitable for systems which are sensitive to inert parts mass fraction and volume.

APPENDIXES

APPENDIX I

MECHANICAL AND PHYSICAL PROPERTIES TEST PROCEDURES

1. UNIAXIAL TENSILE PROPERTIES

a. Test Specimens and Equipment

Two basic test specimens were used to determine the uniaxial tensile properties of convolute-wrapped paper phenolic tubing. The first was the NOL Ring Specimen (Figure 51) used for determining the hoop or with-grain tensile properties; the second was the Tube Tensile Specimen (Figure 52) used to determine the meridian or across-grain tensile properties. These specimen configurations were selected because they could be fabricated from convolute-wrapped tubing and because there were ASTM standards for specimens of this geometry and material type. The requirement that the specimens be fabricated from tubing arose from the dependence of material properties on fabrication technique and the considerable differences in the fabrication techniques for tubing and flat sheet. Gualillo[3] attempted to correlate the results of specimens fabricated from flat stock and from tubing with no success. Since nearly all applications of the material in rocket motors would involve the use of convolute-wrapped tubes, tubular test specimens were chosen.

The NOL Ring specimen was designed in accordance with the requirements of ASTM Standard D2290, and the Tube Tensile Specimen in accordance with the requirements of ASTM Standard D638. The tube specimens were tested in accordance with ASTM D638, using a standard set of V-jaws to apply the load and snug fitting plugs to prevent the V-jaws from buckling the tube walls.

Unfortunately, the test described in ASTM D2290 was not satisfactory for reasons discussed in Section IV-1. We were able to devise a different technique and the apparatus we developed for this technique is shown in Figure 53. Essentially the test consists of a hydroburst of the NOL Ring, free of meridian loads. That portion of the circumferential groove behind the O-ring is pressurized with a suitable fluid and the O-ring serves both as a seal to prevent leakage of the fluid from the cavity and to transmit the pressure loads to the NOL ring. The clearance between the ends of the ring and the walls of the groove is adequate to prevent leakage of the fluid from the cavity and to transmit the pressure loads to the NOL ring. The clearance between the ends of the ring and the walls of the groove is adequate to prevent either meridian or radial restraint of the ring without allowing the O-ring to extrude. To prevent prestressing of the NOL ring, the O-ring was sized so that even when compressed to the maximum by the torqued bolts it would not touch the inner wall of the NOL ring.

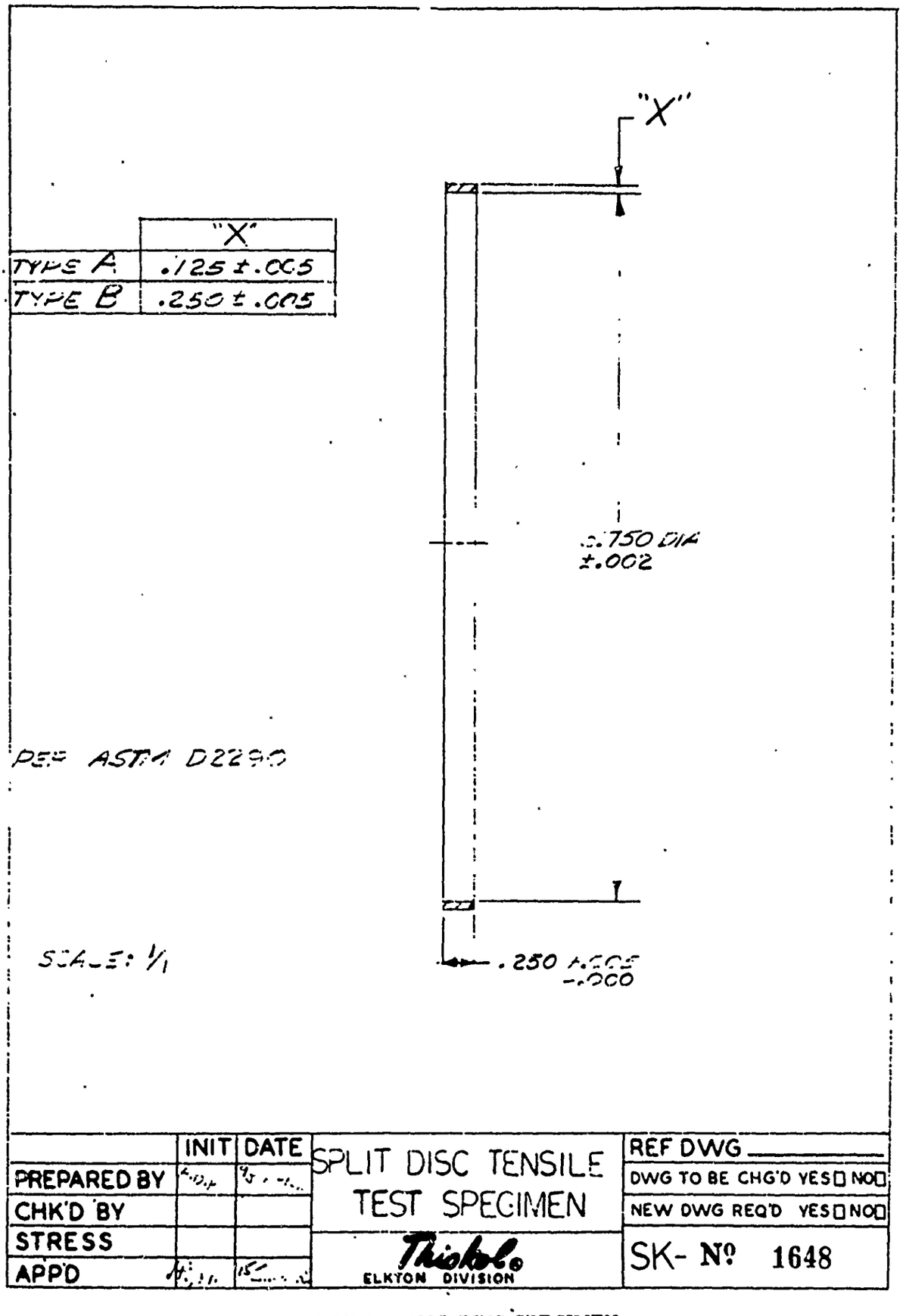


FIGURE 51. NOL RING SPECIMEN

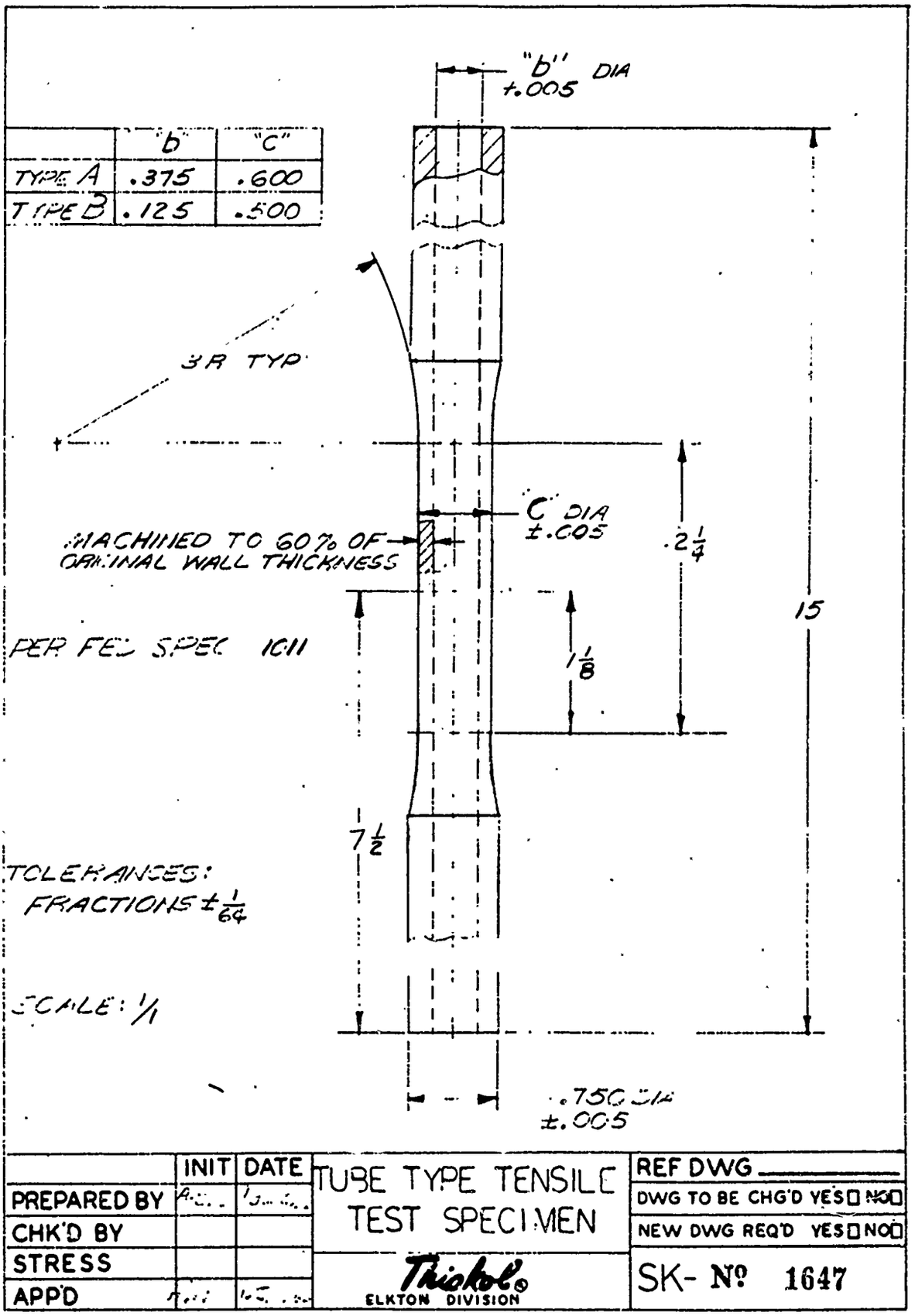


FIGURE 52. TUBE TENSILE SPECIMEN

E258-67-22

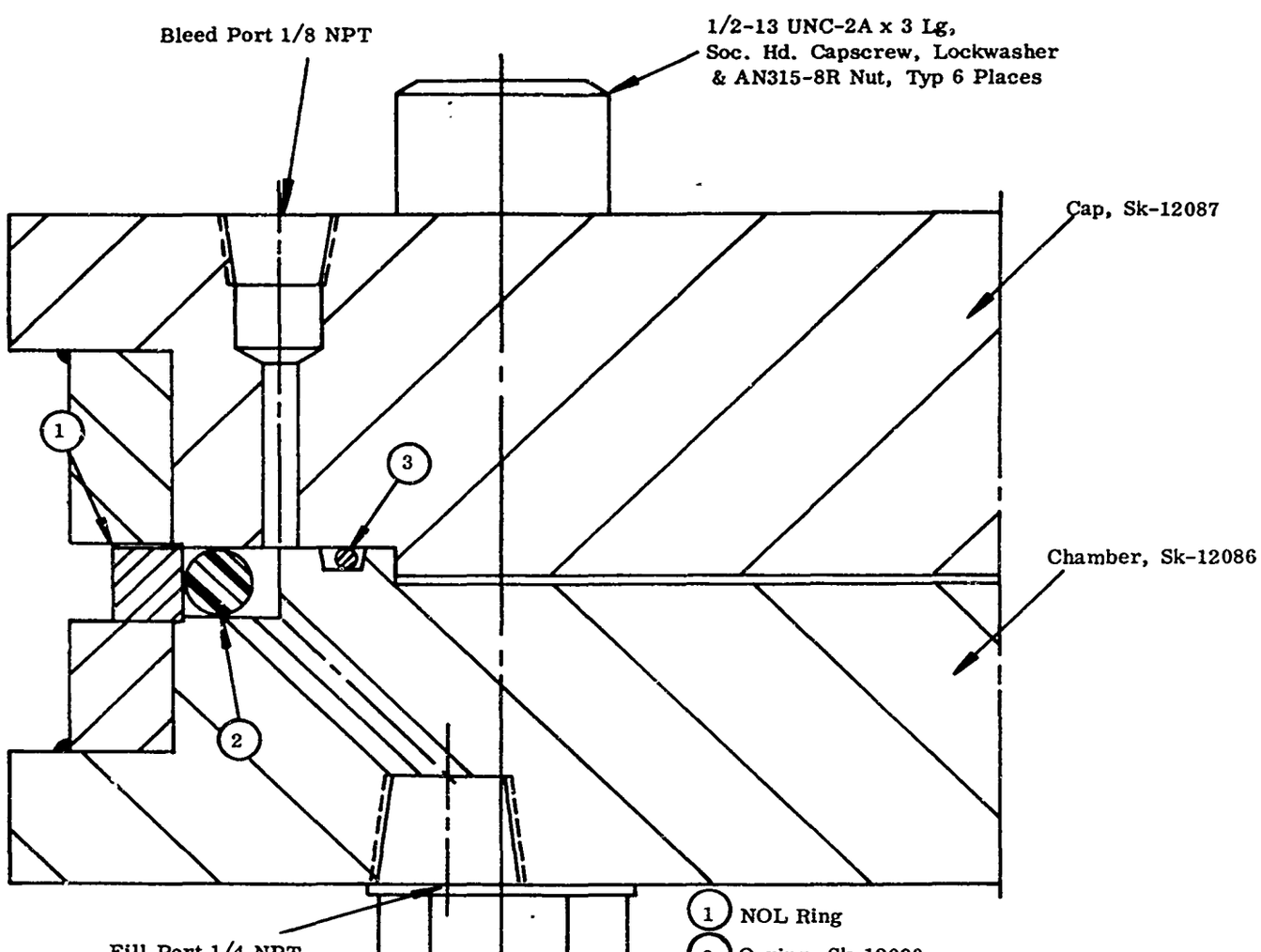


FIGURE 53. HOOP TENSILE TEST APPARATUS

Note that there are two variations of each of the tensile specimens, designated as Type A and Type B. The Type B specimen has a considerably thicker wall and was used only for evaluating the effects of thermal cycling on different wall thicknesses. The Type A specimen was used for all other tests.

b. Test Measurements and Techniques

In these tests, we evaluated the stress-strain-temperature relationship, the effect of strain rate on the stress-strain relationship at room temperature, and the value of three of the six Poisson's Ratios at room temperature. The test program used for determining these relationships is outlined in Table XIII. All tests were made with uncoated specimens.

Strain measurements were made at the locations specified in Figures 54 and 55. Strain gauges were used for all strain measurements of the NOL Ring and the specimen was oriented in the jaws so that the strain gauges were opposite the split in the split disc jaws. The ε_1 measurement on the tube specimen was made with an extensometer and the ε_2 measurement with a strain gauge. In all tests, the output of the various strain sensing devices was recorded on either an X-Y recorder or an oscillograph recorder versus the load applied to the specimen.

2. UNIAXIAL COMPRESSIVE PROPERTIES

a. Test Procedure and Equipment

The compressive test specimen was a tube of convolute-wrapped HY-488 that was 1/2 inch O. D. by 1/4 inch I. D. by 1 inch long. A compression load was applied to each specimen along its longitudinal axis by an Instron testing machine. A Tinius-Olsen self-centering compression fixture was used to maintain the alignment of the specimen during the test. Five specimens were tested at each of three strain rates and all tests were performed with the specimens conditioned to 77°F. Applied load versus compressive strain was continuously recorded on an X-Y recorder during each test.

3. BIAXIAL TENSILE PROPERTIES

Five hydrotests were performed as detailed below to evaluate the biaxial behavior of the paper phenolic. This was a change from the original test plan but it permitted a more effective analysis of the data and made it possible to reduce the number of wall thicknesses and diameters to be investigated. Further, it furnished the best Poisson effect information, and served to define the strain dependence of modulus in a multi-axial field. Secondarily, it gave us a more direct check on the validity of NOL Ring and Tube Tensile Specimen results.

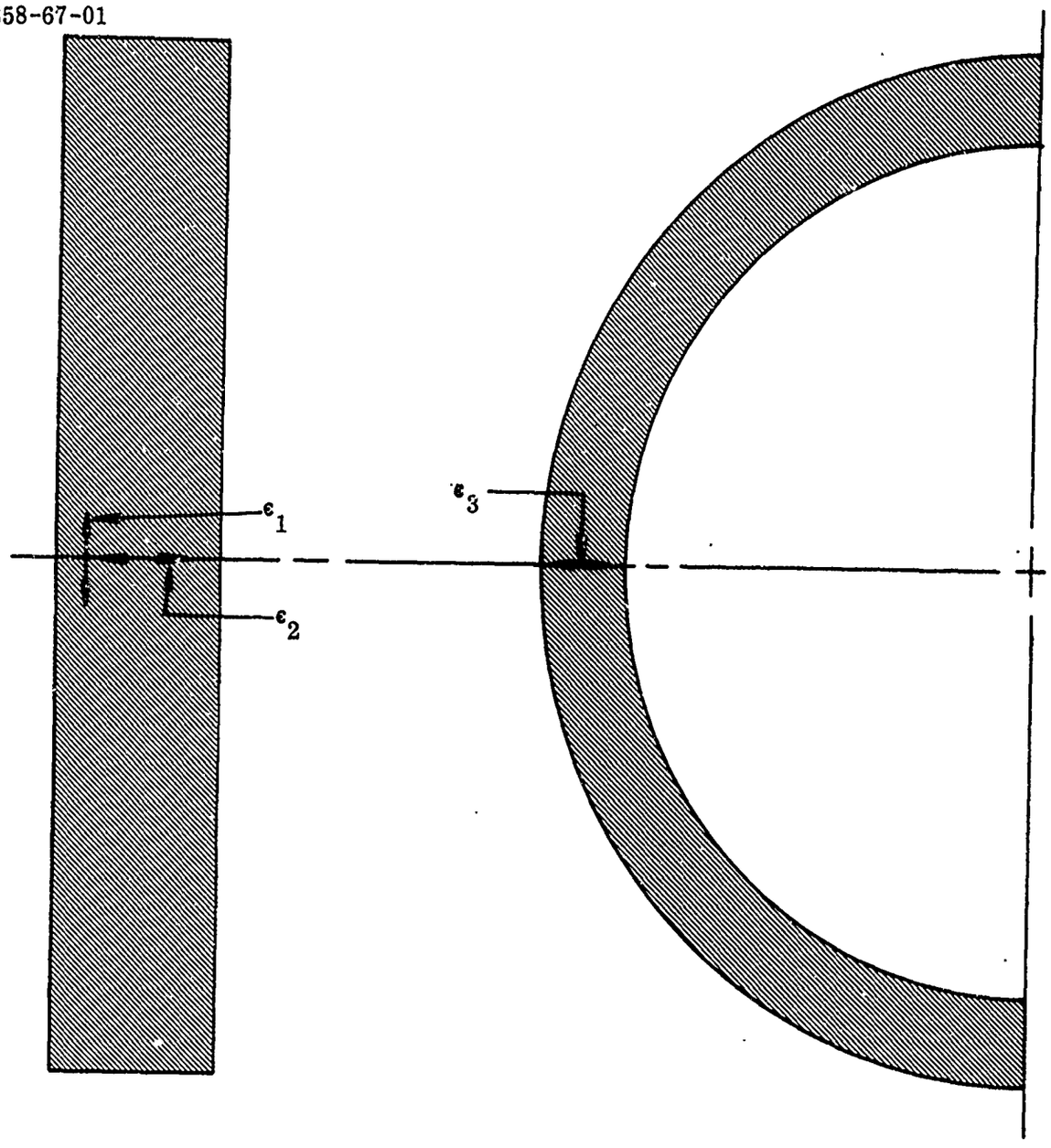
TABLE XIII

UNIAXIAL TENSILE PROPERTIES TEST PROGRAM

Parameter	Ultimate Tensile Strength & Tensile Modulus										Poisson's Ratio		Totals	
Test Temperature	-75°F		0°F		77°F		150°F		225°F		77°F			
Specimens	T	R	T	R	T	R	T	R	T	R	T	R	T	R
Strain Rate, in./min 0.02	-	-	-	-	3	3	-	-	-	-	-	-	3	3
0.10	-	-	-	-	3	3	-	-	-	-	-	-	3	3
0.50	3	3	3	3	3	3	3	3	3	3	5	5	20	20
Totals	3	3	3	3	9	9	3	3	3	3	5	5	26	26

T = Tube Specimen
R = Ring Specimen

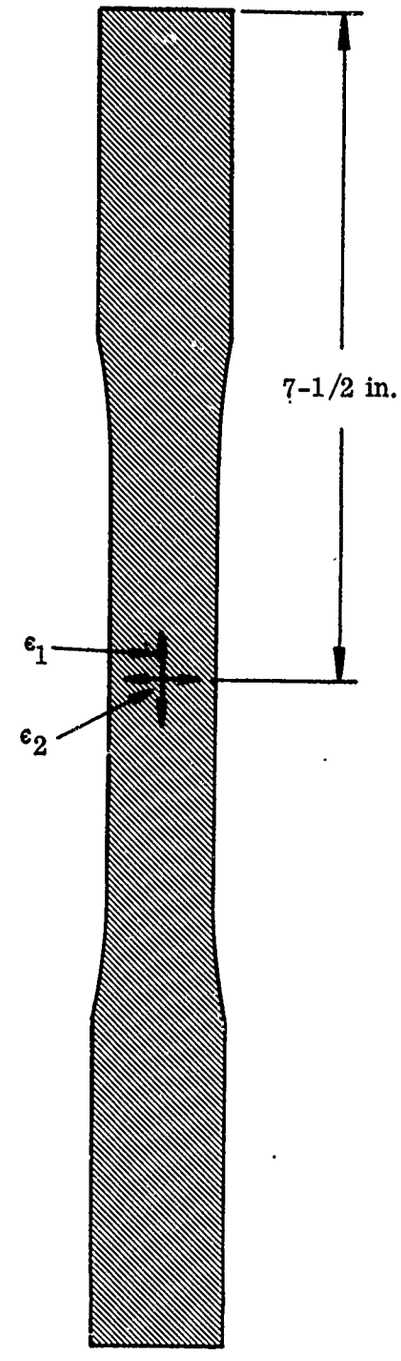
E258-67-01



NOTES:

1. All measurements to be made with strain gauges.
2. ϵ_1, ϵ_2, and ϵ_3 must be in same plane.
3. Specimen per SK-1648. This sketch not to scale.

FIGURE 54. STRAIN MEASUREMENT LOCATIONS FOR THE NOL RING SPECIMEN



NOTES:

1. ϵ_1 to be measured with an extensometer centered on position indicated.
2. ϵ_2 to be measured by an OPSCAN* system at position indicated.
3. Specimen per SK-1647. Not to scale.

FIGURE 55. STRAIN MEASUREMENT LOCATIONS FOR THE TUBE SPECIMEN

*Thiokol trademark.

Inside Diameter of Tube, in.	Tube Length, in.	Wall Thickness, in.	Type of Test
3	12	1/16	Uniaxial*
3	12	1/8	Uniaxial*
3	12	1/16	Biaxial
3	12	1/8	Biaxial
6	24	1/16	Biaxial

Biaxial tests of three inch tubes were performed with the apparatus shown in Figure 56 and the uniaxial tests were performed with the apparatus shown in Figure 57. The biaxial tests of the six inch diameter tube had an internally bonded compression dome closure similar to that discussed in Section IX-5. All of the tubes were instrumented with hoop and meridian strain gauges at the midlength of the case and on both the inner and outer walls.

4. CYCLIC LOADING

The object of these tests was to determine the effect of cyclic tensile loading on the stress-strain relationship and to determine what permanent degradation of material properties will occur. Our test specimens were the standard Type A meridian test specimens described previously. In these tests, five specimens were cycled in tension until failure or for ten cycles, to strain levels of from 1.2% to 1.4%. All tests were performed at 77°F.

Two criteria were used in selecting the test strain level. First, it had to be high enough to stress the material significantly and second, it had to be low enough to demonstrate the absence of gross changes of behavior from cycle to cycle. During the first test, we used a strain corresponding to the minimum value of strain observed at failure at 77°F for the particular specimen, 1.4%. The results indicated the value should be reduced to 1.2%.

All strain measurements were made at the 1 location on the specimen and stress versus applied load was continuously recorded on an X-Y recorder during both load application and load release. Each cycle began and ended at a condition of zero stress on the sample. There was some indication of strain at zero stress after the first cycle and each successive cycle.

5. EFFECT OF ENVIRONMENTAL CONDITIONS ON TENSILE PROPERTIES

During these tests we determined the effect of temperature, humidity, salt spray, vacuum storage, and thermal cycling on the tensile properties of HY-488. The Type A tensile specimens were used for the humidity, salt spray, and vacuum storage tests

E258-67-16

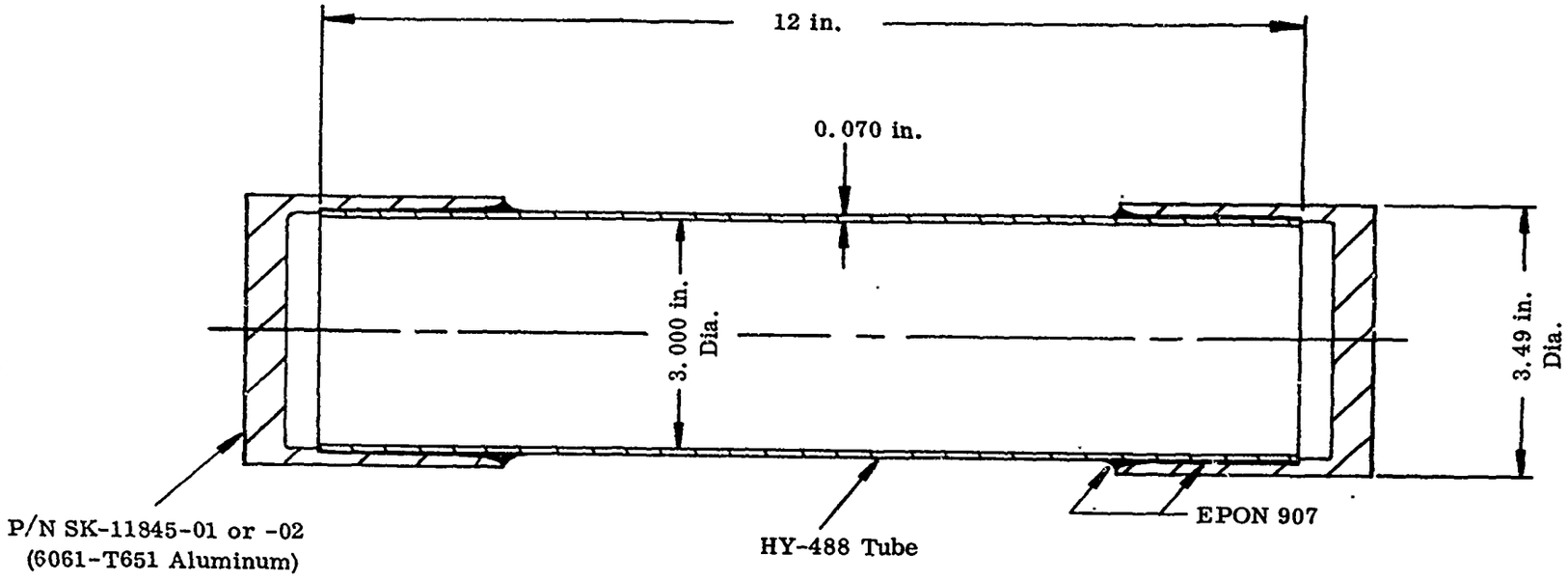


FIGURE 56. 3.000-INCH I.D. X 0.070-INCH WALL BIAXIAL TEST VESSEL

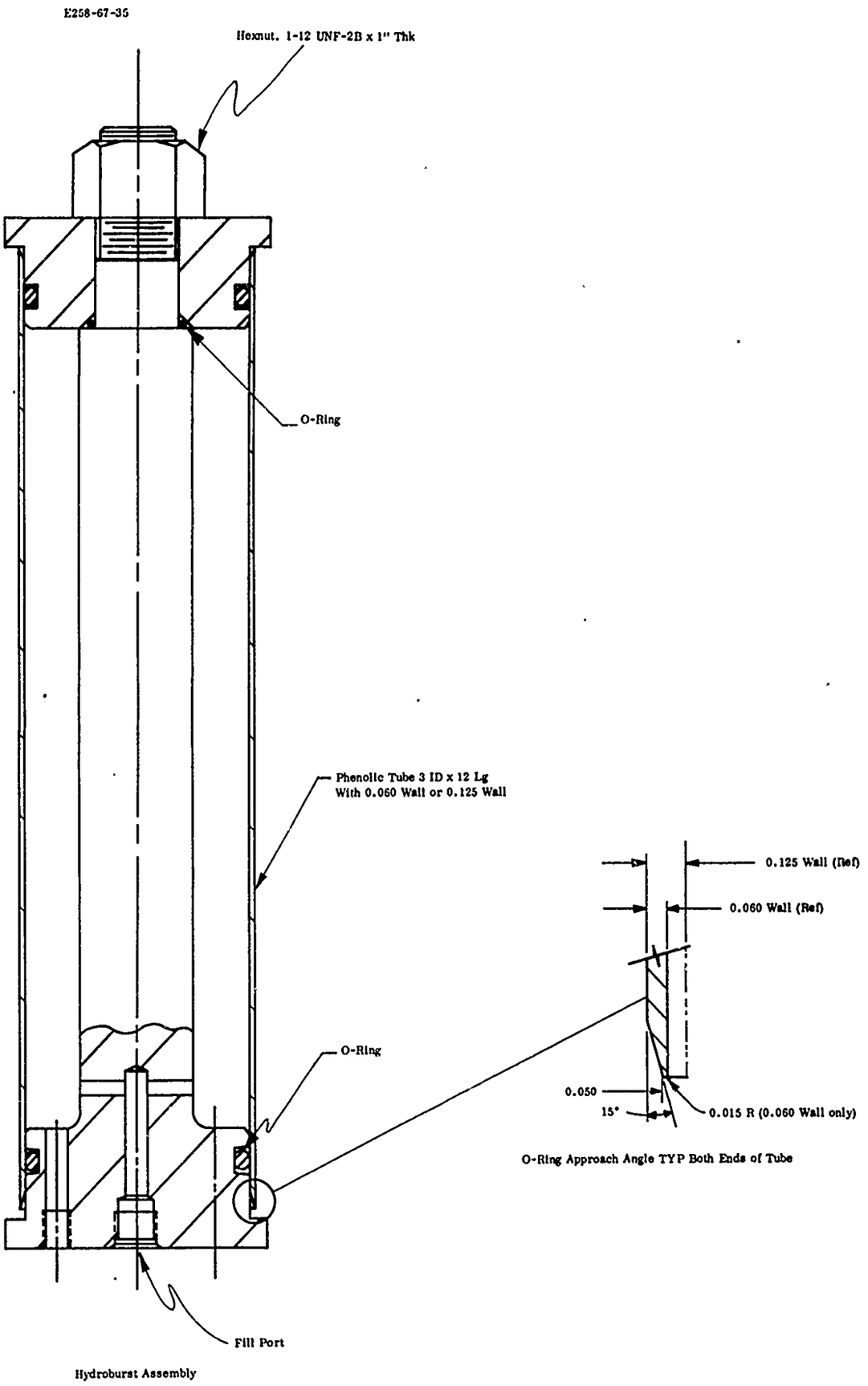


FIGURE 57. 3.00-INCH ID UNIAXIAL TEST APPARATUS

and both Type A and Type B specimens were used for the thermal cycling tests. The tensile testing was performed in accordance with the normal procedures but no strain measurements were made and all tests were at 77°F. Both coated and uncoated specimens were subjected to the humidity, salt spray, and vacuum storage tests as described below, but only uncoated specimens were used for the thermal cycling tests. The hoop specimens used for temperature effect evaluation were tested on the hydrostatic test apparatus but all others were tested on the Split Disc Apparatus.

TA-D-311 was selected as the coating material for the tensile specimens. This resin is an epoxy-amide that was developed by Thiokol for waterproofing paper-phenolic cartridges that are used in casting extremely hygroscopic propellants. It may be applied by either brush or dip coating and a single coat is approximately 0.005-inch thick. Our information on this material indicates that its modulus is considerably less than that of the paper phenolic and thus, the coating should not crack or leak when stresses less than the ultimate strength of the paper phenolic are applied to a coated structure. The coating is so thin that the coating itself does not have any significant effect on the tensile test results. Three coated specimens of each type were used to evaluate the effect of the coating on the tensile specimens. The environmental conditioning for each type of test is discussed in the following paragraphs.

a. Humidity

The coated and uncoated specimens were exposed to 90-percent relative humidity at 80°F. One half of the specimens of each type were exposed for 7 days and the remaining half for 14 days.

b. Salt Spray

The coated and uncoated specimens were exposed to a spray of 5 percent sodium chloride solution at 95°F for 168 hours.

c. Vacuum Storage

The coated and uncoated specimens were exposed to a vacuum of 10^{-6} Torrs at 80°F. One half of the specimens of each type were exposed for 7 days and the remaining half for 14 days.

d. Thermal Cycling

In these tests, our objective was to simulate the most severe combinations of temperature extremes that might be encountered in service use. This would be storage at a low temperature followed by exposure to aerodynamic heating and can be simulated by storage at -75°F followed by a brief exposure to 350°F. Since the

aerodynamic heating exposure is very short and the paper phenolic has a low thermal conductivity, the high temperature effects are going to be highly dependent on the thickness of the specimen. Therefore, specimens of two wall thicknesses were evaluated: The Type A and Type B tensile specimens.

In these tests we were trying to determine only if any permament material degradation would result from thermal cycling. We did not attempt to determine the strength while a specimen was being exposed to aerodynamic heating. All tensile tests were performed at 77°F on specimens which had been conditioned to 77°F. To accomplish this, the specimens were subjected to either one or ten thermal cycles -- all of a particular type. In the first type of cycle, the specimen was exposed to 4 hours at -75°F followed by 5 minutes at 350°F, and in the other it was exposed to 4 hours at -75°F followed by 15 minutes at 350°F.

TABLE XIV

THERMAL CYCLING PROGRAM

Duration of 350°F Exposure	No of Cycles	Type A	Type B	Type A	Type B
5 Minutes	1	4	4	4	4
	10	4	4	4	4
15 Minutes	1	4	4	4	4
	10	4	4	4	4

e. Temperature

Each specimen was exposed to the test temperature for a sufficient period of time for the specimen to reach equilibrium, a minimum of four hours prior to being tested. The test apparatus for all tests was enclosed in a temperature controlled test chamber and the specimen was maintained at test temperature throughout the test. If the transfer time from the pretest conditioning chamber to the test apparatus exceeded three minutes, the specimens were reconditioned for an appropriate period of time.

6. THERMAL AND MASS PROPERTIES

a. Density

The density was determined at 23°C with an air pycnometer, using specimens of tubing 1-1/4-inch OD by 1/4-inch ID by 1/4-inch long. Three specimens were tested.

b. Specific Heat

The average specific heat between 72 and 212°F was determined in a Paar calorimeter per ASTM Method C351 using 1-1/4-inch OD by 3/4-inch ID by 1/4-inch long specimens of tubing. Three specimens were tested.

c. Coefficient of Linear Thermal Expansion

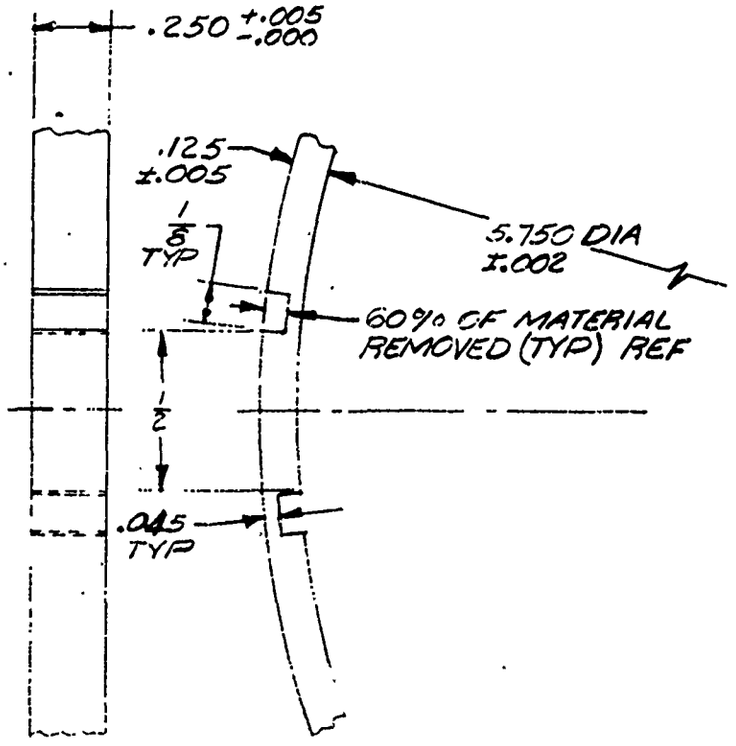
The coefficient of linear thermal expansion was determined with 1/2-inch-diameter by 1-inch-long specimens using the procedures described in ASTM Method D694. The coefficient was determined for the with-grain, across-grain and across-plies directions. Tubing was used for the across-grain specimen but the other specimens were cut from flat sheet of the same density as the tubing. The practical aspects of specimen fabrication precluded using tubing for the with-grain and across-ply specimens. Measurements were made at -75, 72, and 225°F in order to compute average values of the coefficient for the -75 to 72°F and 72 to 225°F temperature ranges.

d. Thermal Conductivity

The thermal conductivity was determined at 100, 160 and 220°F using 9-inch by 9-inch by 1-inch plates in a guarded hot plate apparatus in accordance with ASTM Method C177. A minimum temperature potential of 20°F was maintained between the hot and cold plates and two specimens were tested. Here, again, we have the problem that the test apparatus geometry, the test standard requirements and the configurations of samples that could be cut from tubes of practical dimensions could not be reconciled. It was necessary to use flat sheet of the same density as the tubes for making the specimens.

7. INTERLAMINAR SHEAR STRENGTH

Two techniques were developed for determining the interlaminar shear strength as a function of temperature and strain rate. The first technique determined the shear strength in the with-grain direction and uses the specimen shown in Figure 58. This specimen is an NOL Ring modified similarly to the technique used in Federal Test



SCALE: 3/1

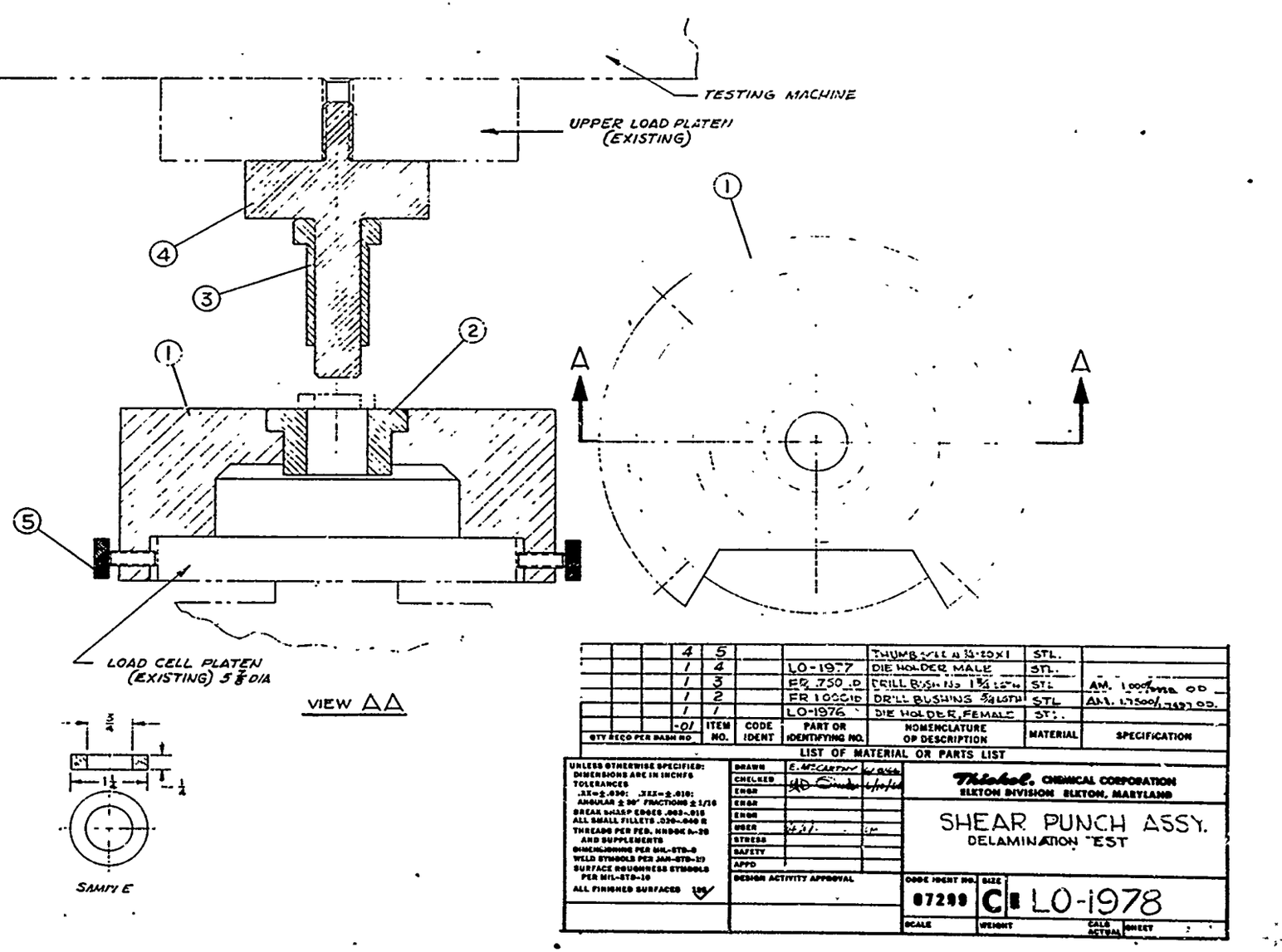
TOLERANCES:
FRACTIONS: ± 1/64
DECIMALS: .000 ± .010

	INIT	DATE	SPLIT DISC INTERLAMINAR SHEAR TEST SPECIMEN	REF DWG
PREPARED BY	A.D.P.	15 JUNE 63		DWG TO BE CHG'D YES ☐ NO ☐
CHK'D BY				NEW DWG REQ'D YES ☐ NO ☐
STRESS			Thiokol ELKTON DIVISION	SK- Nº 2568
APP'D				

FIGURE 58. NOL RING INTERLAMINAR SHEAR SPECIMEN

Method Standard Number 406, Method 1042. The split disc apparatus is used for applying the load to the ring. As would be expected, this technique suffered the same deficiencies as the other split disc techniques and was therefore abandoned.

The second technique uses the apparatus and specimen shown in Figure 59 for determining the across-grain interlaminar shear. As shown in the figure, the testing machine applies a compression load to the male die, which is transmitted to the test specimen as a shear load, parallel to the laminates and normal to the grain direction. The test program for both techniques is outlined in Table XV.



QTY REQD PER DASH NO.	ITEM NO.	CODE IDENT	PART OR IDENTIFYING NO.	NOMENCLATURE OR DESCRIPTION	MATERIAL	SPECIFICATION
	4	5		THUMB SCREW 1/4-20 X 1	STL.	
	1	4	LO-1977	DIE HOLDER MALE	STL.	
	1	3	FR 750 .D	DRILL BUSHING 1 3/4 LG	STL	AM. 1.000 DIA OD
	1	2	FR 1000 D	DRILL BUSHING 5/8 LG	STL	AM. 1.7500/1.7497 OD.
	1	1	LO-1976	DIE HOLDER, FEMALE	ST:.	
	-01					

LIST OF MATERIAL OR PARTS LIST

UNLESS OTHERWISE SPECIFIED: DIMENSIONS ARE IN INCHES. TOLERANCES .XX = ±.030; .XXX = ±.010; ANGULAR ± 30' FRACTIONS ± 1/16. BREAK SHARP EDGES .003-.015. ALL SMALL FILLETS .030-.040 R. THREADS PER FED. HNDBK H-28 AND SUPPLEMENTS. DIMENSIONING PER MIL-STD-8. WELD SYMBOLS PER JAN-STD-21. SURFACE ROUGHNESS SYMBOLS PER MIL-STD-10. ALL FINISHED SURFACES 125

DRAWN E. McCARTHY 4/8/68
CHECKED 4/9/68
ENGR
ENGR
ENGR
USER
STRESS
SAFETY
APPD
DESIGN ACTIVITY APPROVAL

Thiokol CHEMICAL CORPORATION
ELKTON DIVISION ELKTON, MARYLAND

SHEAR PUNCH ASSY.
DELAMINATION TEST

CODE IDENT NO. 07299 | SIZE C | LO-1978

SCALE | WEIGHT | CALC ACTION | SHEET

FIGURE 59. PUNCH INTERLAMINAR SHEAR APPARATUS

TABLE XV

INTERLAMINAR SHEAR STRENGTH TEST PROGRAM

Parameter	Interlaminar Shear Strength										Totals	
Test Temperature	-75°F		0°F		77°F		150°F		225°F			
Specimen	AG	WG	AG	WG	AG	WG	AG	WG	AG	WG	AG	WG
Strain Rate, in./min 0.02	-	-	-	-	3	3	-	-	-	-	3	3
0.10	3	3	3	3	3	3	3	3	3	3	15	15
0.50	-	-	-	-	3	3	-	-	-	-	3	3
Totals	3	3	3	3	9	9	3	3	3	3	21	21

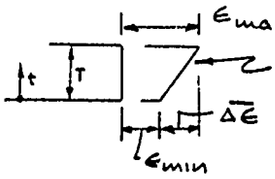
AG = Across Grain Specimen
WG = With Grain Specimen

Thiokol CHEMICAL CORPORATION
ELKTON DIVISION, ELKTON, MARYLAND

TITLE: Analytic Treatment of flexural effects	MOTOR	PREPARED V. Singer	DATE	PAGE OF
	DWG. NO.	CHECKED	DATE	J.O. NO.

MARGIN OF SAFETY

Consider first a cross-section experiencing extreme fiber strains of the same sign.



At any point thru the thickness,

$$\epsilon_t = \epsilon_{min} + \frac{t}{T}(\epsilon_{max} - \epsilon_{min})$$

$$= \epsilon_{min} + \frac{t\,\Delta\bar{\epsilon}}{T}$$

Polynomial for secant modulus at any point:

$$E_t = A + B\epsilon_t + C\epsilon_t^2 = A + B\epsilon_{min} + C\epsilon_{min}^2 + \frac{t\,\Delta\bar{\epsilon}}{T}(B + 2C\epsilon_{min}) + \frac{Ct^2\Delta\bar{\epsilon}^2}{T^2}$$

Since $\sigma_t = E_t\epsilon_t$,

$$\sigma_t = (A\epsilon_{min} + B\epsilon_{min}^2 + C\epsilon_{min}^3) + \frac{t\,\Delta\bar{\epsilon}}{T}(A + 2B\epsilon_{min} + 3C\epsilon_{min}^2)$$
$$+ \frac{t^2\Delta\bar{\epsilon}^2}{T^2}(3C\epsilon_{min} + B) + \frac{Ct^3\Delta\bar{\epsilon}^3}{T^3}$$

Now integrating across the thickness,

F = total axial force $= \int_0^T \sigma_t\,dt$ and

M_{edge} = moment about lower edge $= \int_0^T \sigma_t\,t\,dt$

The following expressions obtain:

$$\frac{F}{T} = (A\epsilon_{min} + B\epsilon_{min}^2 + C\epsilon_{min}^3) + \frac{\Delta\bar{\epsilon}}{2}(A + 2B\epsilon_{min} + 3C\epsilon_{min}^2)$$
$$+ \frac{\Delta\bar{\epsilon}^2}{3}(B + 3C\epsilon_{min}) + \frac{C\Delta\bar{\epsilon}^3}{4}$$ and

RE 2-1

$$M_{edge}/_{T^2} = \frac{1}{2}(A\epsilon_{min} + B\epsilon_{min}^2 + C\epsilon_{min}^3) + \frac{\Delta\bar{\epsilon}}{3}(A + 2B\epsilon_{min} + 3C\epsilon_{min}^2) + \frac{\Delta\bar{\epsilon}^2}{4}(B + 3C\epsilon_{min}) + \frac{C\,\Delta\bar{\epsilon}^3}{5}$$

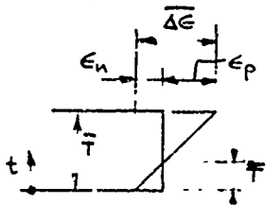
Representing $F/_T$ by X and $M/_{T^2}$ by Y, the resultant axial force is found to act at a station thru the thickness of $\bar{t}$, where

$$\bar{t} = M_{edge}/_F = YT/X$$

Thus the moment about the mid thickness is

$$M_t = F\left(\bar{t} - \frac{T}{2}\right) = \frac{2Y - X}{2}$$

Consider now extreme fiber strains of opposite sign:



ϵ_n is a negative quantity such that

$$\Delta\bar{\epsilon} = \epsilon_p - \epsilon_n$$

At any point t,

$$\epsilon_t = \epsilon_n + \frac{t\,\Delta\bar{\epsilon}}{T}$$

At $t = \bar{T}$, $\epsilon_t = 0$. Thus $\bar{T} = -\frac{T\epsilon_n}{\Delta\bar{\epsilon}}$, a positive quantity.

The polynomials for secant modulus are:

At $t \geq \bar{T}$; $E_p = A_p + B_p\epsilon_t + C_p\epsilon_t^2$;

At $t \leq \bar{T}$; $E_n = A_n + B_n\epsilon_t + C\epsilon_t^2$

And the stress at any point is given by

$$\sigma_{tp} \text{ or } \sigma_{tn} = \overbrace{(A\epsilon_n + B\epsilon_n^2 + C\epsilon_n^3)}^{\text{first parenthesis}} + \frac{t\,\Delta\bar{\epsilon}}{T}\overbrace{(A + 2B\epsilon_n + 3C\epsilon_n^2)}^{\text{second parenthesis}}$$

$$+ \frac{t^2\,\Delta\bar{\epsilon}^2}{T^2}\underbrace{(B + 3C\epsilon_n)}_{\text{third parenthesis}} + \frac{C\,t^3\,\Delta\bar{\epsilon}^3}{T^3}$$

where the n or p values of A, B, and C are used, according to the station thru the thickness

Again integrating across the thickness,

$$F = \int_0^{\bar{T}} \sigma_{tn}\,dt + \int_{\bar{T}}^{T} \sigma_{tp}\,dt \qquad \text{and}$$

$$M_{edge} = \int_0^{\bar{T}} \sigma_{tn}\,t\,dt + \int_{\bar{T}}^{T} \sigma_{tp}\,t\,dt.$$

Using the notation $(1st)_p \equiv$ first parenthesis in σ_t expression for p values of A, B, and C, etc. the following expressions obtain:

$$\frac{F}{T} = \frac{\epsilon_n}{\Delta\bar{\epsilon}}\left[(1st)_p - (1st)_n\right] + \frac{\epsilon_n^2}{2\,\Delta\bar{\epsilon}}\left[(2nd)_n - (2nd)_p\right]$$

$$+ \frac{\epsilon_n^3}{3\,\Delta\bar{\epsilon}}\left[(3rd)_p - (3rd)_n\right] + \frac{\epsilon_n^4}{4\,\Delta\bar{\epsilon}}(C_n - C_p)$$

$$+ (1st)_p + \frac{\Delta\bar{\epsilon}}{2}(2nd)_p + \frac{\Delta\bar{\epsilon}^2}{3}(3rd)_p + \frac{C_p\,\Delta\bar{\epsilon}^3}{4}$$

and

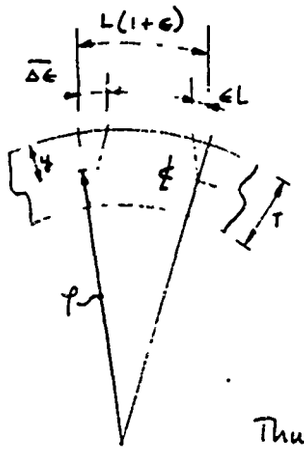
$$\frac{M}{T^2} = \frac{\epsilon_n^2}{2\,\Delta\bar{\epsilon}^2}\left[(1st)_n - (1st)_p\right] + \frac{\epsilon_n^3}{3\,\Delta\bar{\epsilon}^2}\left[(2nd)_p - (2nd)_n\right]$$

$$+ \frac{\epsilon_n^4}{4\,\Delta\bar{\epsilon}^2}\left[(3rd)_n - (3rd)_p\right] + \frac{\epsilon_n^5}{5\,\Delta\bar{\epsilon}^2}(C_p - C_n)$$

$$+ \frac{1}{2}(1st)_p + \frac{\Delta\bar{\epsilon}}{3}(2nd)_p + \frac{\Delta\bar{\epsilon}^2}{4}(3rd)_p + \frac{C_p\,\Delta\bar{\epsilon}^3}{5}$$

Again, $$M_t/T^2 = \frac{2Y - X}{2}$$

Consider now the curvature of an initially straight flexural element:



$$\frac{1}{\rho} = \frac{\varepsilon}{y} = \frac{\overline{\Delta\varepsilon}}{T}$$

Assuming an equivalent linearly elastic material with modulus E_f,

$$\frac{1}{\rho} = \frac{M_t}{E_f I} = \frac{\overline{\Delta\varepsilon}}{T}$$

where $I = \frac{T^3}{12}$ for unit width

Thus

$$E_f = \frac{T}{\overline{\Delta\varepsilon}} \times \frac{M_t}{I} = \left(\frac{M_t}{T^2}\right) \times \frac{12}{\overline{\Delta\varepsilon}}$$

In effect, the value E_f is an artificial modulus covering the fact that for the actual non-linear material, $I/y \neq t^2/6$

Thiokol CHEMICAL CORPORATION
ELKTON DIVISION, ELKTON, MARYLAND

TITLE: Extensions of Hooke's Law	MOTOR	PREPARED	DATE	PAGE OF
	DWG. NO.	CHECKED	DATE	J.O. NO.

MARGIN OF SAFETY

For material exhibiting linearly elastic anisotropy in elements where thickness effects can be neglected, represent the properties as follows:

E_θ, E_ϕ = moduli for uniaxial loading in the subscripted direction

$\nu_{\theta\phi} = \left| \frac{\epsilon_\phi}{\epsilon_\theta} \right|$ in a uniaxial field in the θ direction

$\nu_{\phi\theta} = \left| \frac{\epsilon_\theta}{\epsilon_\phi} \right|$ in a uniaxial field in the ϕ direction

With parameters thus defined, Hooke's law for a biaxial field is

$$\epsilon_\theta = \frac{\sigma_\theta}{E_\theta} - \nu_{\phi\theta} \times \frac{\sigma_\phi}{E_\phi} \quad \text{and} \quad \epsilon_\phi = \frac{\sigma_\phi}{E_\phi} - \nu_{\theta\phi} \cdot \frac{\sigma_\theta}{E_\theta}$$

From the second expression,

$$\frac{\sigma_\phi}{E_\phi} = \epsilon_\phi + \nu_{\theta\phi} \times \frac{\sigma_\theta}{E_\theta} = \frac{E_\theta \epsilon_\phi - \nu_{\theta\phi}\sigma_\theta}{E_\theta}$$

Thus $$E_\phi = \frac{E_\theta \sigma_\phi}{E_\theta \epsilon_\phi + \nu_{\theta\phi}\sigma_\theta}$$

Similarly, from the first expression,

$$\frac{\nu_{\phi\theta}\sigma_\phi}{E_\phi} = \frac{\sigma_\theta}{E_\theta} - \epsilon_\theta = \frac{\sigma_\theta - E_\theta \epsilon_\theta}{E_\theta}$$

Thus $$\nu_{\phi\theta} = E_\phi \times \left[\frac{\sigma_\theta - \epsilon_\theta E_\theta}{\sigma_\phi E_\theta} \right] = \frac{E_\theta \sigma_\phi}{E_\theta \epsilon_\phi + \nu_{\theta\phi}\sigma_\theta} \times [\sim] = \frac{\sigma_\theta - \epsilon_\theta E_\theta}{E_\theta \epsilon_\phi + \nu_{\theta\phi}\sigma_\theta}$$

RE 2-1

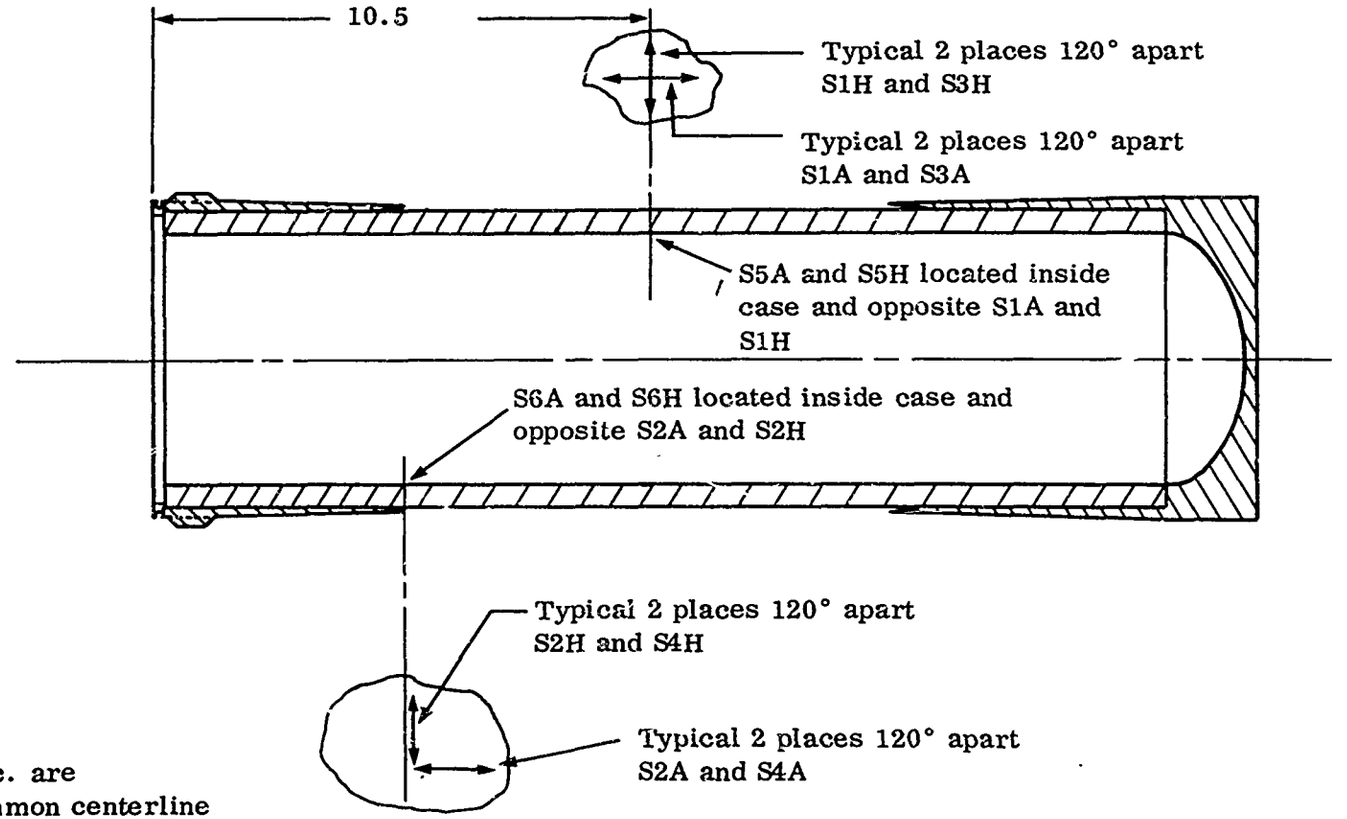
APPENDIX IV

TABLE XVI

STRAIN DATA FOR TE-M-49-1, CONCEPT III, HYDROBURST I

Strain Gauge No.	Maximum Pressure, psi	Maximum Strain, microinch/inch
S1A	3200	4906
S1H	3200	5892
S2A	3200	7310
S2H	3200	5829
S3A	3200	5305
S3H	3200	5364
S4A	3200	7995
S4H	3200	5253
S5A	3200	5335
S5H	3200	8004
S6A	3200	Lost Data
S6H	3200	

Strain gauge locations are shown in Figure 60.



NOTES:

S1A, S1H, S2H, etc. are
located along a common centerline
and similarly with S3A, S3H, S4A, etc.

FIGURE 60. STRAIN GAUGE LOCATIONS FOR CONCEPT III HYDROBURST

APPENDIX V

TABLE XVII

STRAIN AND TEMPERATURE DATA FOR TE-M-49-1 STATIC TEST

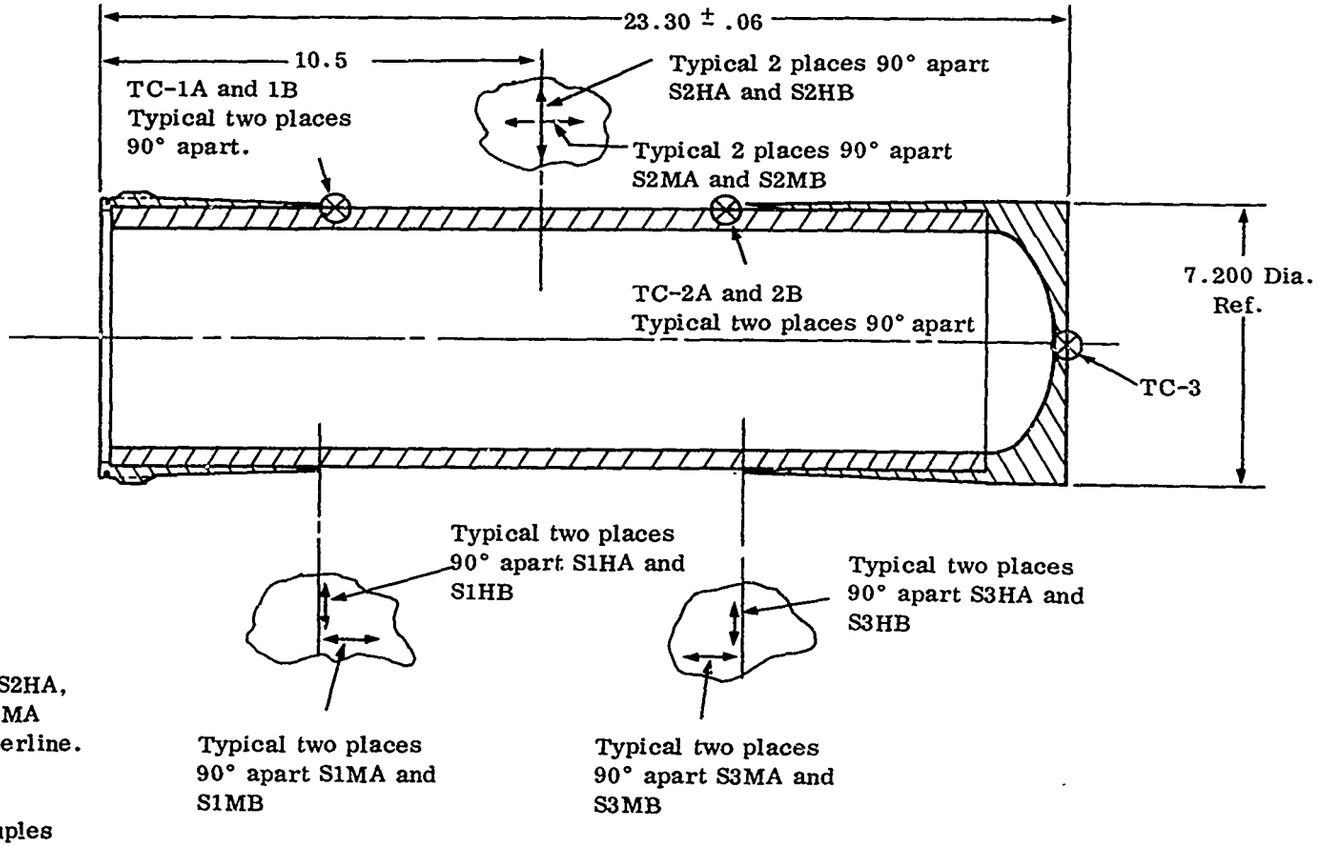
Strain Gauge Location	Maximum Strain, microinch /inch
S1HA	1673
S1HB	1820
S1MA	2331
S1MB	2379
S2HA	1664
S2HB	1727
S2MA	--
S2MB	3158
S3HA	3949
S3HB	4160
S3MA	5301
S3MB	2550

NOTES:

1. All maximum strains occurred at peak pressure.

2. There was no significant rise in case temperature at the end of action time at any point.

3. Strain gauge and thermocouple locations are shown in Figure 61.



NOTES:

1. Align S1HA, S1MA, S2HA, S2MA, S3HA, and S3MA along a common centerline.

2. Locate all thermocouples along star valleys.

FIGURE 61. STRAIN GAUGE AND THERMOCOUPLE LOCATIONS FOR CONCEPT III STATIC TEST

REFERENCES

1. Heteny, Beams on Elastic Foundations, Univ. of Mich. Press, 1946.

2. Timoshenko and Woinowsky-Krieger, Theory of Plates and Shells, McGraw-Hill, 1959.

3. Gualillo, S. P., Final Technical Report, Study of Meteorological Rocket Falling Mass Hazards, Report No. 45-65, Control No. U-65-45A, TCC, Huntsville, Ala., Sept. 1965.

4. Engineering Methods for Grain Structural Integrity Analysis, Lockheed Propulsion Co. Report No. 578/556-F-3, May 1963.

5. Bullard, D. & Holdan, J., Design and Development of 2.75-inch Mark 4 Mod 0 Rocket Motor, NAVWEPS Report 8647, NOTS-TP-3688, AD No. 467508, Naval Ordnance Test Station, China Lake, California, April, 1965.

6. Design Study, Program Plan and Budgetary Cost Estimate for an Improved 2.75 Inch Diameter FFAR, Report No. TE-66-2114, Huntsville Div., TCC, Huntsville, Ala.

7. Personal communication with J. Duda of Naval Propellant Plant, Indian Head, Md.

8. Model Specification, Motor, Rocket, Solid Propellant, M58A2, Specification No. SP-83C, Thiokol Chemical Corporation, Redstone Div., Huntsville, Ala.

9. Air Launched Propulsion System Study, Technical Report No. AFRPL-TR-65-46, Edwards AFB, California, February, 1965.

Unclassified

Security Classification

DOCUMENT CONTROL DATA - R & D

(Security classification of title, body of abstract and indexing annotation must be entered when the overall report is classified)

1. ORIGINATING ACTIVITY (Corporate author)	2a. REPORT SECURITY CLASSIFICATION
Thiokol Chemical Corporation Elkton Division Elkton, Maryland 21921	Unclassified 2b. GROUP N/A

3. REPORT TITLE

FINAL REPORT — STUDY AND DEMONSTRATION OF PAPER PHENOLIC COMPONENTS

4. DESCRIPTIVE NOTES (Type of report and inclusive dates)

Final Report, 3 May 66 to 13 November 67

5. AUTHOR(S) (First name, middle initial, last name)

John W. Edwards
V. Singer
F. W. Mueller

6. REPORT DATE	7a. TOTAL NO. OF PAGES	7b. NO. OF REFS
February, 1968	156	9

8a. CONTRACT OR GRANT NO.	9a. ORIGINATOR'S REPORT NUMBER(S)
AF04(611)-11621 b. PROJECT NO. 3059 c. Program Element No. 62405184 d.	E258-67 9b. OTHER REPORT NO(S) (Any other numbers that may be assigned this report) AFRPL-TR-67-320

10. DISTRIBUTION STATEMENT

Qualified requestors may obtain copies of this report from DDC.

11. SUPPLEMENTARY NOTES	12. SPONSORING MILITARY ACTIVITY
---	Air Force Rocket Propulsion Laboratory Research and Technology Division Edwards AFB, California Air Force Systems Command, USAF

13. ABSTRACT

The structural, thermal and mass properties of convolute-wrapped paper phenolic tubing were determined. This information was used to develop a satisfactory technique for performing a stress analysis for the preliminary design of several rocket devices, and for the detailed design and successful feasibility demonstration firing of a paper phenolic case, M58A2 rocket motor. The material is degraded by high temperature and humidity, although the effect is generally not permanent and the humidity problem can be overcome with a protective coating. The principal problem in the stress analysis technique was compensating for the non-linear anisotropic character of the material. The low strength-to-weight ratio and shear strength of the paper phenolic resulted in a decrease of seven percent in burnout velocity for the M58A2 and, consequently, a reduction of fifteen percent in cost effectiveness when compared to a metal case. In some applications, however, where the performance criterion is not sensitive to inert weight and where other properties of the paper phenolic offer overriding advantages (e.g., non-usability of debris) the material can be competitive.

DD FORM 1 NOV 68 1473 REPLACES DD FORM 1473, 1 JAN 64, WHICH IS OBSOLETE FOR ARMY USE.

Unclassified

Security Classification

14. KEY WORDS	LINK A		LINK B		LINK C	
	ROLE	WT	ROLE	WT	ROLE	WT
Paper Phenolic Materials						
Rocket Motor Cases						
Materials Testing Methods						
Production Methods						
Dimensional Limitations						
Physical Properties						
Improvement of Physical Properties						
Cost Effectiveness						
Stress Analysis Technique						